Western █ Graduate&PostdoctoralStudies

Electronic Thesis and Dissertation Repository

Investigation and Validation of Imaging Techniques for Mitral Valve Disease Diagnosis and Intervention

Claire Vannelli
The University of Western Ontario

Supervisor
Peters, Terry M.
The University of Western Ontario

Recommended Citation

Abstract

Mitral Valve Disease (MVD) describes a variety of pathologies that result in regurgitation of blood during the systolic phase of the cardiac cycle. Decisions in valvular disease management rely heavily on non-invasive imaging. Transesophageal echocardiography (TEE) is widely recognized as the key evaluation technique where backflow of high velocity blood can be visualized under Doppler. In most cases, TEE imaging is adequate for identifying mitral valve pathology, though the modality is often limited from signal dropout, artifacts and a restricted field of view. Quantitative analysis is an integral part of the overall assessment of valve morphology and gives objective evidence for both classification and guiding intervention of regurgitation. In addition, patient-specific models derived from diagnostic TEE images allow clinicians to gain insight into uniquely intricate anatomy prior to surgery. However, the heavy reliance on TEE segmentation for diagnosis and modelling has necessitated an evaluation of the accuracy of the oft-used mitral valve imaging modality.

Dynamic cardiac 4D-Computed Tomography (4D-CT) is emerging as a valuable tool for diagnosis, quantification and assessment of cardiac diseases. This modality has the potential to provide a high quality rendering of the mitral valve and subvalvular apparatus, to provide a more complete picture of the underlying morphology. However, application of dynamic CT to mitral valve imaging is especially challenging due to the large and rapid motion of the valve leaflets. It is therefore necessary to investigate the accuracy and level of precision by which dynamic CT captures mitral valve motion throughout the cardiac cycle. To do this, we design and construct a silicone and bovine quasi-static mitral valve phantom which can simulate a range of ECG-gated heart rates and reproduce physiologic valve motion over the cardiac cycle. In this study, we discover that the dynamic CT accurately captures the underlying valve movement, but with a higher prevalence of image artifacts as leaflet and chordae motion increases due to elevated heart rates.

In a subsequent study, we acquire simultaneous CT and TEE images of both a silicone mitral valve phantom and an iodine-stained bovine mitral valve. We propose a pipeline to use CT as the ground truth to study the relationship between TEE intensities and the underlying valve morphology. Preliminary results demonstrate that with an optimized threshold selection based solely on TEE pixel intensities, only 40% of pixels are correctly classified as part of the valve. In addition, we show that emphasizing the centre-line rather than the boundaries of high intensity TEE image regions provides a better representation and segmentation of the valve morphology. This work has the potential to inform and augment the use of TEE for diagnosis and modelling of the mitral valve in the clinical workflow for MVD.

Keywords: Mitral Valve Disease, Transesophageal Echocardiography, Dynamic 4D-CT.

Acknowledgments

It is imperative to first acknowledge my supervisor Dr. Terry Peters for his guidance, mentorship and inspiration throughout my time as both an undergraduate and graduate student in his lab. Terry, thank you for giving me countless opportunities to be exposed to, immersed in and excited about cutting-edge medical imaging research. Your generous spirit and kind-hearted nature fosters a supportive, close-knit and productive lab environment which I will greatly miss. John Moore, thank you for your open-door, "no question is a bad question" policy in your role as the VASST lab manager. Your ideas, wisdom and technical expertise were all essential components of the completion of this thesis. To Wenyao Xia, I cannot thank you enough for your keen interest and leadership in collaboration on various projects over the past two years. I am so grateful that both our paths and research interests crossed while in graduate school, and I will miss your vigor, quick-wit and masterful chess skills. Goli, you have been my role model since my first day in the lab and I have learned so much from you. I will aim to emulate your poise, tenacity and attention to detail in my future endeavors, and will forever cherish the time we spent in Berlin. To the past and present members of the Virtual Augmentation and Simulation for Surgery and Therapy lab, I have thoroughly enjoyed working alongside such incredible, brilliant individuals.

To my advisory committee, Dr. James Lacefield, Dr. Ana Luisa Trejos, and Dr. Daniel Bainbridge, I would like to acknowledge your guidance, input and advice throughout the past two years. Dr. Aaron So and Jennifer Hadway, thank you for all of your assistance.

The most surprising aspect of my time at Western was the close relationships I was fortunate to form, cultivate and strengthen. To the hommies– John, OG and Rob, we've kept each other honest, motivated and resilient. Justin, your advice, friendship and support was invaluable over the past two years. Dante, my long-lost cousin, I am so thankful that Robarts brought us together and that we forged such a strong friendship– you kept me in good spirits and always restored my confidence and motivation. Terenz, you have been such a steadfast source of endless support, wisdom and perspective. Thank you for being so generous with your technical skills, your profound ability to listen to and reason through problems and your counsel learned through experience. To all of my fellow graduate student colleagues, thank you for the grad club afternoons, beach volleyball games and impromptu board game sessions.

Finally, to my family–Mom and Dad, it is through your unstoppable work ethic, generosity and selflessness that our family operates as such a tight-knit, supported unit. Gma, the real OG, I have loved being in such close proximity to you over the past three years. Joe, thank you for never screening my calls and always sharing your positive, fun-loving self. Kate, my Supersis and role model since Day 1, I hope we never stop talking daily, no matter where in the world we find ourselves. I love you all.

Contents

List of Figures

List of Abbreviations, Symbols, and Nomenclature

Terminology

BNC	Bayonet Neill-Concelman
CAD	Computer-aided Design
CMF	Continuous Max Flow
DC	Direct Current
ECG	Electrocardiogram
FP	False Positive
MED	Mean Euclidean Distance
MI	Mutual Information
MV	Mitral Valve
MVD	Mitral Valve Disease
MVP	Mitral Valve Prolapse
MVR	Mitral Valve Regurgitation
NCC	Normalized Cross Correlation
PLA	Polylactic Acid
PPV	Positive Predictive Value
RMSD	Root Mean Squared Distance
ROI	Region Of Interest
STL	Stereolithography
TAVI	Transcatheter Aortic Valve Implantation
TP	True Positive
USD	United States Dollars
VHD	Valvular Heart Disease
2D	Two-Dimensional
3D	Three-Dimensional
4D	Four-Dimensional

Medical Imaging Terminology

CT	Computed Tomography
MRI	Magnetic Resonance Imaging
SSFP	Steady-State Free Precession
TEE	Transesophageal Echocardiography
TTE	Transthoracic Echocardiography
US	Ultrasound

Chapter 1

Introduction

1.1 Background

This chapter consists of a general overview of the anatomy and physiology of the human heart, with special attention given to the mitral valve. As well, this introductory section outlines the current standard of care for imaging, diagnosis and intervention of mitral valve disease, and previous work that is pertinent to the core focus of this thesis. Heart disease has become the number one cause of global death, with one in four deaths attributed to cardiovascular complications. The economic impact of treating cardiovascular diseases is significant, costing $320.1 billion USD annually, with the total number of cardiac operations and procedures increasing by 28% over the last twenty years [49]. With the significant increase in life expectancy over the past century, valvular heart disease has been referred to as the next cardiac epidemic [12] and deadliest plague [29] facing modern medicine. Transesophageal echocardiography (TEE) is widely recognized as the standard of care evaluation technique to diagnose mitral valve disease (MVD). In most cases, TEE imaging is adequate for identifying pathology, however due to limitations such as signal dropout, limited resolution and user-variability in interpreting images, the diagnostic value of TEE is often limited. A study of 242 patients who had undergone TEE-guided mitral valve repair for degenerative mitral valve disease found the rate of recurrence of mitral valve regurgitation to be 5% after 1 month and 40% after 4 years [19]. To meet the current demand for innovative solutions to cardiovascular issues, medical companies have been developing a wide range of devices, tools, imaging systems and techniques for improved diagnosis and intervention. Conventional open-heart cardiac surgery is often too invasive and not feasible for the aging population. A recent US study estimates the prevalence of valvular heart disease (VHD) to be 2.5% progressively increasing with age up to 13.2% at 75 years of age [51]. Conversely, beating-heart surgery employs image-guided, minimally-invasive tools to repair and replace heart valves while minimizing procedural patient trauma [22]. To develop

these techniques, dynamic cardiac simulators are needed for testing, validation and surgical training; referred to as phantoms, these simulators remove the need for multiple animal studies and expedite the implementation of ideas from the lab bench to the operating room. However, no two valves function or fail in the same manner. Cardiac surgeons have identified a need for patient-specific valve models in their preparation for minimally-invasive procedures [33]. This work was motivated by the increasing complexity of diagnosis and treatment of mitral valve regurgitation. Dynamic cardiac computed tomography (CT) is emerging as a valuable tool for diagnosis and assessment of cardiac function. We have conducted various studies to investigate the accuracy of dynamic CT for diagnosis and patient-specific modelling of mitral valve regurgitation. In addition, we have used dynamic CT as a ground truth to assess the efficacy of trans-esophageal ultrasound for accurately capturing valve morphology and motion. It is our aspiration that the outcome of this thesis will provide clinicians with the ability to better diagnose, model and address problems with the mitral valve.
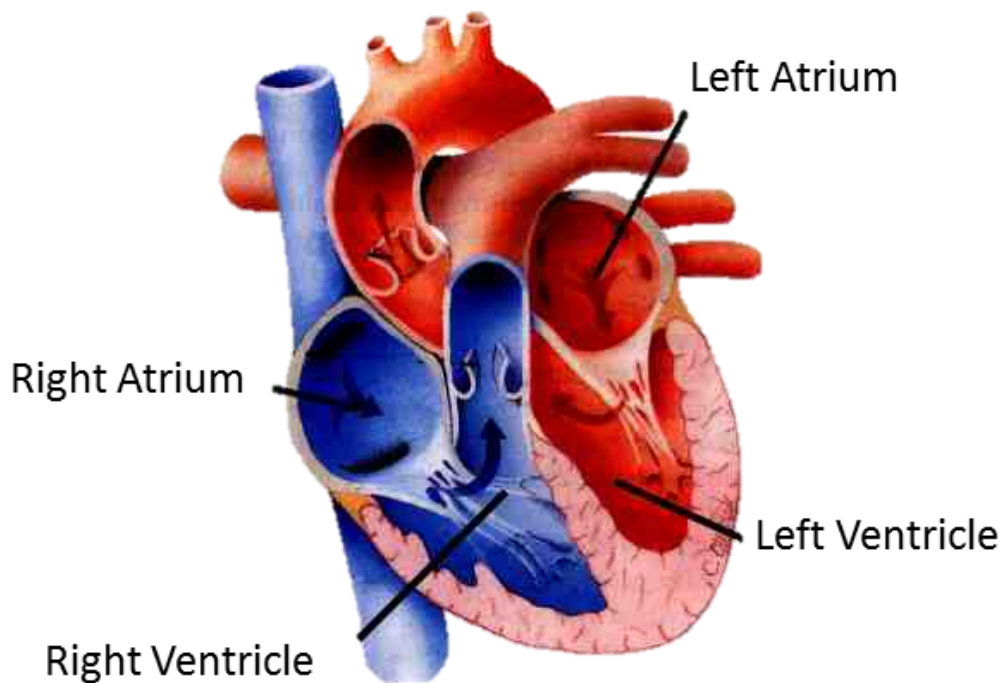
Figure 1.1: Cardiac Chambers (Image Courtesy of The Cardio Research Web Project)

1.2   Anatomy and Physiology of the Human Heart

1.2.1   Overview of Anatomy and Circulation

The heart is a muscular organ central to the distribution of blood through a vast network of arteries and veins that comprise the cardiovascular system. This enables systemic circulation of oxygen and nutrients to the tissues, along with removal of carbon dioxide and other wastes. Divided into four chambers, blood from the venous system is received at the right atrium, travels to the right ventricle where it is pumped to the lungs to be oxygenated. The left atrium then receives oxygen-rich blood from the lungs, which is pumped to the left ventricle and then through the aorta into systemic circulation (Figure 1.1).

1.2.2   Electrical Activity of the Heart

An electrocardiogram (ECG) is acquired from strategically-placed electrodes on the patients limbs and records the electrical activity of the heart (Figure 1.2). A new ECG waveform is produced for each cardiac cycle. The first stage of the ECG is the P-wave, representing atrial depolarization. The PR interval tracks the start of the P-wave to the start of the Q-wave, indicating the time taken for the electrical signals to be conducted between the atria and ventricles. The QRS complex covers the depolarization of the ventricles, as seem by three related waves (Q, S and R waves). Next, the ST-segment begins after the S-wave and finishes at the start of the T-wave; this period represents the time between depolarization and repolarization of the ventricles. During the T-wave, ventricular repolarization occurs.
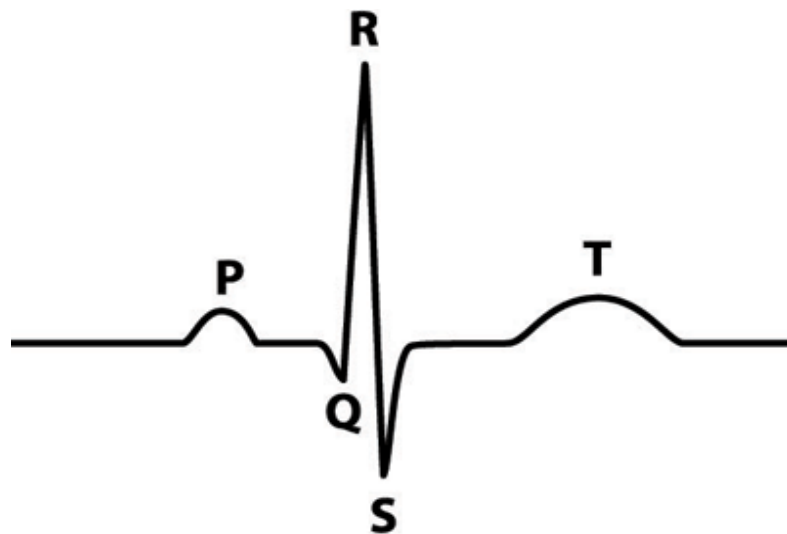
Figure 1.2: ECG waveform which tracks the electrical activity of the heart divided into the P, QRS and T waves (Image Courtesy of EKG Academy)

Other terminology used to characterize the ECG wave is the R-R interval, which starts at the peak of one R wave and ends at the peak of the subsequent R-wave, denoting the time between two QRS complexes. As well, the QT-interval outlines the time taken for the ventricles to depolarize and repolarize, starting at the beginning of the QRS complex and finishing at the end of the T-wave [34].

The overall cardiac cycle can be divided into two distinct phases of electrical activity: (1) diastole and (2) systole. During diastole, the ventricles are relaxed and for most of this period, blood flows passively from the left and right atria to the left and right ventricles, respectively. To achieve this flow pattern, blood passes through the atrioventricular valves (mitral on the left and tricuspid on the right) which separate atria and ventricles. Systole is the time of simultaneous left and right ventricular contraction when blood is ejected to the aorta and pulmonary artery, respectively (Figure 1.3). During systole, the atrioventricular valves are closed to ensure one-way, forward motion of blood, while the aortic and pulmonary valves are opened [66].

1.2.3 Heart Valves

The movement and direction of blood flow through the four chambers are regulated by four heart valves. The tricuspid valve separates the right atrium and ventricle, while the pulmonary valve sits between the right ventricle and the pulmonary artery. On the left side of the heart, the mitral valve directs blood flow between the atrium and ventricle, while the aortic valve separates the ventricle and aorta (Figure 1.4). Under normal circumstances, blood flow is
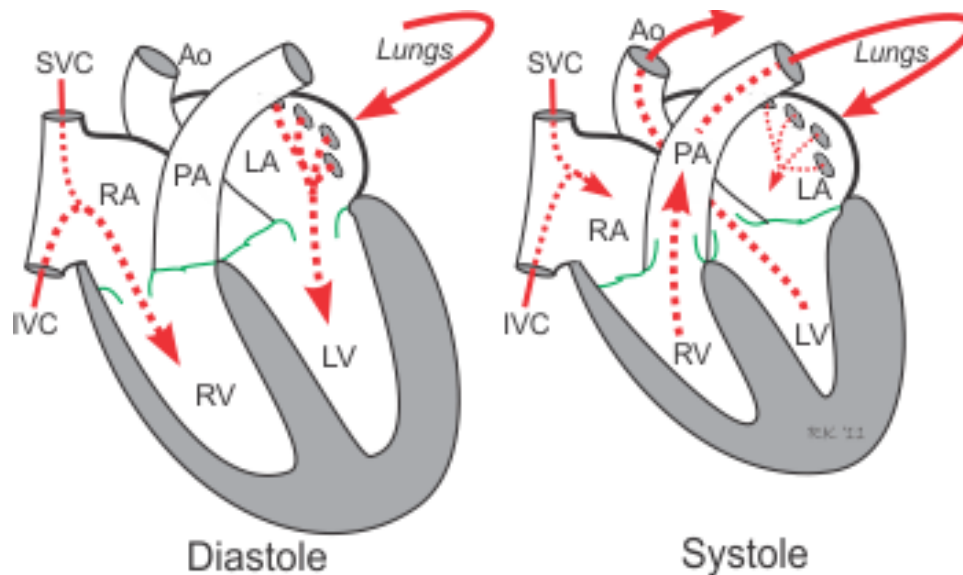
Figure 1.3: Blood flow through the heart chambers and valves during diastole and systole (Image Courtesy of Cardiovascular Physiology Concepts)

unidirectional through the heart, entering the right atrium and rejoining systemic circulation after passing through the left ventricle. This flow pattern is facilitated by heart valves which act as one-way inlets of blood on one side of the ventricle and one-way outlets of blood on the other ventricular side. When heart muscle contracts and relaxes over the length of the cardiac cycle, the valves open and shut, directing and alternating blood flow through the four chambers.

Heart valves can malfunction in two ways: (1) regurgitation and (2) stenosis. A regurgitant valve does not close completely, causing backflow of blood into the preceding chamber rather than forwards through the valve. In a stenotic valve, the opening was either formed incorrectly or has become narrowed such that blood flow is impeded; as a result, the heart must pump blood with greater force to move blood through the stiff, stenotic valve [65].
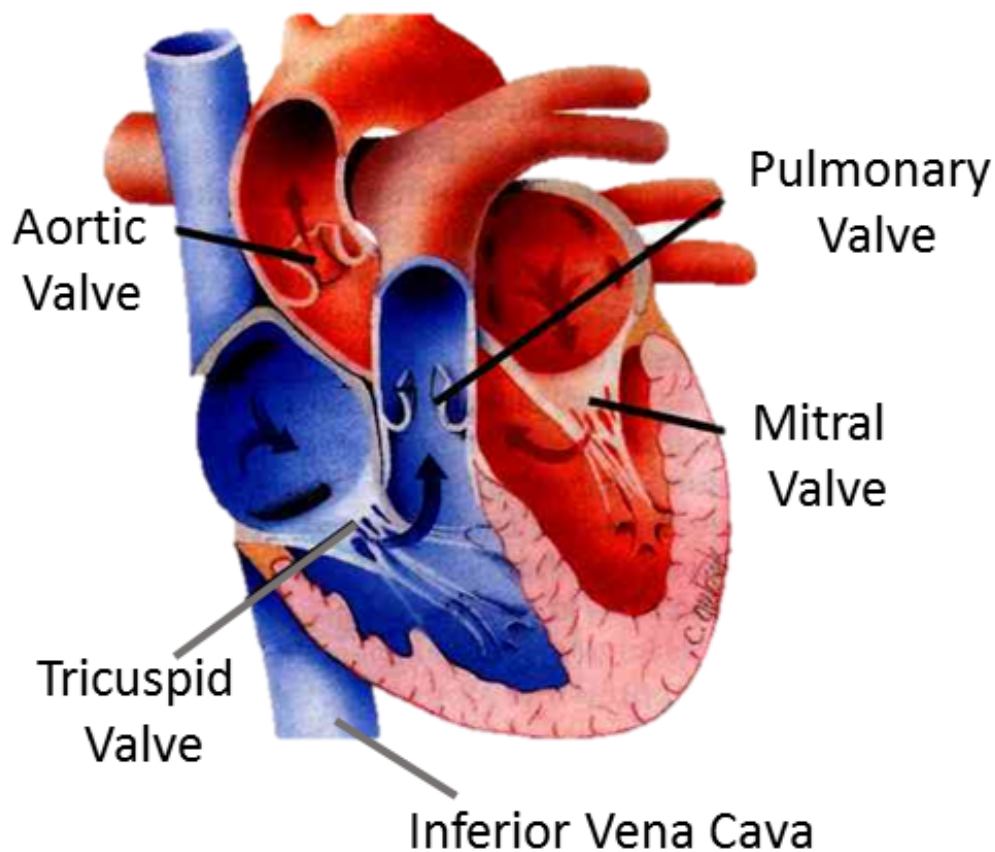
Figure 1.4: Cardiac Valves (Image Courtesy of The Cardio Research Web Project)

1.2.4   The Mitral Valve

The mitral valve (MV) separates the left atrium and ventricle, and is the main anatomical focus of this thesis. Embryologic development of the mitral valve is a complex process, which occurs in the endocardial cushion between the fifth and fifteenth weeks of gestation. As one of the most unique tissues in the human body, mitral valve structure is highly variable. The fully developed valve complex comprises an annulus, two valve leaflets (posterior and anterior), chordae tendineae, and papillary muscles (Figure 1.5). Peripheral to the valve apparatus are the walls of the left atrium and ventricle. The non-planar, saddle-shaped valve complex is obliquely located in the heart, immediately adjacent to the aortic valve [32].
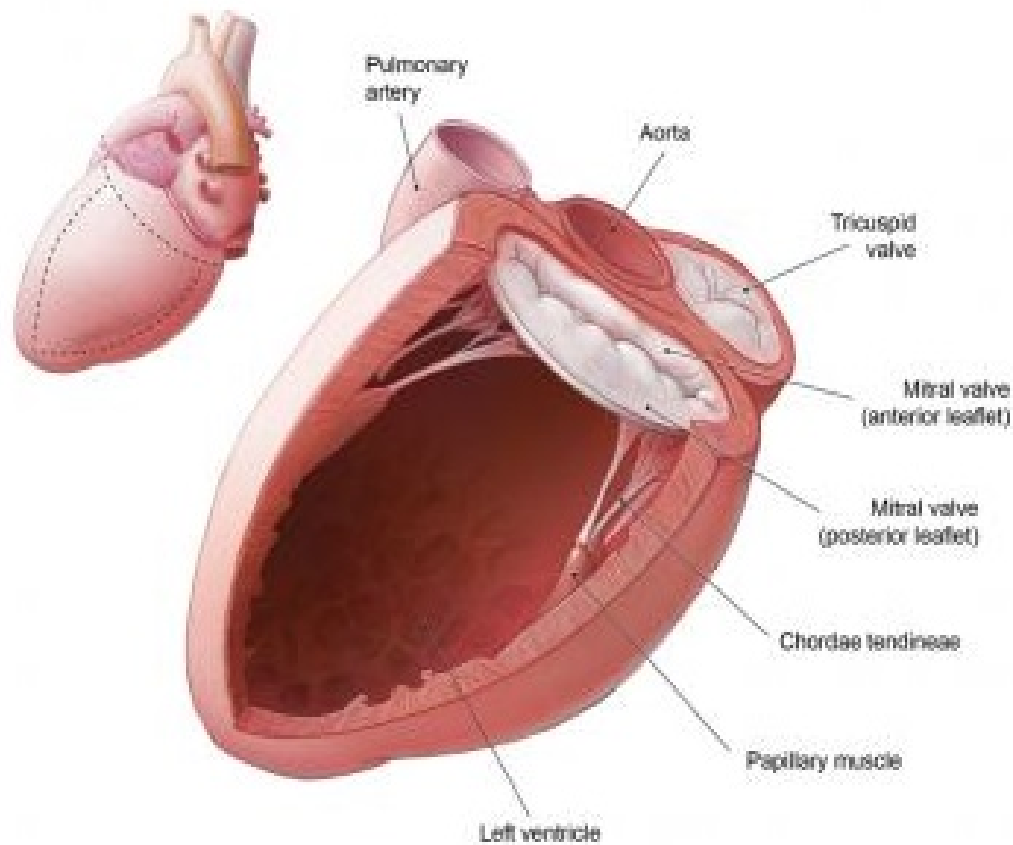
Figure 1.5: Components of the Mitral Valve (Image Courtesy of Medscape)

The mitral annulus describes the tissue juncture of the endocardial layer of the left atrium, the valve tissue, and the endocardium and myocardium of the ventricle [68]. Mitral valve leaflets (posterior and anterior) are distinctly different in circumference and shape to the leaflets of the other atrioventricular valve, the tricuspid valve. Along with the leaflets, the valve has variable, accessory tissue termed commissural scallops to occlude medial and lateral gaps during leaflet coaptation. In a normal, healthy state, mitral valve leaflets are thin, soft, pliable and translucent. Both leaflets have an atrial and ventricular surface. The posterior leaflet is crescent-shaped with a short radial length and long circumferential base; to facilitate clinical communication regarding diagnosis and intervention, the leaflet can be divided into lateral (P1), central (P2) and medial scallops (P3). The anterior leaflet is trapezoid-shaped and attached to the fibrous part of the annulus. This leaflet is longer, thicker and larger than the posterior leaflet, and can similarly be distinguished by lateral (A1), central (A2) and medial scallops (A3) [11]. The chordae tendineae are string-like structures which attach the ventricular-facing leaflet surface to the papillary muscles (Figure 1.6). Due to their collagenous structure, the chords do not stretch beyond 10% in physiologic conditions. The muscular components of the mitral apparatus are the papillary muscles and left ventricular wall. Two papillary muscles are positioned along the mid to apical region of the left ventricular wall [28].
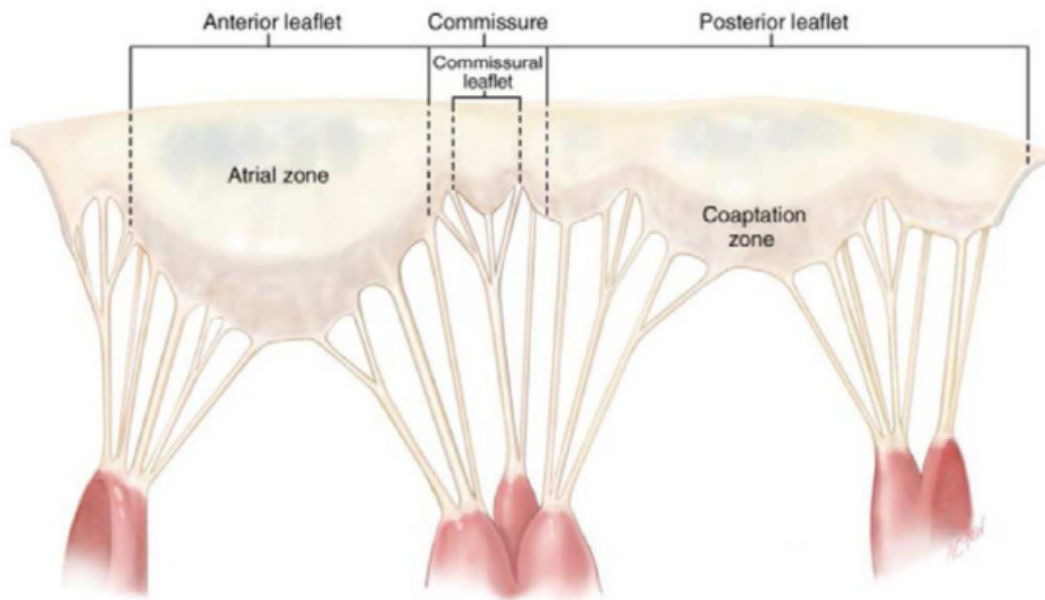
Figure 1.6: An unfolded mitral valve depicting the atrial leaflet surface, papillary muscles attached to the chordae tendineae and the anterior, posterior leaflets and commissures [11]

Normal function of mitral valve allows unimpeded blood flow into the left ventricle during diastole, and prevents backflow of blood into the left atrium during systole. The healthy mitral valve undergoes substantial dynamic changes in both size and shape over the length of the cardiac cycle. After left ventricular contraction, the aortic valve closes and the mitral valve opens, allowing blood to flow from the atrium to ventricle. Complete closure (defined as coaptation) and correct symmetrical overlap of the posterior and anterior leaflets are essential for normal, non-regurgitant valve function [41]. The mitral valve has a distinctive motion pattern during the cardiac cycle, which can be correlated to electrical activity tracked by the ECG wave (Figure 1.7) [71].

The valve remains closed early in diastole, during the isovolumic ventricular relaxation phase; as the ventricular muscle relaxes in late ventricular diastole, pressure in the chamber drops below pressure in the atrium and the mitral valve opens to allow blood to flow down its pressure gradient from the atrium to the ventricle. Ventricular systole follows depolarization of the myocardial cells in the ventricle wall (the QRS complex on the ECG). Due to specific innervation, papillary muscles contract before the ventricular wall which keeps the chordae under tension. With ventricular wall contraction, the pressure in the chamber rises higher than diastolic atrial pressure [63], causing the mitral valve to close to prevent backflow of blood to the atrium, in preparation for the ventricular ejection phase at the end of systole. After valve closure, papillary muscles are stretched during ventricular contraction, facilitating optimal valve coaptation [26].

1.3   Mitral Valve Disease

Normal mitral valve function relies on a carefully coordinated mechanism and interplay between the individual components of the valve complex. Both congenital and acquired disorders can impair this mechanism and the result is a regurgitant, diseased or overall incompetent valve. This section outlines different pathophysiologic variants of mitral valve disease.

1.3.1   Mitral Valve Regurgitation

Mitral valve regurgitation (MVR) is the most common valve dysfunction in US population [51]. Regurgitant valves have incomplete or insufficient leaflet coaptation. As a result, part of left ventricular stroke volume flows backwards into the atrium rather than forwards through aorta during systole. During diastole, when the valve is open, the regurgitant volume is returned to the left ventricle and leads to ventricular volume loading. MVR has a wide range of causes, including mitral valve prolapse, flail leaflets (Figure 1.8c), damaged or ruptured chor-
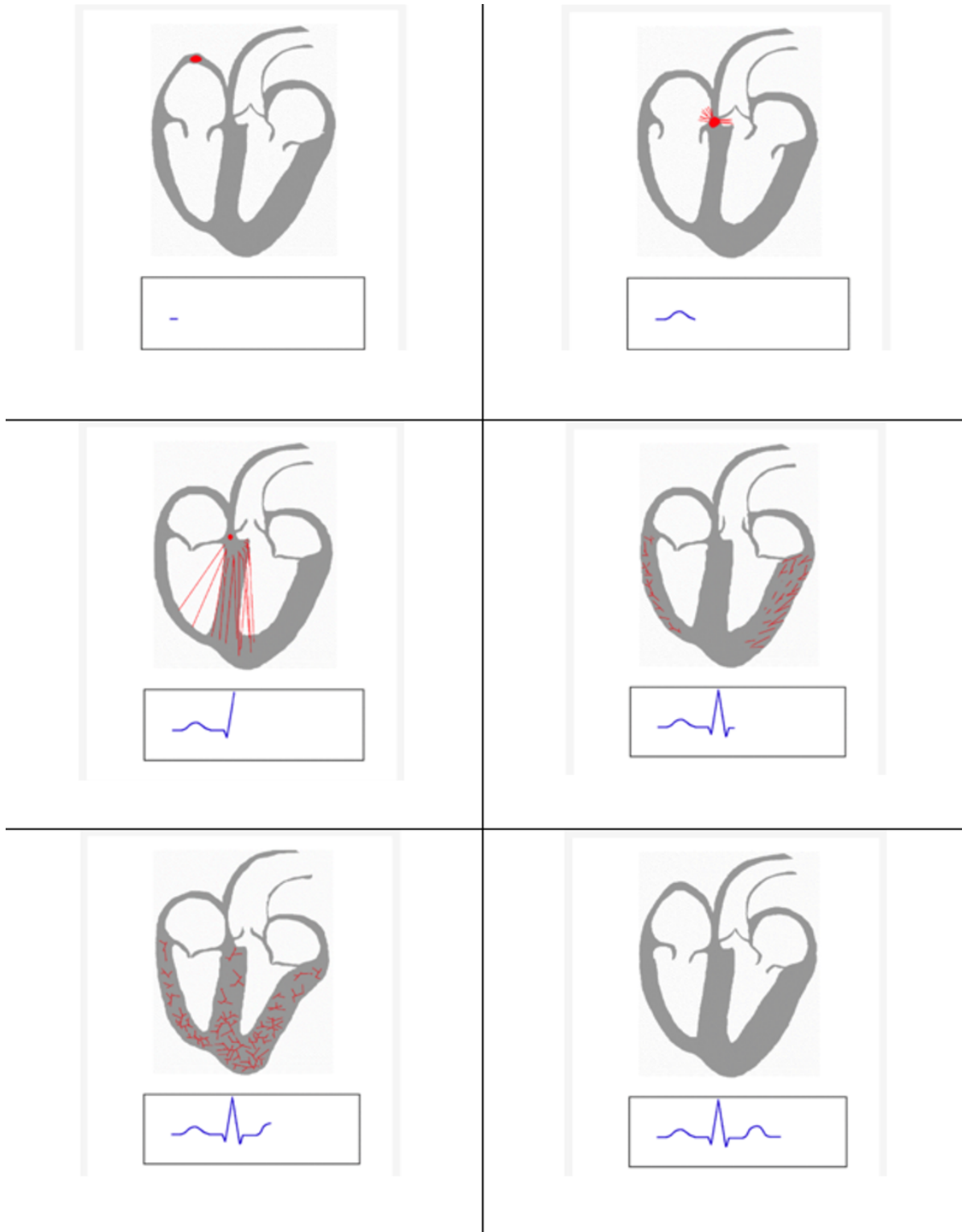
Figure 1.7: Mitral valve motion correlated to the stages of the ECG wave [71]

dae, rheumatic fever, endocarditis, congenital heart defects, untreated high blood pressure and general valve damage due to wear and tear. Symptoms of mitral valve regurgitation include: heart murmur due to turbulent flow through the heart, shortness of breath (especially during exertion or lying down), fatigue, lightheadedness and heart palpitations. The severity of MVR is assessed on a graded scale from mild to severe; individuals can live with functional, mild MVR without treatment but once classified as severe, a course of intervention is determined for valve repair or replacement [1].

1.3.2 Mitral Valve Stenosis

Mitral stenosis is the narrowing of the valve opening such that blood flow is obstructed between the left atrium and ventricle. Typically, mitral stenosis arises with valve scarring from rheumatic fever, however some individuals can be born with the condition. Unless classified as severe, mitral stenosis does not present with symptoms. Severe mitral stenosis causes similar symptoms to mitral valve regurgitation such as shortness of breath, fatigue, dizziness and heart palpitations [6].

1.3.3 Mitral Valve Prolapse

Mitral valve prolapse (MVP) is characterized by an abnormal protrusion or bulging of parts of the valve leaflet into the atrium (beyond the plane of the mitral annulus) during ventricular systole (Figure 1.8b). MVP is the leading cause of mitral regurgitation and is cited as the most oft-occurring reason for mitral valve surgery, affecting nearly one in 40 individuals [21]. However, MVP has a wide range of presentations and the cause can either be primary or secondary. Primary MVP includes cases where the main abnormality exists in the mitral leaflet, while secondary MVP indicates dysfunction in the subvalvular mitral apparatus [5]. Though mitral valve prolapse is typically a lifelong disorder, the symptoms experienced by individuals are greatly variable with some never experiencing any signs of prolapse or regurgitation. Any symptoms that prolapse patients present with are typical of mitral valve regurgitation, initially with mild severity and developing gradually.

1.3.4 Degenerative Mitral Valve Disease

Degenerative mitral valve disease (MVD) is the most common form of organic mitral valve disease in developed countries, with incidence in the US estimated to be 2-3% [21]. MVP is the most common functional abnormality associated with degenerative MVD, as a result of both leaflet redundancy (from abnormal connective tissue) and chordae elongation (making
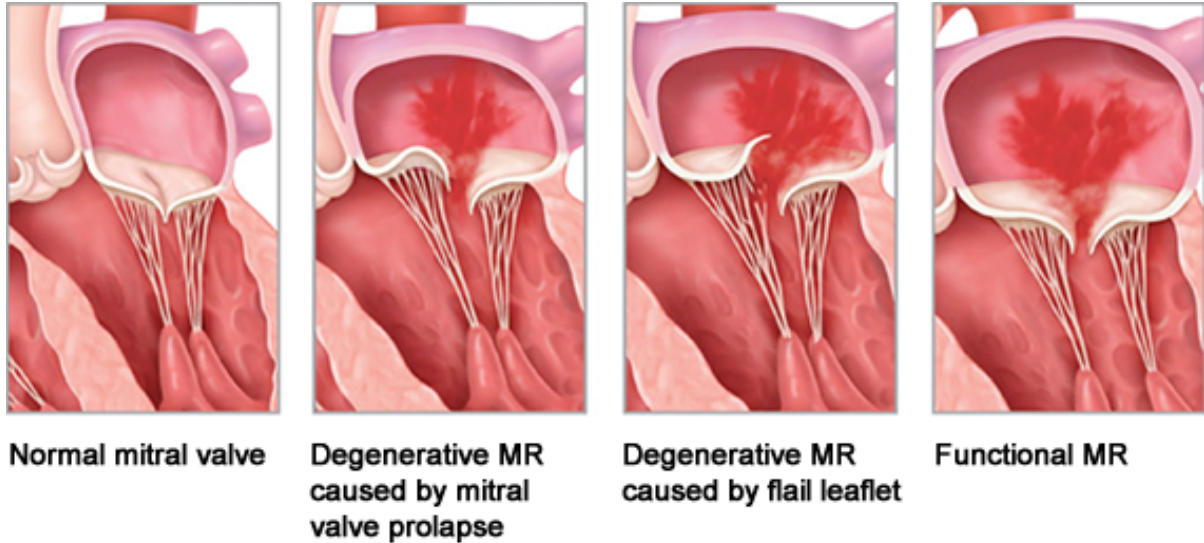
Figure 1.8: Mitral valve in systole for (a) normal case (b) degenerative MVR due to prolapse (c) degenerative MVR due to flail leaflet and (d) functional MVR (Image Courtesy of Abbott Vascular)

them prone to rupture). There is high variation in the pathological characteristics of individuals with degenerative MVD. Severe regurgitation follows rupture of elongated chordae, due to unsupported and flail leaflets. With increased severity of MVR, so does the risk of heart failure, atrial fibrillation and death due to cardiovascular complications [20].

1.4 Mitral Valve Imaging

As structural heart disease interventions continue to evolve, accurate and reliable imaging is necessary for diagnosis, pre-operative selection of cases, intra-operative guidance, post-operative evaluation and longitudinal follow-up of patients. Though much is known about mitral valve behavior in healthy and abnormal individuals, a complete understanding of the complexity of valve anatomy and function remains an active area of research. It is an ongoing challenge to fully capture the dynamic movements and interaction of valvular components to describe physiology during the cardiac cycle. Medical imaging is the key assessment tool to non-invasively comprehend details of dynamic mitral valve morphology and disease for decision-making and treatment planning [20]. For all medical imaging, visualization in 3D is preferred over 2D as it allows better understanding of the spatial relationships between adjacent anatomic structures.

1.4.1 Ultrasound

Due to its ability to capture images in real time, ultrasound is ideally situated to capture the rapid, dynamic movement of the mitral valve over the length of the cardiac cycle. The mitral valve is complex, with a unique arrangement of its component parts within the left ventricle. Cross-sectional imaging techniques including 4D echocardiography allow the valve to be visualized in its entirety by acquiring a whole series of planes [31]. Echocardiography is the preferred modality for diagnosing the presence of severity of MVD in addition to assessing the underlying etiology.

Colour Doppler Imaging

Colour Doppler 3D TEE is a valuable technique, widely used to identify both the location of the regurgitant orifice and the severity of MVR [73]. With the capabilities of Doppler volumetric methods, there are several parameters available to determine severity of MVR such as the area ratio between the regurgitant jet and left atrium, vena contracta width and effective regurgitant orifice area (Figure 1.9). However, no single parameter can grade the severity of MVR on its own, and an integrated approach with a combination of volumetric data is necessary for thorough analysis. Measurements made with Doppler imaging are limited to an estimation of the MVR, as colour images are easily confounded by variations in patient hemodynamics and operator-selected gain settings. As such, colour flow imaging is effective for diagnosis of MVR but should not serve to quantify the regurgitation [25].

Transthoracic Echocardiography

Transthoracic echocardiography (TTE) is the main tool used for an initial assessment of mitral valve pathology in daily cardiology practice [55]. TTE images are acquired by sliding, rotating and tilting an ultrasound transducer on the gel-covered surface of the chest. First, a parasternal long axis view is acquired to assess the leaflet thickness and evaluate their motion during the cardiac cycle. Next, a short axis parasternal view captures the attachment of leaflets to the chordae, and mitral valve area can be measured. Finally, apical four chamber and long axis views are acquired to visualize leaflet coaptation and estimate the degree of possible regurgitation with Doppler. While TTE is sufficient and oft-employed for initial valve imaging, when visualizing the mitral valve, TTE is limited by the structures surrounding the heart, such as the lungs and ribs. Since these images are acquired superficially, the ultrasound waves are often obstructed by these areas before reaching and providing a clear picture of the valve.
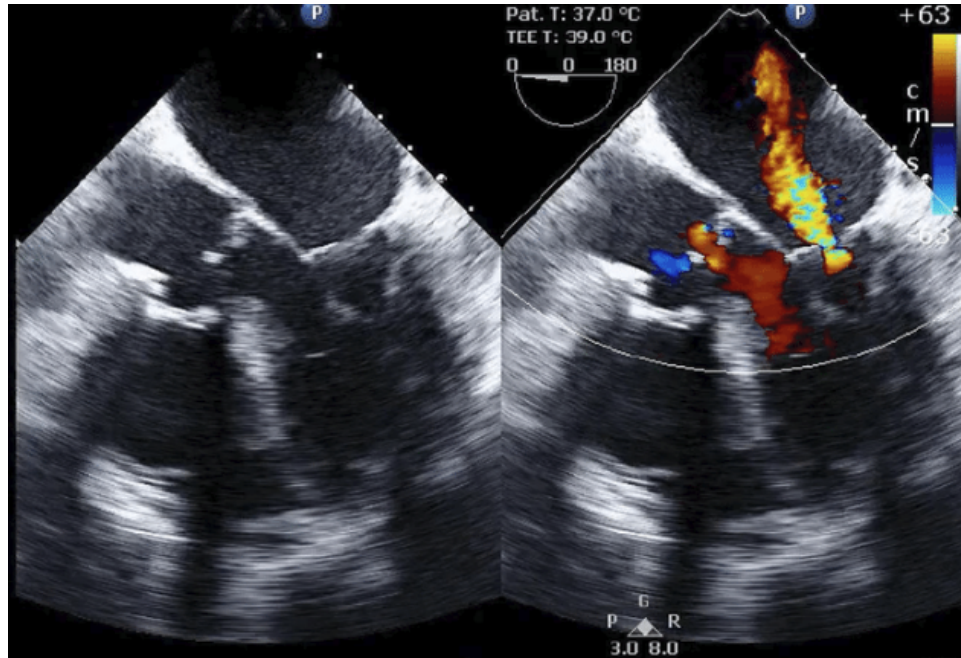
Figure 1.9: Diagnostic, preoperative TEE images of the mitral valve (left) and color Doppler image (right) depicting mild to moderate functional MVR [47]

Transesophageal Echocardiography

While TTE is the primary modality for diagnosis and evaluation of MVD, transesophageal echocardiography (TEE) is an important adjunct for patients in need of more detailed visualization of left atrium and valve morphology. Due to the proximity of the esophagus to the upper chambers of the heart, acquisition with a TEE probe can provide very clear and detailed images of different cardiac structures and valves. TEE has become an invaluable diagnostic tool, detailing the underlying anatomical mechanism for clinician preparation prior to a surgical or percutaneous repair. The first use of 2D TEE during cardiac surgery was in 1979, which promoted the development of 3D TEE to reduce the cognitive load on clinicians. Further, 3D echocardiography moves beyond the 2D cross-sectional heart views to anatomic images that correspond to a Cartesian coordinate system [64]. 3D TEE is also used intro-operatively to guide percutaneous procedures for valve repair, as well as post-operatively to assess outcomes of valve surgery. Images are acquired from an ultrasound probe inserted into a patient's esophagus in some cases while they are under a local anesthetic. Along with progression down the length of the esophagus, the probe head can be rotated and tilted to different angles and provide a range of cardiac views.

There are three prerequisites for optimal 3D TEE acquisition of dynamic MV morphology: (1) high temporal resolution for a frame-by-frame analysis of leaflets (2) high spatial resolution to visualize and classify fine morphological details 3) large volumetric dataset which
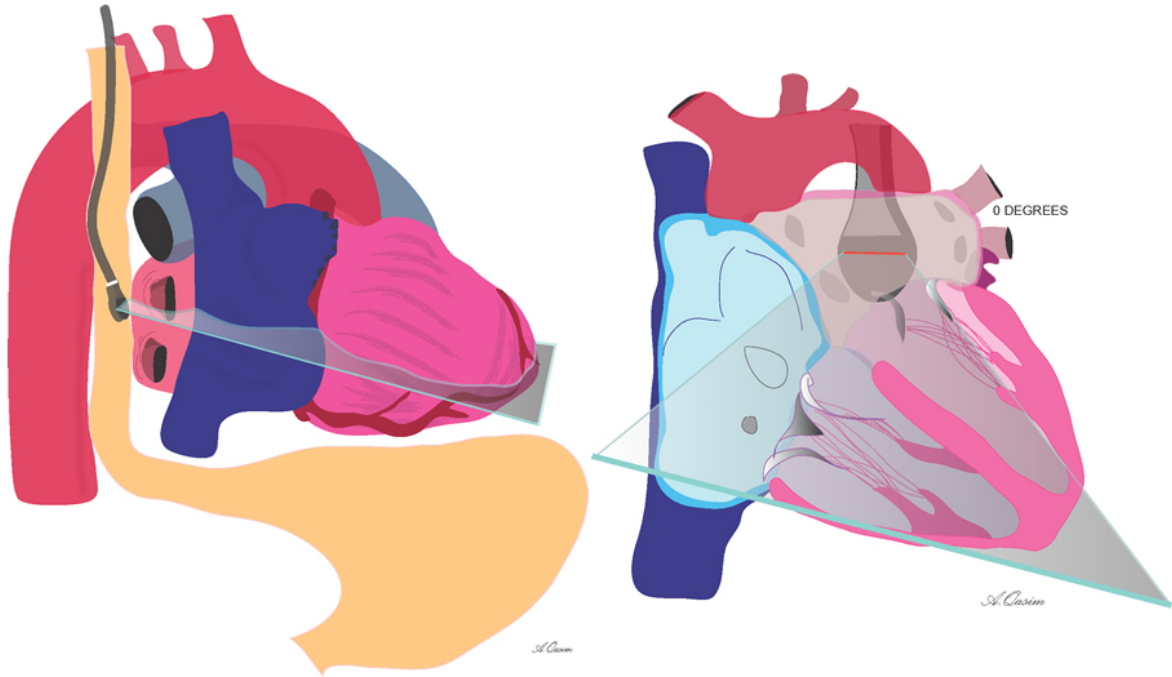
Figure 1.10: Stylized depiction of TEE probe in the mid-esophagus and the subsequent short axis, four chamber view (Image Courtesy of Toronto General Hospital Department of Anesthesia)

captures MV from commissure to commissure [73] (Figure 1.10). However, in real-time 3D TEE imaging there is a tradeoff between temporal resolution (frame or volume rate) and size (width and depth) of the data set. In comparison to TTE, TEE imaging is superior for diagnosis of infective endocarditis. Drawbacks of using TEE for imaging the mitral valve include its invasiveness and the spatial constraints of the esophagus. These confines necessitate small and subtle probe motions to obtain adequate imaging windows. As well, TEE is resource intensive, often uncomfortable for patients and associated with complication risks [3]. Both temporal and spatial resolutions impact the image quality of 3D TEE, as well as the cognitive limitations of comprehending the 3D echo images displayed on a 2D screen (with colour used to demonstrate depth and reality). As with other 3D imaging modalities, 3D TEE is impacted by artifacts such as stitching artifacts, dropout (dropout artifacts can mimic valvular perforations and periprosthetic leaks [59]), blurring or thickening of structures. The evaluation of the submitral apparatus is challenging from the conventional TEE approach [54]. The conventional mid-esophageal approach at the mitral valve level allows for clear visualization of the mitral annulus and leaflets (as the ultrasound beam is nearly perpendicular to the annular plane). However, in this orientation the beam is parallel to the chordae and the long axis of the papillary muscles and therefore any imaging of the subvalvular apparatus is sub-optimal [27].
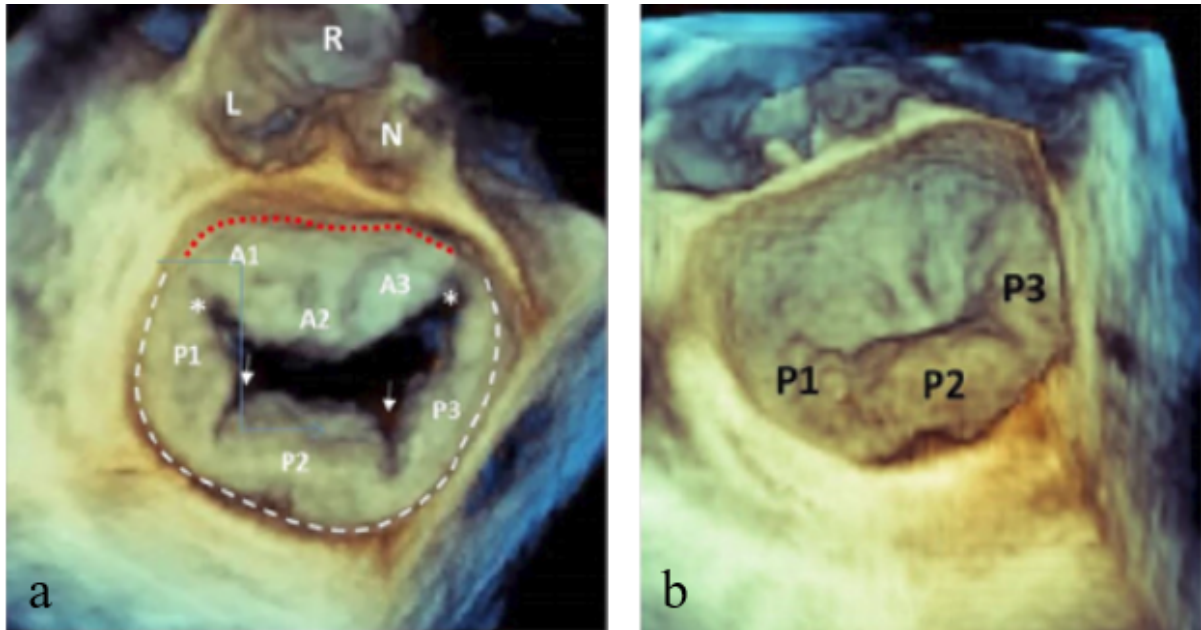
Figure 1.11: (a) 3D TEE image of mitral valve in mid-diastole from overhead (surgeon's) perspective; three scallops of posterior leaflet, inter-scallop indentations/minor commissures (arrows), 3 divisions of anterior leaflet; asterisks point to two commissures and (b) 3D TEE image of closed mitral valve in systole with three scallops of posterior leaflet labelled [73]

Transgastric Echocardiography

Transgastric echocardiography is an extension of TEE; the transgastric views are acquired when the TEE probe is progressed along the length of the esophagus and into the stomach (Figure 1.12). These images provide optimal evaluation of the left and right ventricular function through ejection fraction calculation and post-operative wall motion assessment. As well, deep transgastric views (with the probe inserted far into the patients stomach) can assess the degree of aortic stenosis or regurgitation. It is relatively unknown how effective transgastric echocardiography would be for imaging the mitral valve; since image acquisition is highly operator-dependent, the experience and technique of the clinician maneuvering the TEE probe will significantly impact which structures are visualized by the transgastric view. However, a recent study demonstrated that visualization of the submitral apparatus using transgastric 3D TEE imaging was both feasible and enabled accurate measurements of primary chords [54]. In the transgastric position, the ultrasound probe is mostly perpendicular to chords and papillary muscles, enabling a clearer view of submitral apparatus. Drawbacks of transgastric echocardiography imaging are that acquisition is extremely operator-dependent, resulting scans are still subject to relatively poor image quality and often depict ambiguous structures. Post-processing work done to improve transgastric echo images is time-intensive with highly variable outcomes.
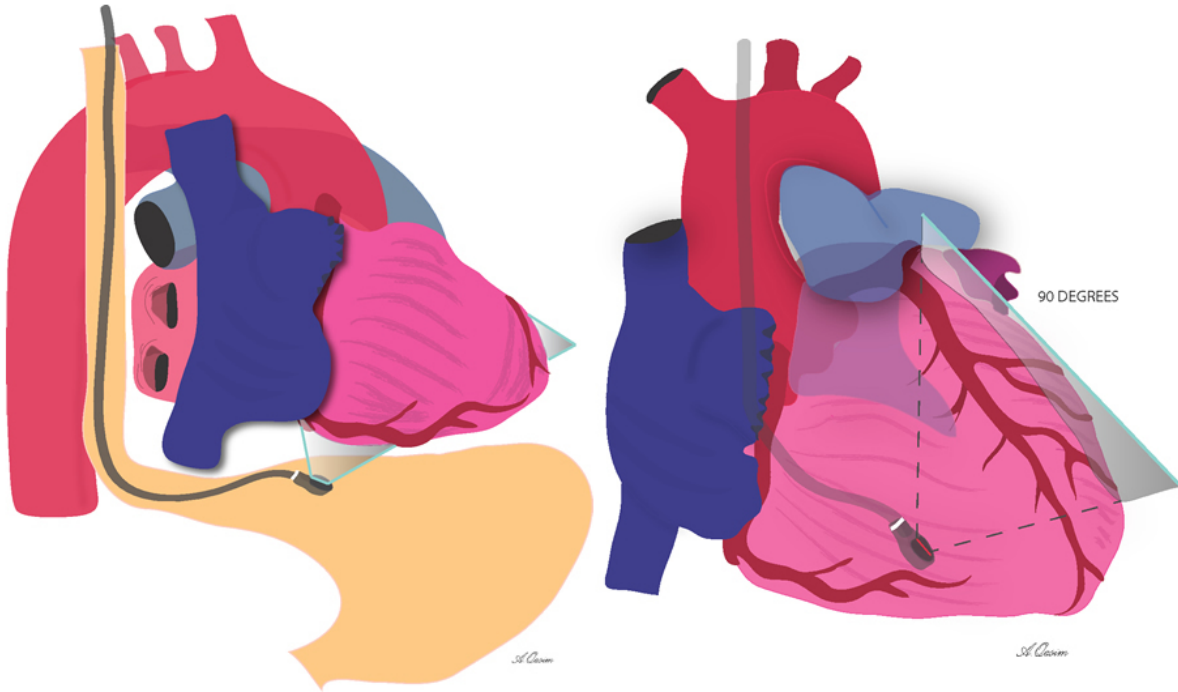
Figure 1.12: Stylized depiction of TEE probe in the transgastric position and the subsequent long axis, four chamber view (Image Courtesy of Toronto General Hospital Department of Anesthesia))

1.4.2   Computed Tomography

Computed Tomography (CT) is an increasingly important adjunct to echocardiography for the evaluation of MV disease and regurgitation [48]. CT has an important role in identification of acquired or congenital conditions with resultant regurgitation or stenosis. Additionally, CT is used to detect and monitor postoperative complications after mitral valve repair and replacement procedures.

The main application of cardiac CT is in angiography studies, which involves injection of a contrast medium and acquisition is structured to allow for assessment of the coronary arteries along with valvular structure and function. These scans are typically performed on a multidetector scanner with a minimum 64-row capacity with retrospective ECG gating. For patients with functional MVR, multidetector row CT can detect the presence of leaflet remodelling [37].The benefits of cardiac CT include total visualization of cardiac anatomic features, including coronary arteries, paravalvular structures and cardiac wall motion [35]. As with other applications of CT, the radiation dose is modulated in accordance with the "as low as reasonably achievable" principle.
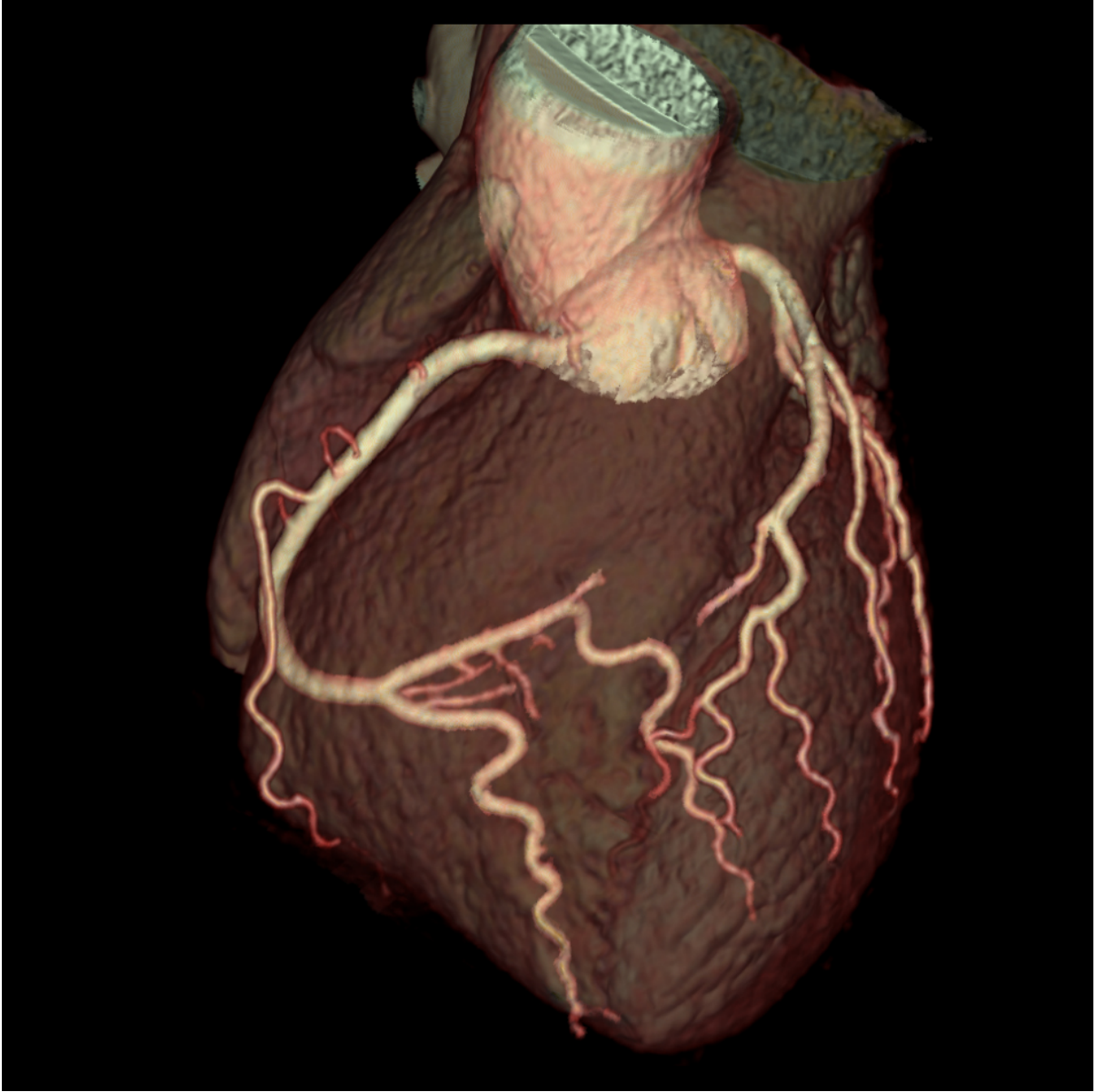
Figure 1.13: Cardiac low dose coronary artery map derived from a surface reconstruction from a 3D acquisition using the GE Revolution CT Scanner (GE Medical Systems, Waukesha, WI)

ECG Gating

The main challenge with cardiac CT is temporal resolution. Image acquisition follows rotation of the gantry (containing both the xray source and detector), and this must occur faster than cardiac movement during contraction to avoid image blurring. In addition, the acquired images capture distinct events occurring over the cardiac cycle, and there must be synchrony between the acquired data and the ECG waveform. Two methods (prospective and retrospective ECG gating) can be used to accomplish this phase-matching. For prospective ECG gating or triggering, the patient's ECG is monitored and the scanner only acquires images during cardiac diastole (typically, the heart has minimal motion during ventricular filling) (Figure 1.13). The scanner interprets a delay after the QRS complex and then triggers the "step and shoot" technique, repeating this for subsequent cardiac cycles until the entire heart has been covered. In contrast, retrospective ECG gating acquires images continually throughout the cardiac cycle, and selectively reconstructs image volumes from a desired phase after the entire scan is completed (Figure 1.14). Since the scan acquires images at all phases of the cardiac cycle, it is possible to reconstruct images in systole, diastole or any point between the two stages [62]. Considerations for which method to use include desired temporal resolution, temporal flexibility, radiation dose and ECG dose modulation.
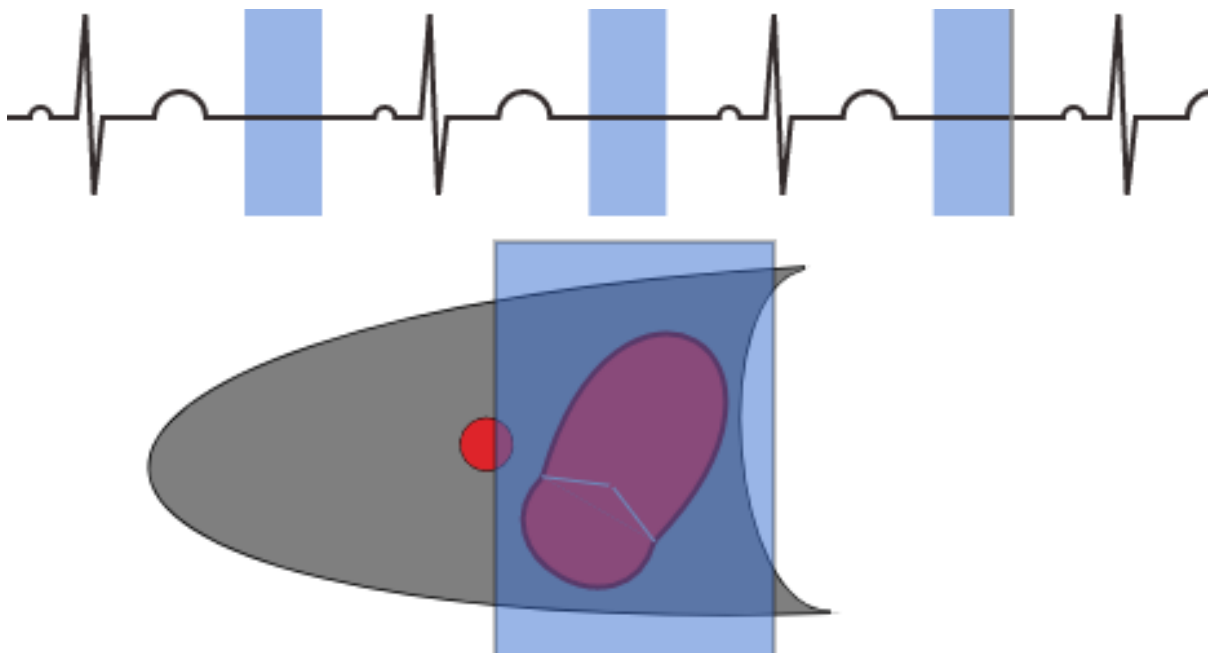
Figure 1.14: Prospective Gating for Cardiac CT (Image Courtesy of XRay Physics)
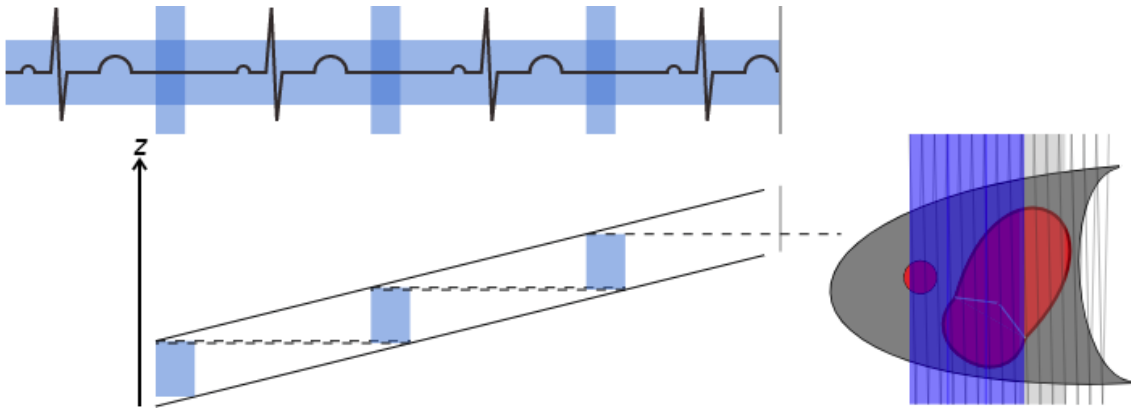
Figure 1.15: Retrospective Gating for Cardiac CT (Image Courtesy of XRay Physics)

CT Image Artifacts

Artifacts are often encountered in both clinical and research applications of computed tomography. These artifacts corrupt the resulting images as they can obscure or simulate pathology. Common CT imaging artifacts include noise, beam hardening, scatter, motion, cone beam, hlical, ring and metal artifacts. Techniques have been developed to reduce artifacts, such as iterative reconstruction or combining data from multiple scans. These methods are advantageous, as they enable lower radiation dose for the patient, higher resolution scans and more accurate diagnoses. Dual and multi-energy CT can reduce beam hardening artifacts and enhance tissue contrast [8].

Image artifacts relevant to this thesis are those most prevalent in 4D-CT images. These are due primarily to cardiac and respiratory motion. There are generally four types of artifacts which impact 4D-CT image acquisition: (1) blurring, (2) duplicate structure, (3) overlapping structure, and (4) incomplete structure. Blurring artifacts result from organs moving faster than the CT gantry rotation speed. Duplicate, overlapping and incomplete structure artifacts occur at the interface between two adjacent slices, and result in images with omitted, distorted or simulated underlying tissue [70].

4D Dynamic Computed Tomography (4DCT)

Dynamic, 4D-Computed Tomography is an exciting, relatively new imaging modality which is used primarily for perfusion studies to visualize blood flow and overall cardiac movement (Figure 1.15). It is relatively unknown how dynamic CT would perform for valve imaging, but it has the potential to provide both a high quality rendering of the valve and subvalvular apparatus and reliable volumetric data. However, there are challenges to imaging valve motion with CT. First, the CT gantry must rotate faster than the valve moves during the cardiac cycle.

Figure 1.16: GE Revolution CT Scanner for acquisition of dynamic, 4D-CT images (GE Medical Systems, Waukesha, WI)

Valve motion becomes more rapid at higher heart rates, typical of regurgitation patients and the period between diastole and systole shortens. Determining the ability and accuracy of 4DCT for mitral valve imaging is one of two main objectives of this thesis.

1.4.3 Magnetic Resonance Imaging

Cardiac Magnetic Resonance Imaging (MRI) provides the gold standard of visualizing gross cardiac function and anatomy. MRI is based on the magnetization properties of nuclei in common atoms throughout the body; patients are scanned within a powerful, uniform, external magnetic field used to align protons within water molecules *in vivo* within the tissue under examination. Depending on the type of subsequent external RF pulse sequence, different types of images are created of patient anatomy. Cardiac MRI typically involves ECG gating and breath-hold acquisitions. For mitral valve imaging, balanced steady-state free precession (SSFP) sequences applied in the short-axis plane of the heart [48] produces morphologic evaluation of the mitral valve and identification of jets indicative of regurgitation or stenosis (Figure 1.16). Since
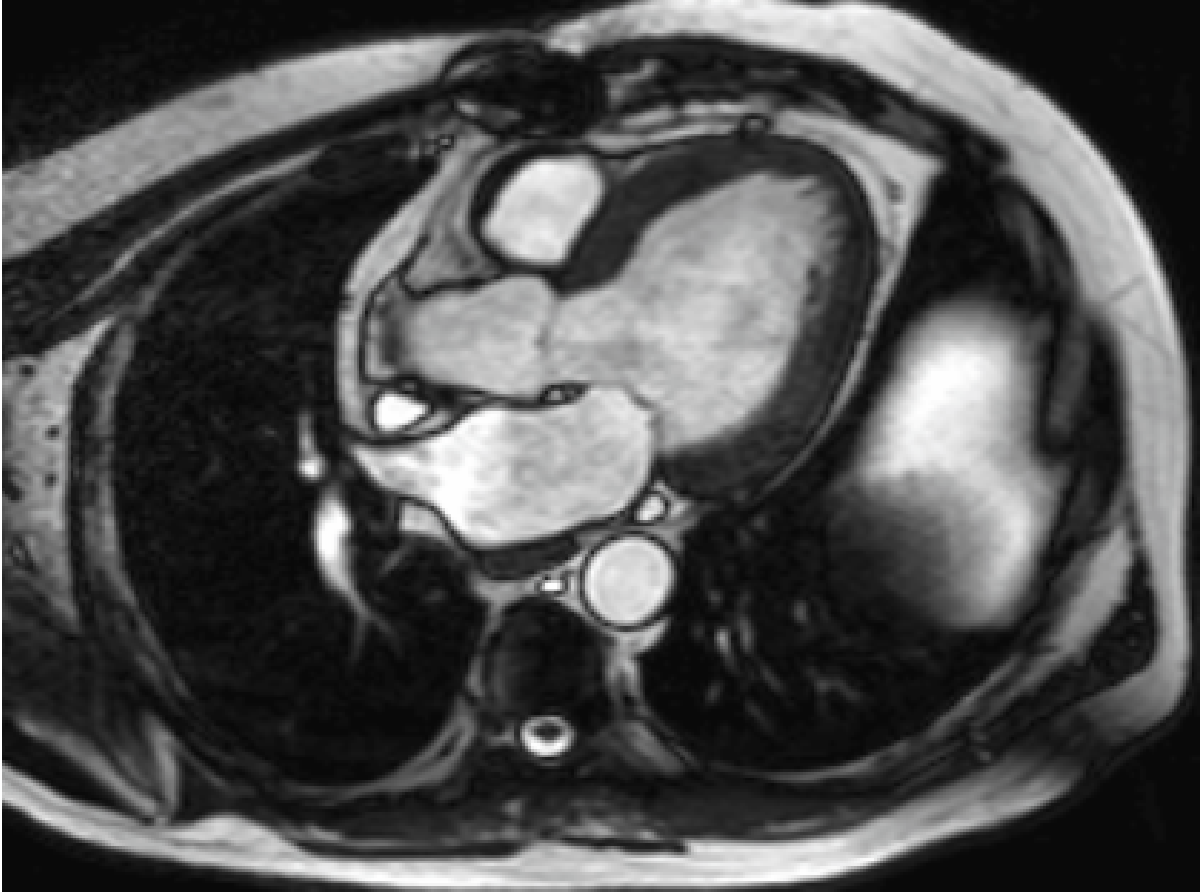
Figure 1.17: Cardiac MRI image depicting the left atrium, left ventricle, aorta, mitral valve and aortic valve (Courtesy of Center for Medical Imaging and Physiology, Department of Clinical Physiology at Lund University)

the size and length of the jet visible in SSFP images depends on a large number of factors, these morphological characteristics cannot estimate the severity of mitral valve dysfunction. Cardiac MRI is ideally suited for providing accurate, noninvasive quantification of mitral regurgitation

1.5   Mitral Valve Image Processing

Image processing describes different methods used to perform operations in order to extract useful information or enhance an image, and is analogous to signal processing, where the input is an image and the output can be an image or different features associated with the image. Medical image processing applies these techniques to medical images derived for both diagnostic and therapeutic purposes, encapsulating the analysis, enhancement and display of images acquired with x-rays, ultrasound, MRI, nuclear medicine and optimal imaging modalities.

1.5.1   Segmentation

Medical image segmentation extracts a region of interest (ROI) either by an automatic or semi-automatic process. Often, the ROI is a particular tissue or organ. For patients with MVD, the ROI is often the valve complex, segmented from a 3D TEE image. Thresholding is based on the assumption that images are divided into regions of different grey level, and is one of the quickest and easiest methods for segmentation. The corresponding histogram has varying peaks and valleys which serve to divide the image into different sections, often background and area of interest. Region growing is an interactive segmentation method which requires initialization by user-selected seed points to begin the process. With this technique, regions are grown around the user-defined seed point based on areas of intensity homogeneity. Other methods employ boundaries such as active contours and graph cuts to delineate the region of interest.

1.5.2   Registration

Image registration involves the alignment of two or more images into a common spatial region. The goal of image registration is to find the optimal transform which best aligns the regions of interest in the two input images. Applications of medical image registration include overlapping images of the same patient from different modalities, aligning temporal sequences of images to compensate for motion artifact between scans and image-guided interventions. Current algorithms can automatically register images that are related by a rigid body transformation, such that tissue deformation is negligible. As well, non-rigid or deformable registration algorithms can compensate for tissue deformation. Methods such as landmark-based, homologous-point registration and Normalized Cross Correlation (NCC) are used in this thesis.

1.6   Mitral Valve Interventions

In accordance with current guidelines, patients with symptomatic organic MVR along with asymptomatic patients with left ventricular dysfunction, significant pulmonary hypertension and atrial fibrillation are advised and referred for surgery [67].

1.6.1   Mitral Valve Repair

Mitral valve repair is widely accepted as the preferred and optimal surgical intervention of valve dysfunction and disease [45]. Supporting evidence for regurgitation due to degenerative mitral valve disease strongly favours repair over replacement. A successful repair is based

on proper understanding of the anatomic and functional changes of the diseased valve, classified by Carpentiers analysis of leaflet motion [9]. The main goal of repair surgery is to preserve as much of the native valve tissue and subvalvular apparatus as possible. This involves patching holes in and rebuilding the valve, reconnecting leaflets, removing excess tissue to increase leaflet coaptation, replacing cords and separating fused leaflets. Another example is mitral valve annuloplasty, an oft-employed surgical technique used to repair a regurgitant valve through implantation of an annuloplasty ring device. These devices are designed to increase leaflet coaptation while preserving the native valves annular shape and motion [57].

The advantages of valve repair include lower operative mortality, better preservation of left ventricular function and improved valve durability post-repair. A majority of surgeons have adopted mitral valve repair as the method of choice for correction of MVR. For patients with the most common form of isolated prolapse of the middle scallop and posterior leaflet, success rates for repair surgery are nearly 100% [14]. The main advantage of repair is freedom for patients from the side-effects to the alternative replacement procedure; annuloplasty does not require lifelong anticoagulation, and there are no thromboembolic complications which can occur with valve replacements. However, there are limitations of the repair procedure, and the feasibility of repair depends both on patient pathology and the experience of the clinical team. In particular for patients with secondary severe MVR and a low ventricular ejection fraction. In such cases, eliminating the regurgitation increases the left ventricular afterload and may induce post-operative low cardiac output syndrome [61].

Traditionally, mitral valve repair has been performed with invasive, open-heart surgery where the patient is connected to the heart-lung bypass machine. However, recent developments in biomedical engineering and robotics have employed image-guided tools to enable minimally-invasive, beating-heart mitral valve repair [13]. This reduces the overall impact on patients, surgical risk and recovery times that are a side-effect with open heart surgery. These minimally-invasive approaches rely on the insertion of catheters through a small incision into particular arteries and veins in the body in order to access the heart and its valves. One commonly-accessed entry point is the femoral vein, through which a catheter can be progressed to the inferior vena cava and into the right atrium. Percutaneous transcatheter mitral valve repair with a MitraClip device has resulted in good outcomes for patients with primary regurgitation and high surgical risk [50]. For this procedure, the catheter is used to puncture the septal wall (separating the right and left atria) to cross into the left side of the heart, access the mitral valve and deploy a clip(s) to hold the two leaflets of a regurgitant valve together for improved closure during systole [30]. An analogous, minimally-invasive procedure used to treat aortic valve stenosis in transcatheter aortic valve implantation (TAVI); guided through a small incision in the groin or chest, a catheter deploys and implants a new aortic valve on top

of the stenotic tissue.

1.6.2   Mitral Valve Replacement

In the event that the patients native valve cannot be repaired, clinicians may recommend mitral valve replacement. There are various options for valve replacements, including replacing the native valve with either a mechanical (titanium and carbon) or bioprosthetic (bovine, porcine or human heart tissue) valve. Among consideration for valve selection is patient age since bioprosthetic valves have a shorter lifespan and will need to be replaced in 10 years, so they are typically acceptable for patients greater than 60 years of age. The tradeoff with the mechanical valve is that the patient will require blood-thinning medications for the remainder of their life to prevent clots; however, when replacement is the only option for restoring mitral valve function, a mechanical replacement is most suitable for younger patients. Whenever possible with replacement surgery, chords are preserved and attached to the new mitral valve. There is evidence that preservation of chordae and papillary muscles during replacement for chronic MVR is beneficial for postoperative left ventricular function [50]. Prosthetic valve-related complications include thromboembolism, anticoagulant-related hemorrhage and endocarditis.

1.7   Patient-Specific Mitral Valve Models

Surgical simulation involves imitation of an operation on cadavers, animals, models or simulators in order to teach and train a clinicians skills, decision-making and exposure to complex cases. In cardiac surgery, personalized analytical heart models have become a crucial component of the clinical workflow, especially with complex disorders such as valvular heart disease [39]. As technology has developed to facilitate minimally-invasive procedures, clinicians must also acquire and practice new skill sets for navigating tools and interpreting patient anatomy with image guidance. Image-guided procedures enable beating-heart surgery, but pose new challenges and risks by removing the clinicians direct line of sight [46]. The success of these interventions relies on patient-specific simulators for pre-operative planning: this includes attempting different access routes, deploying sutures and analyzing their accuracy, navigating variations in patient anatomy and repeating the procedure under image-guidance so as to reduce the cognitive load when performing the actual operation. As a way of expanding beyond the "see one, do one, teach one" concept for surgical training [36], simulators and patient-specific models can provide a realistic environment which is compatible with various imaging modalities. Patient-specific modelling allows clinicians to gain insight into uniquely intricate anatomy prior to a medical intervention.
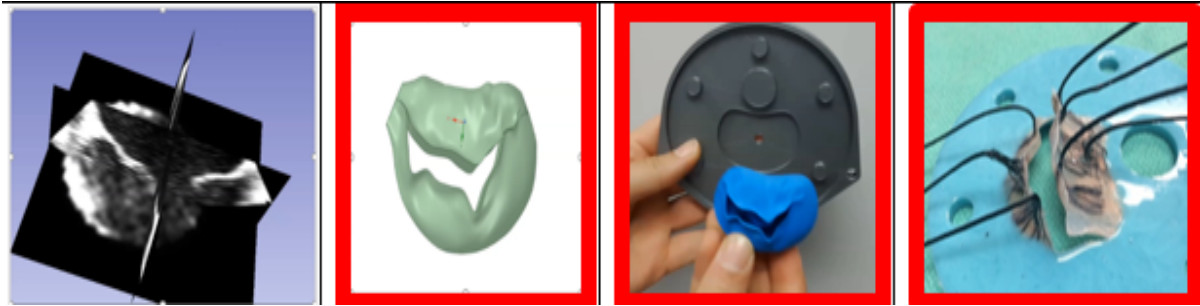
Figure 1.18: Workflow for creation of pre-operative, patient-specific mitral valve models

It is widely accepted that the mitral valve has a highly complex and variant dynamic structure with a direct impact on the hemodynamic changes following left ventricular contraction during the cardiac cycle [52]. Dynamic valve models can simulate the morphology and function of a diseased, regurgitant valve such that clinicians can interact with and practice different repair or replacement techniques prior to the actual surgery. The workflow for creation of these patient-specific mitral valve models is depicted in Figure 12. The mitral valve is segmented from a patients diagnostic TEE and rendered as a volume for rapid prototyping into a silicone, tissue-mimicking valve [24]. Next, the valve is inserted into a dynamic left ventricular phantom with blood-mimicking fluid which provides realistic, apical-to-basal motion patterns at varying heart rates. This phantom can be used to simulate valvular repair and replacement procedures with magnetic tracking, augmented reality, fluoroscopy and ultrasound guidance [69]. Currently, echocardiographic-based mitral valve models are in the early clinical validation phase.

In addition to providing a realistic training and pre-operative planning environment for clinicians, surgical simulators also act as a platform for validating new image-guided, virtual and augmented reality techniques. To ensure these systems provide accurate tracking, image information and will reduce the cognitive load during surgery, they are validated and tested using physiologically-relevant models [38], [44], [43]. Surgical phantoms with generalized or patient-specific anatomy allow for simulation of a specific procedure. Throughout the literature, there is evidence that incorporating surgical simulators and patient-specific models into the education and training of clinicians can reduce negative outcomes for patients [42], [4].

1.8 Clinical Challenges with TEE

Reliance on imaging for diagnosis and intervention of mitral valve disease introduces a host of challenges to the clinical team. Images will be impacted by the quality, age and calibration of the scanner. By depending on imaging modalities for comprehensive information of patient structure and pathology, clinicians can make decisions regarding the tools and devices
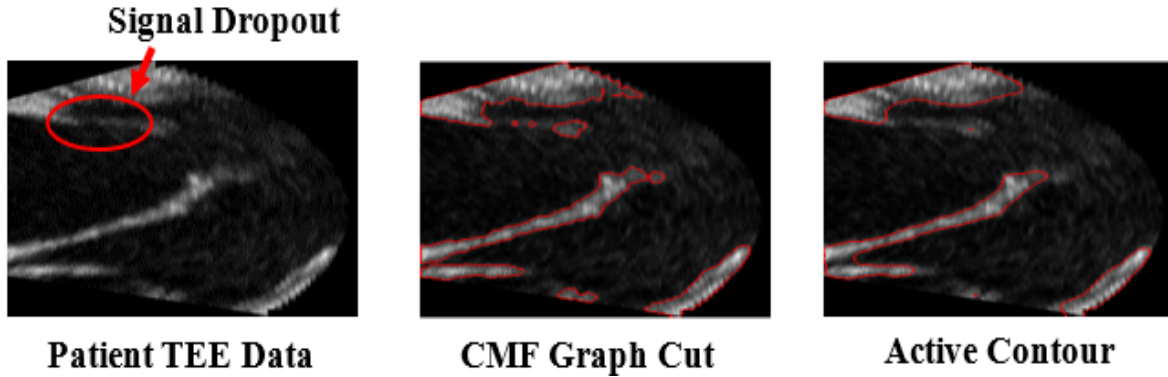
Figure 1.19: Effects of signal dropout in patient TEE images on valve segmentation

best suited to intervention; in many cases, preoperative imaging provides sufficient informa-
tion to allow clinicians to make informed decisions and perform the procedure with confidence.
However, there are the cases where a patient has complex anatomy, or the cause of regurgita-
tion remains unclear without an understanding of subvalvular structures. Additional imaging
may be needed, though the clinician can still be left without a complete understanding of the
best course of action for intervention. For complex, atypical cases and patients undergoing
minimally-invasive, beating-heart mitral valve repair or replacement, patient-specific models
and simulators are a useful preoperative planning tool. Currently, the development of these
models is limited by the quality of the patient images from which they are derived.

Multiple pervading issues with TEE images impair diagnosis of regurgitation in the clinical
workflow and challenge the implementation of the patient-specific modelling pipeline. The first
is the prevalence of signal dropout, appearing as gaps within the valve leaflet in regions that
should present as contiguous tissue (Figure 1.19).

For diagnosis, images affected by dropout make it difficult for clinicians to determine the
cause of regurgitation; for modelling, the valve cannot be completely segmented and the result-
ing models have holes (Figure 1.20). Thus, there is a loss of some patient-specific morphology
and the efficacy of the models is decreased. The second issue is the presence of additional im-
age artifact which appear as high intensity regions in the TEE images and can be misconstrued
as leaflets or other anatomical structures (Figure 1.21).

Similarly, regions of artifacts affect the diagnostic value of the TEE and pose challenges to
the modeling process. In addition, the TEE images provide a limited view of the valve, without
any indication of the structure or function of the subvalvular anatomy. Often, the source of
regurgitation is indeterminable due to the absence of information on the annulus, chordae and
papillary muscles. In addition, there is evidence that intra-operative use of TEE for mitral valve
repair has resulted in a rate of recurrent regurgitation of 5% after 1 month and 40% after 4 years
[19]. Steps towards both improving and augmenting TEE applications in mitral valve imaging
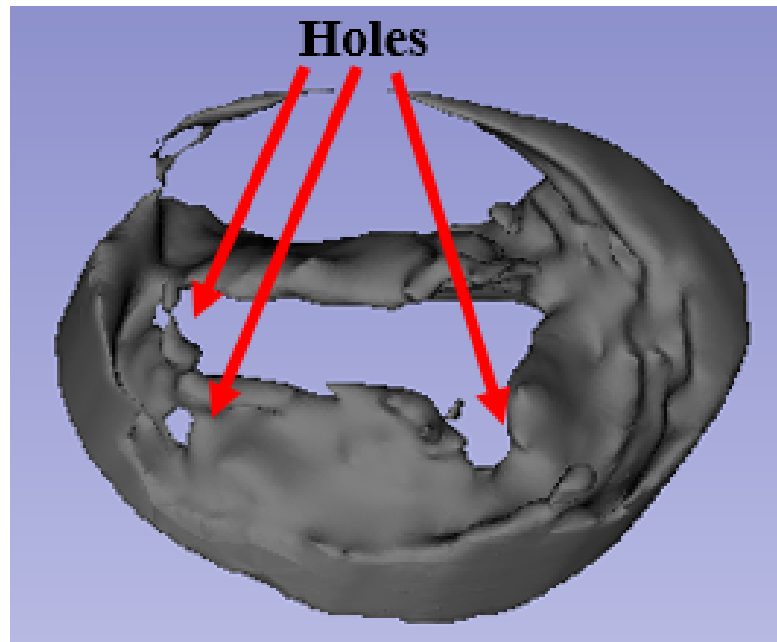
Figure 1.20: Volume rendering of TEE segmentation with holes due to regions of signal dropout
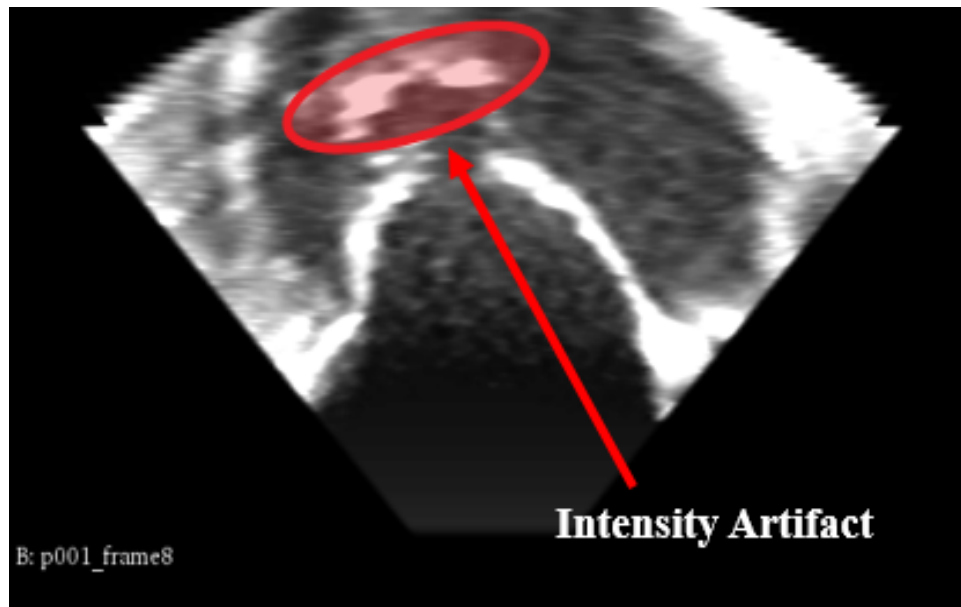
Figure 1.21: Intensity artifact in TEE image often misconstrued as valve tissue

will be beneficial for diagnosis, modelling and pre-, intra- and post-operative evaluation of valve function.

1.9   Summary

Given the high, interpersonal variability of mitral valve tissue, patients affected with MVD and subsequent regurgitation each have a unique path from diagnosis to intervention and recovery. Decisions in mitral valve disease management rely heavily on non-invasive imaging. Echocardiography, specifically acquired with a transesophageal probe, is considered the standard-of-care for diagnosis, intervention planning and guidance, and post-operative assessment. In most cases, TEE imaging is sufficient for identifying pathology and underlying causes of regurgitation. However, due to limitations such as signal dropout, artifacts, limited resolution and operator-dependence for image interpretation, the diagnostic value of TEE is often impacted. As well, due to the high volume of elderly patients unable to undergo invasive, open heart surgery for valve repair or replacement, new tools and techniques have been developed for image-guided, beating-heart approaches. For these new procedures, patient-specific models have an essential role in training clinicians and validating new devices for guidance and surgery. These models rely on segmentation of the mitral valve from a TEE, which has its own set of challenges. It remains unknown whether intensity-based segmentation methods are accurately and reliably delineating the mitral valve complex from TEE images.

Due to advancements and recent developments in imaging modalities, there is an increasing ability for clinicians to acquire a complete understanding of their patients intricate, dynamic anatomy. Dynamic computed tomography (4D-CT) is emerging as a valuable tool for both diagnosis and assessment of cardiac diseases. However, it is virtually unknown how this modality would perform for mitral valve imaging. Before initiating animal or patient studies, a proof-of-concept phantom study is needed to identify and quantify the abilities of the 4D-CT for mitral valve imaging.

With the widespread use of relatively inexpensive rapid prototyping techniques, simulators modelled off of patient anatomy are widely available. For minimally-invasive cardiac surgery, this application of modelling is particularly important, as clinicians are required to operate on a beating heart, without a direct line of sight into the area of interest. As well, for valve repair and replacement procedures, pathologic patient anatomy is highly variable as no two valves function or fail by the same mechanism. With mechanically-controlled motion and deformations, physical cardiac phantoms provide a platform for developing image-guidance and image-processing techniques. The first step to any patient-specific modelling pipeline is segmentation of diagnostic imaging, and in the case of mitral valve disease, segmenting

a patients TEE. Segmentation is also used for pre-operative quantitative analysis to inform subsequent interventions and treatment. However, intensity-based segmentation methods of the mitral valve from TEE images must be validated and assessed for their accuracy to delineate valve leaflets, used to create simulators.

The potential benefits and challenges of dynamic, 4D-CT for mitral valve imaging are the motivations for this work. We investigate and evaluate how reliably dynamic CT captures the morphology and behavior of the mitral valve in a beating heart. As well, we explore how mitral valve movement in dynamic CT might degrade image quality or introduce artifacts. Finally, we use a dynamically-acquired set of CT images from both silicone and bovine phantoms as ground truth in a comparative study with simultaneous TEE imaging.

1.10   Objective 1

1.10.1   How accurately does dynamic CT capture mitral valve morphology and dynamics?

At the outset of this research, it was largely unknown how dynamic, 4D-CT of the mitral valve with the GE Revolution scanner would capture valve morphology and function. With evidence of limitations of TEE for diagnosis, intra-operative guidance and patient-specific modelling of complex MVD cases, the first objective of this thesis was to evaluate 4D-CT capability of imaging the valve complex under physiologic conditions. To address this, we created a quasi-static phantom with both silicone and bovine valves to mimic normal valve motion patterns and be arrested at precise cardiac phases. The methodology and results of this proof-of-concept, phantom study are presented in Chapter 2.

1.11   Objective 2

1.11.1   How accurately does transesophageal echocardiography identify the mitral valve?

With the phantom construction and results from Chapter 2, the focus of validation could return to the realm of TEE and patient-specific modelling. The second objective of this thesis was to use both statically- and dynamically-acquired images of silicone and iodine-stained bovine mitral valve phantoms to serve as ground truth for comparison to simultaneously-acquired TEE images. The motivations for this project are the limitations and ambiguity of TEE mitral valve segmentation, which has an important role in quantitative assessment of valve function pre- and

post-operatively as well as in patient-specific modelling. Our primary goal was to demonstrate how accurately and reliably an intensity-based segmentation of a mitral valve from a TEE image actually delineates the valve complex. The results and statistical analysis from these experiments are reported in Chapter 3.

1.12   Thesis Outline

The chapters are as follows:

- *Chapter 2* develops the construction of a quasi-static, silicone and bovine valve phantom for construction of a ground truth dataset to validate 4D dynamic CT with mitral valve imaging.

- *Chapter 3* presents the results from a study using a CT ground truth dataset to validate TEE for mitral valve imaging and segmentation, as used in patient-specific models.

- *Chapter 4* provides a detailed discussion of the work from Chapters 2 and 3 in addition to outlining the future directions of this research.

Each chapter is prefaced with an additional introduction illustrating recent work similar to the topic at hand.

Chapter 2

Accuracy of mitral valve imaging in dynamic 4D-CT

This chapter is largely based on the podium presentation:

- "Accuracy of mitral valve imaging in dynamic CT" in the session on Advanced Imaging for the Heart and Heart Valves at Computer Assisted Radiology and Surgery (CARS), June 2018 in Berlin, Germany

2.1 Introduction

With the significant increase in life expectancy over the past century, valvular heart disease (VHD) has been identified as the next cardiac epidemic. A recent study estimates that prevalence of VHD to be 2.5%, progressively increasing with age up to 13.2% at 75 years of age [5]. Transesophageal echocardiography is widely recognized as the standard of care evaluation technique to diagnose mitral valve diseae. In most cases, TEE imaging is adequate for identifying pathology, however due to limitations such as signal dropout, limited resolution and user-variability in interpreting images, the diagnostic value of TEE is often limited. TEE images are unable to capture subvalvular anatomy and for some patients, the cause of regurgitation is ambiguous and remains unknown. As a result, pre-operative planning is limited and the surgical outcome is affected. For inter-operative TEE-guidance with mitral valve repair, the modality is often unable to provide a comprehensive view of the underlying valve disfunction, such that there are nontrivial rates of post-operative, reccurent regurgitation [4]. Conversely, the use of dynamic 4D-CT to capture a complete picture of the valve and subvalvular apparatus could enable surgeons to personalize their approach to intervention and reduce the rate

of recurring MVR. In addition, the emerging availability of beating-heart valve replacements necessitates pre-operative stent sizing. TEE cannot provide accuate volumetric data which is used to pre-operatively size neochordae and valve stents for beating heart replacements. As well, post-processing of TEE images for further analysis or patient-specific modelling is limited by signal dropout, artifacts and ambiguity of high-intensity regions. These factors motivate the use of 4D-CT to augment TEE in the clinical workup of MVD for quantification of patient anatomy. Dynamic cardiac computed tomography is emerging as a valuable tool for diagnosis and assessment of cardiac disease. However, application of dynamic CT to mitral valve imaging is particularly challenging due to the large and rapid motion of the mitral valve leaflets. Therefore, it is important to investigate the level of precision with which dynamic CT captures mitral valve morphology throughout the cardiac cycle. CT has the potential to provide a high quality rendering of the mitral valve apparatus and subvalvular anatomy, which is lacking in other cardiac imaging modalities. In this work, we propose a method to assess the accuracy of dynamic CT imaging of the mitral valave, validated through comparison with a static but adjustable ground truth phantom. Outcomes of this study will assist in evaluating the potential of dynamic CT as an effective tool in mitral valve applications. The results from this work can inform the use of dynamic CT in the clinical workflow for diagnosis and intervention of patients with mitral valve disease–, as well as assess the efficacy of transesophageal ultrasound for accurately capturing valve morphology and dynamic motion.

The main objective of this chapter is to take the initial steps to evaluate the reliability of dynamic CT for imaging the mitral valve under laboratory conditions in a custom-made, beating mitral valve model as well as a bovine valve. To achieve this objective, we evaluate dynamic CT against static CT that was treated as ground truth. To design the study, we first developed the phantom and methodology of acquiring synchronized data with static and dynamic CT to perform a quantitative analysis based on acquired volumetric data and a qualitative assessment of motion artifacts introduced in the dynamic scan.

2.2 Methods

2.2.1 Overview

The morphology and behavior of the mitral valve is dependent on hemodynamics, which cannot easily be replicated in a static environment. To address this, we designed and constructed a quasi-static valvular model, which mimics normal mitral valve morphology and motion patterns, but can be arrested at precise cardiac phases. This motorized phantom simulated valve movements over one complete cardiac cycle, from systole to systole. Valve motion was

achieved by cyclical adjustment of the chordae tendinae, operated by two Arduino-controlled servomotors. To assess the accuracy of gated, dynamically-acquired mitral valve images, we arrested the quasi-static valve model at distinct points in the cardic cycle which we compared with phase-matched, dynamic images. CT images of the silicone valve were acquired in air, both with the valve in motion and at predefined static positions. CT images of the bovine valve were acquired in water.

2.2.2 Phantom Design and Construction

Physical Design

After many iterations of modulating the physical design, an orientation was selected which both optimized the physiologically-accurate valve motion pattern and enabled the system to be imaged in water with both CT and ultrasound for the validation study in Chapter 3. The final design consisted of a translucent, plastic container with physical dimensions 21 x 16 x 12 cm, volume of 3L and wall thickness of 1cm. All electronics were mounted either outside of, or atop the walls of the container in order to avoid contact with water during the simultaneous CT-TEE validation study (Chapter 3). A custom-designed valve stand with six screw holes (tapped during post-processing) was modelled in SpaceClaim (http://www.spaceclaim.com/en/default.aspx) to fit the dimensions of a mitral valve annulus, and at an angle that mimics a patient lying supine. The Stereolithography (STL), Computer-Aided Design (CAD) file for the valve stand was converted to G-code with Ultimaker's software Cura 3.3 (https://ultimaker.com/) and 3D-printed with polylactic acid (PLA) on an Ultimaker 3 Extended 3D-printer. After construction, the stand was cemented to the base of the container in a location which allowed TEE probe access from the esophageal side of the valve. A flange made of Smooth-on Dragon Skin^{TM} silicone (https://www.smooth-on.com/product-line/dragon-skin/) cured into a custom-made, 3D-printed circular mold with six screw holes, a diameter of 11cm and thickness of 2mm was prepared to support the valve phantoms (silicone and bovine, whose preparation is described in subsequent sections). The flange was fitted on the valve stand and the holes in the silicone aligned to the stand screw holes. A ring-shaped, 3D-printed component with an outer diameter of 11 cm, inner diameter of 5.5 cm and thickness of 0.5 cm and six evenly-spaced, tapped screw holes (for 10-24 1/2" screws) was constructed to secure and immobilize the silicone flange and valve phantom to the 3D-printed stand (Figure 2.1, purple component). Strategically-placed along the top of the container walls were four customized (modelled in SpaceClaim), 3D-printed cylindrical pulleys which rotate around the centroidal axis. Two servomotors (HiTEC, https://www.hitecrcd.com, HS-625MG) were screwed into custom-designed (SpaceClaim) holders and attached to atop the walls on either side of the container.

These were deliberately placed behind the valve (with no parts of the motor overlapping the field of view for imaging studies) in order to avoid streaking artifacts from CT of metal components, which corrupted images acquired with previous phantom prototypes. The output shafts of both servomotors were fitted with custom-designed (SpaceClaim), 3D-printed lever arm which extends 3cm outwards from the center of the rotating servomotor shaft. A 2cm long, 1/4" screw was threaded vertically into the far end of the lever arm, making a radial sweep from 0° to 180° when the servomotor is operated.

Silicone Mitral Valve Phantom Preparation

Two types of dynamic mitral valve phantoms were designed in our study. The first was a proof-of-concept, Dragon Skin^{TM} silicone valve which was constructed following the patient-specific valve modelling workflow outlined in Chapter 1, Figure 1.18. Attenuation and speed of sound concerns usually make silicone a sub-optimal media for ultrasound phantoms. However, the anatomical structure of interest in this phantom (the mitral valve) is rarely more than 2mm thick, which greatly minimizes the adverse effects of attenuation and speed of sound discrepancies between the ultrasound probe and simulated tissue. First, images were acquired from a diagnostic, dynamic 3D TEE of a patient with mitral valve regurgitation. Next, the mitral valve was segmented with both automatic and manual techniques from the valve position during diastole (ventricular filling, leaflets are open), since the two leaflets cannot be distinguished from the systolic view of the valve with TEE. A volume rendering was completed in SpaceClaim to generate a CAD model of the valve. From there, the CAD model was converted to G-code using Cura software and the positive valve mold was 3D-printed with PLA filament using the Ultimaker 3 Extended 3D printer. Chords were prepared by taking four thin strings, and fraying the ends that would rest against the silicone leaflet. To construct the valve, we mixed Smooth-on Dragon Skin^{TM} silicone, known for its strength and stiffness which is advantageous for the design constraint of the valve phantom being arrested and immobilized at a specific, repeatable position for static ground truth creation. We placed the patient-specific, 3D-printed positive mold inside the circular flange mold and poured the silicone. We then positioned the frayed ends of the string-chords along the 3D-printed mold of the leaflets and painted silicone with a brush overtop of the strings to cover the leafelts. Next, the silicone-filled flange and valve mold apparatus was inserted into a rotating curing device consisting of an Arduino-controlled servomotor which ensured evenly spread silicone throughout the mold [24]. Once cured, the silicone flange was screwed onto the stand (as outlined in the previous section). The string-chordae cured within the silicone leaflets were positioned around the pulleys and secured to the screw on the lever arm attached to the rotating shaft of the servomotors. The Arduino-controlled servomotor-and-pulley system adujsted the chordae and which precisely controlled

their position to simulate a realistic systolic-to-diastolic valve motion pattern over a range of heart rates (details provided in the next subsection). The silicone valve phantom (Figure 2.1) has the advantage of an indefinite shelf life, and excellent CT image quality.

Figure 2.1: Silicone valve closed at peak systole and flange secured in 3D-printed stand mimicking patient lying supine with chords connected to pulleys and servomotors in the Arduino-controlled motorized valve manipulator. Servomotors both at 0° angle position.

Bovine Valve Phantom Preparation

For more realistic valvular anatomy, we performed experiments with a bovine valve. To prepare this phantom, we assembled and replicated the physical design previously described for the silicone valve phantom. We acquired another container which could accomodate the modular pulleys and servomotor stand attachments since the dimensions were identical. Next, we created a second Dragon Flex silicone flange (using the same 3D-printed mold as the flange for the silicone valve phantom), adding a layer of mesh to the mold before pouring silicone in order to facilitate sutures of the bovine valve. An entire bovine heart was procured from a local abbatoir and dissected down to preserve the mitral valve leaflets, chordae and papillary muscles. Next, the bovine valve annulus was sutured to the silicone flange. Any silicone which was cured over the region of the leaflets was cut away. Strings (identical to the strings used as chordae in the silicone valve model) were then sutured into the papillary muscles. This enabled the bovine valve phantom to be inserted into and actuated by the Arduino-controlled motorized valve manipulator (described in the next subsection). One week before the date of the imaging study, a Lugol's iodine stock solution was prepared. For ten hours prior to scanning, the sutured bovine valve was immersed in a diluted volume of this stock solution to increase tissue contrast in CT, following a protocol for iodine-staining of biological tissue for CT imaging [16]. The workflow for bovine valve preparation is presented in Figure 2.2. During the 7 days between bovine heart acquisition and imaging, the tissue was sealed and stored in a refrigerator at 0°C. Once assembled with the physical design, the container was filled with water, submering the stained bovine valve. This introduced hydrodynamics and ensured compatibility of the bovine phantom with both CT and TEE imaging. The bovine valve was used primarily for a qualitative analysis of image quality. This configuration is compatible for imaging in both air and water to for the study with simultaneous TEE imaging for validation, as presented in Chapter 3.
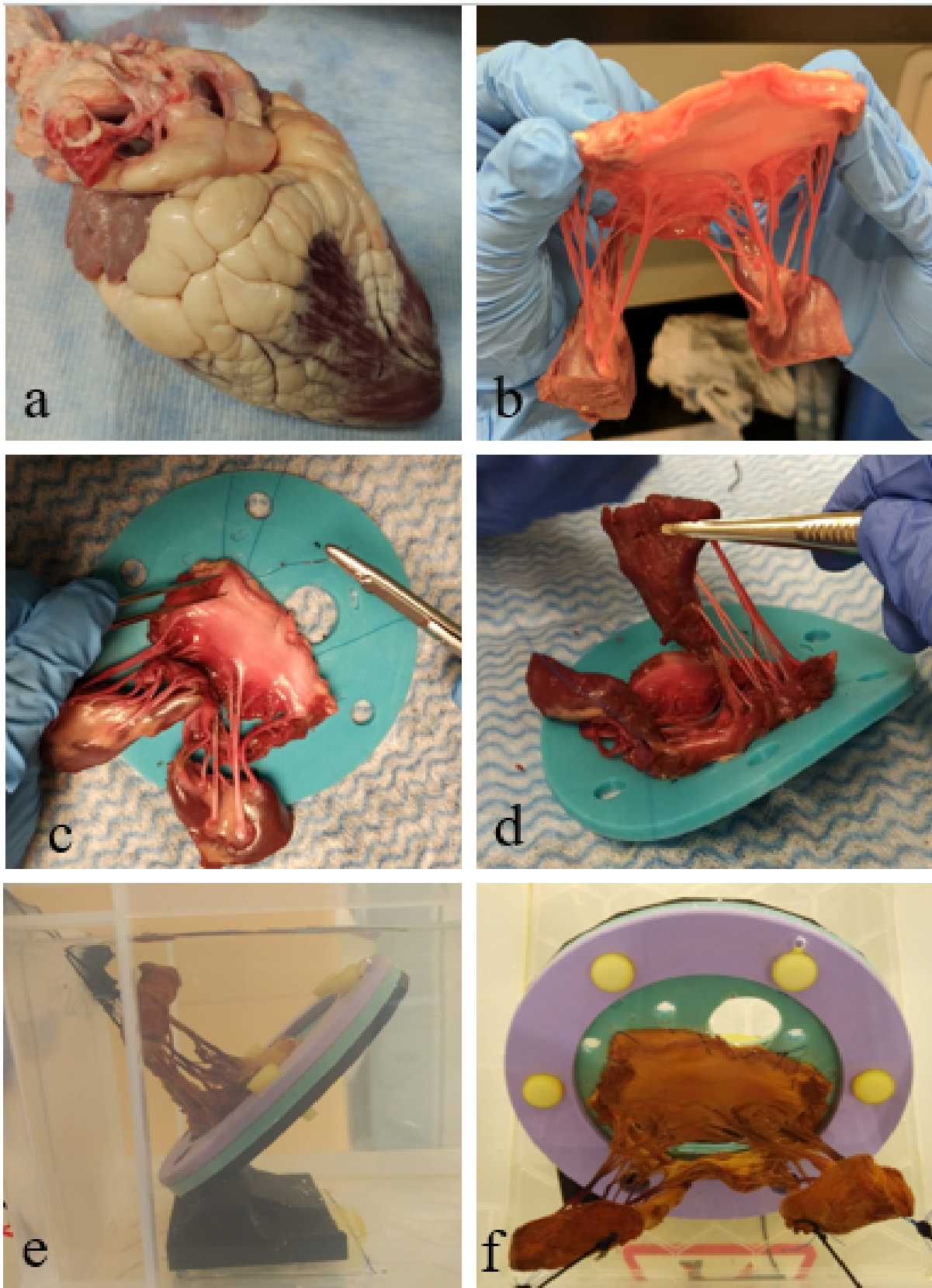
Figure 2.2: Preparation of the stained bovine mitral valve phantom (a) entire bovine heart (b) dissected mitral valve leaflets, chordae and papillary muscles (c) annulus sutured to silicone flange (d) papillary muscles sutured to strings (e) side view of stained valve submerged in water (f) apical view of the stained bovine valve with strings sutured in the papillary muscles

Motorized Valve Manipulator

We constructed a motorized system that provides repeatable, ECG-gated, realistic valve movements over a complete cardiac cycle. The apparatus comprises two Arduino-controlled (https://www.arduino.cc) servomotors (HiTEC, https://www.hitecrcd.com, HS-625MG), strategically positioned pulleys for adjusting the papillary muscles, and chordae to open the valve leaflets. The first prototype of the motorized valve manipulator consisted of two Faulhaber motors and incremental encoders (2224U012SR, https://www.faulhaber.com/en/home/) used to manipulate the leaflet positions. However, due to the limited capabilities of the motion manager software for imaging off-site, we decided to revist motor options for the second prototype. For the second iteration, servomotors were selected over Direct Current (DC) motors to ensure precise control of the quasi-static valve model by modulating their angular position. The unmodified servos used for this system have a fixed range of rotation from 0° to 180° and control is achieved by sending a pulse of a particular length and duration to reach the desired position. The Adafruit Motor Shield v2.3 (https://www.adafruit.com/) was soldered, assembled and interfaced with the Arduino to utilize the built-in servo command library for streamlined position control. Servos typically draw more current than the Arduino can supply, so we added a 24V external power supply to run the motors [7].

The system mimics the full range of cardiac motion from diastole to systole. For heart rates below 80 bpm (around most resting heart rates), the length of one cardiac cycle is approximately into the two phases as follows: one-third of the time in systole and two-thirds in diastole [58]. For higher heart rates (greater than 80 bpm), the proportion of time spent in diastole shortens as ventricular filling occurs over less time. This translates to mitral valve motion which is gradual opening (diastole) and fast closing (systole), where the valve "snaps shut". The motorized valve manipulator was programmed to operate at 30, 60 and 90 bpm. In order to modulate the valve leaflets similar to their motion pattern *in vivo*, the four chords were paired (one attached to each leaflet) and wrapped around the pulleys and attached to the lever arm on the end of both servomotors. Initially in the position corresponding to 0° (the systole phase, leaflets are closed, Figure 2.1), as the servomotors rotate clockwise to 90°, the lever arm pulls the chords which subsequently open the leaflets. When the servomotors reach 90°, the valve is in full diastole (leaflets are open, ventricular filling occurs, Figure 2.3).
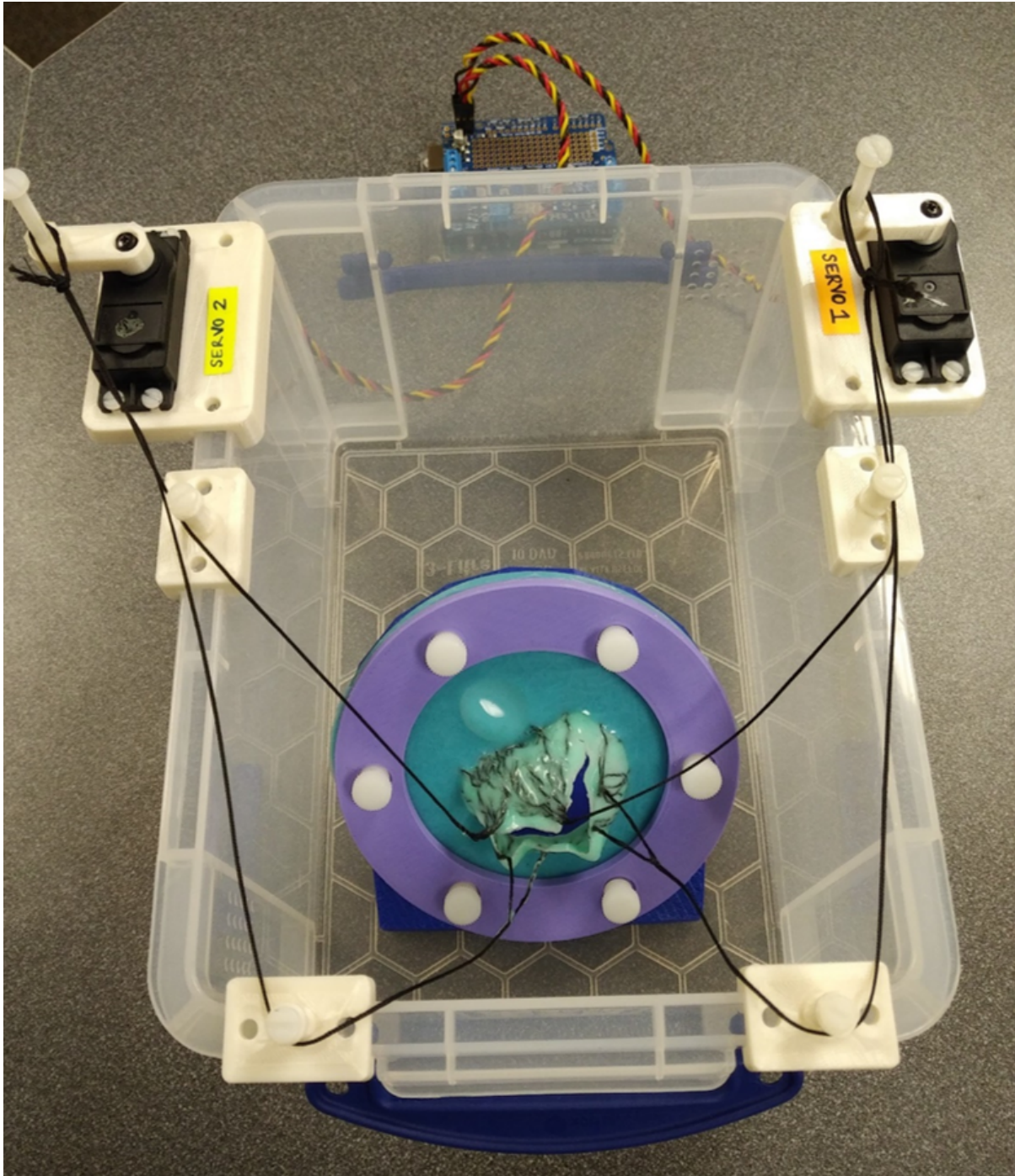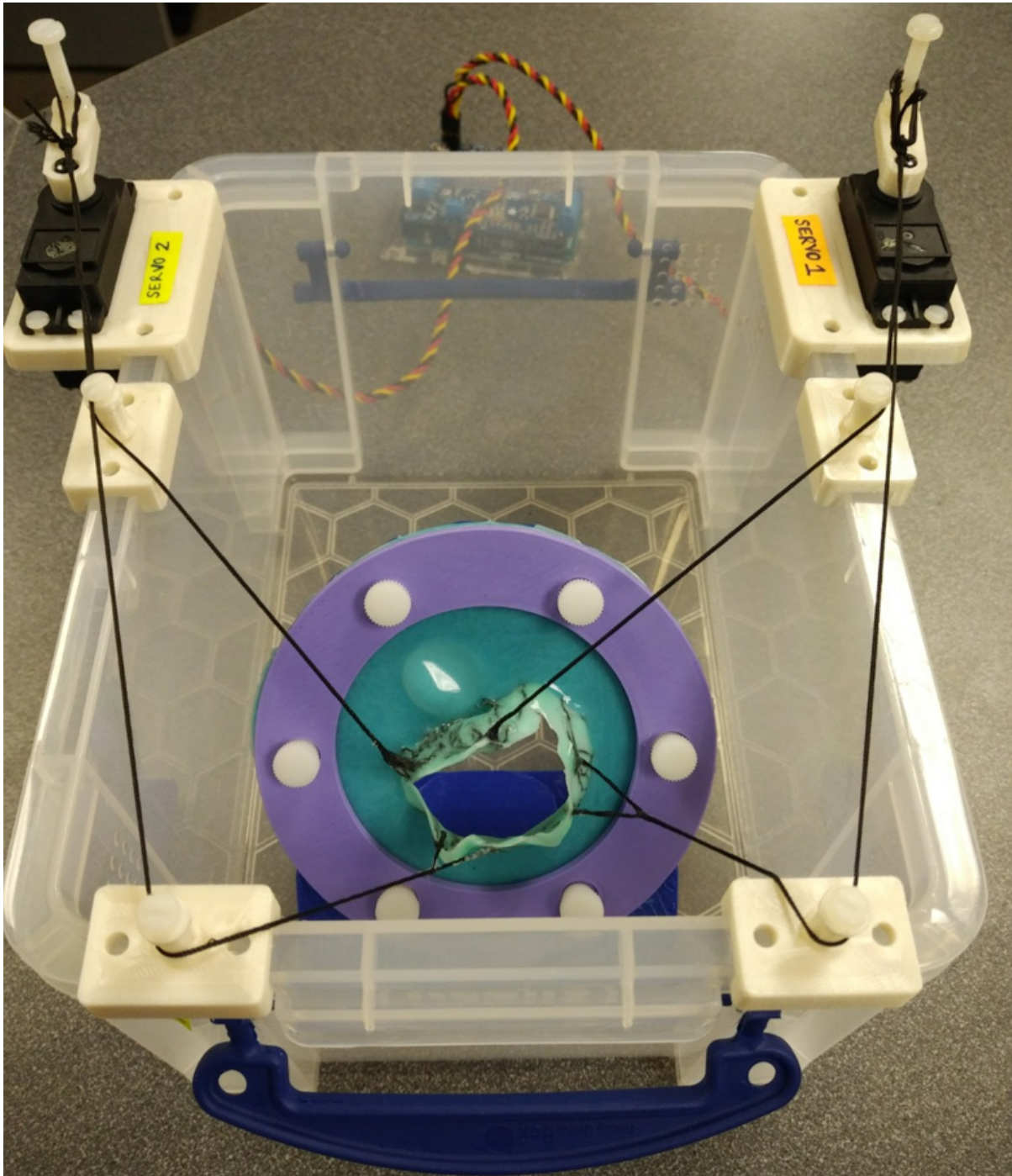
Figure 2.3: Silicone valve open at peak diastole and flange secured in 3D-printed stand mimicking patient lying supine with chords connected to pulleys and servomotors in the Arduino-controlled motorized valve manipulator. Servomotors both at 90° angle position.

For 30 and 60 bpm, the period or length of the cardiac cycle is 2s and 1s, respectively with 2/3rd of the period in diastole and 1/3rd of the cycle in systole. For 90 bpm, the period of the cardiac cycle is 0.667s and the ratio between length of diastole and systole decreases to roughly 3/5th and 2/5th, respectively [18]. The parameters used to program the servomotors and the Adafruit shield were the cardiac cycle length (or period) and the fraction of time spent in diastole and systole. Valve motion was modulated by the servomotor-controlled lever arms rotating from 0° to 90° continuously over the length of diastole (valve leaflets opening) and from 90° to 0° rapidly over the length of systole (valve leaflets snapping shut). The angular position and speed of the servomotors were controlled using the pos() and microseconds() commands built-in with the servos library. The millis() command was used to keep track of time in lieu of the delay() command, which is a global blocking function. For dynamic scans, the motors operate continuously to mimic valve movement at either 30, 60 or 90 bpm As the motorized valve manipulator was operated, the string-chordae were adjusted to simulate a realistic systolic-to-diastolic valve motion pattern.

The final design constraint for the motorized valve manipulator is precise, repeatable arresting of the valve phantoms at specific time points. This function is necessary for constructing the static ground truth images which are compared to the phase-matched images acquired during the dynamic, continuous scan to determine the accuracy of the 4D-CT for dynamic mitral valve motion. The six time points selected for static imaging (corresponding to the cardiac cycle and ECG wave, Figure 2.4) were chosen according to stages of transition or movement of the valve from one position to another. The time points span the R-R interval, and correspond to precise servomotor angular positions which arrest the valve leaflets in particular positions. With the anglular positions controlled in the static scans, we were able to correlate the static volumes to the phase-matched volume acquired in the continuous, dynamic scan for 30, 60 and 90 bpm.

ECG Gating

ECG gating was used to phase-match the dynamic and static scans, acquired retrospectively. An output gating signal (5V, 32ms square wave) from the Adafruit Motor Shield coinciding with the R-wave of the cardiac cycle of the motorized valve manipulator connects to a commerically-available Passive ECG Adapter (Model PI-ECG1 ver 1.3 PROT, Shelley Medical Imaging Technologies, London ON,
http://www.simutec.com/) with a Bayonet Neill-Concelman (BNC) cable. This device converts the 5V square wave to a real QRS complex which is recognized by both the Revolution CT and Philips iE33 TEE machine, analgous to ECG-gating for patient scans. With gated acquisition of dynamic images, we could conduct phase-matching between static and dynamic scans.
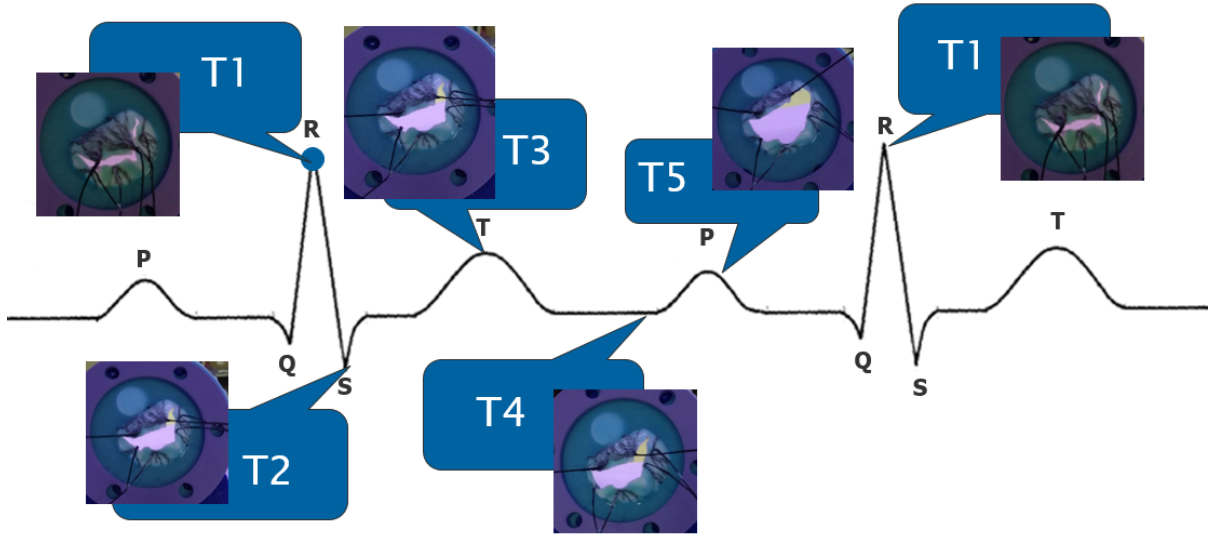
Figure 2.4: ECG wave with six corresponding time points selected for static ground truth images and photos of the valve leaflet orientation at each position

Overall, this methodology provided us with two quasi-static phantoms for TEE and CT image collection of both static and dynamic scenarios. From this we conducted two imaging studies: (1) an analysis of the 4D-CT for capturing the mitral valve motion, with comparison between dynamic and static, ground truth scans and (2) validation of TEE for mitral valve imaging with simultaneous CT and TEE image acquisition, with the CT datasets used a ground truth for comparison.

2.2.3 Image Acquisition

To provide ground-truth images, this phantom can be arrested at distinct points over the cycle for comparison with a continuous, dynamic scan from both CT and ultrasound. For both the silicone and bovine valve phantoms, 4DCT data were acquired with parameters appropriate for maximum temporal resolution and image quality. The static ground truth dataset was acquired first, followed by a continuous, restrospective scan of two dynamic cardiac cycles. The silicone phantom was first imaged (static and dynamic) in air, and then the container was filled with water for a second set of scans. The stained bovine valve was submerged in water for the entire length of the scanning. In preparation for the TEE validation study performed in Chapter 3, simultaneous TEE and CT images were acquired of both the silicone and bovine valves. All of the 3D TEE scans were acquired using a Philips iE33 (Philips, Amsterdam, NL), using the X7-2t transesophageal probe. Three strategically placed holes on opposite sides of the annulus served as fiducials that were visible in both CT and TEE for landmark-based registration. The 4D-CT scans were conducted on the GE Revolution Discovery multi-slice scanner (GE Medi-

cal Systems, Waukesha, WI) for the cardiac protocol in cine mode at a resolution of
512 x 512 x 1792 and the pixel spacing of 0.398 x 0.398 x 0.398mm. These data were acquired
with retrospective gating and the scan parameters were set as follows: 120 keV, 120 mA, 0.28 s
gantry rotation, 2.2 s length of scan and 0.625 mm slice thickness. Each image reconstruction
used data acquired from a full 360° rotation of the gantry. The experimental setup is depicted
in Figure 2.5.

Acquisition of ground-truth static dataset

To establish a ground truth dataset, we acquired static images at different phases of the cardiac
cycle. Over the R-R interval, the valve was adjusted by the motorized system and arrested
at six chosen time points before acquiring a static image in the dynamic CT scanner (Figure
2.4). To do this, the silicone mitral valve phantom attached to the motorized valve manipulator
was programmed to adjust the angular position of the servomotors to a predefined location and
arrest the valve in position for 5s. During the pause, a 3D-CT volume was acquired. Then the
lever arm was adjusted to the next angular position, and another image was acquired. This step
was repeated until six static CT images were acquired, corresponding to distinct points over
the cardiac cycle. Once completed, the motorized valve manipulator components were moved
to the container with the submerged bovine valve phantom and the scanning was repeated.

Acquisition of continuous, phase-matched, dynamic dataset

After acquisition of the static ground-truth images, the silicone phantom in air within the mo-
torized valve manipuator was actuated continuously. This enabled acquisition of 3 sequential
dynamic scans with uninterrupted, ECG-gated mitral valve movement at 30, 60 and 90 bpm,
respectively. Two cardiac cycles were imaged for each heart rate. The phases of the images
acquired throughout this dynamic sequence correspond to the same phases provided by the
quasi-static ground truth series. Next, the container was filled with water and three scans were
acquired at 30, 60 and 90 bpm. Upon completion, the components of the motorized valve ma-
nipulator were attached to the submerged, bovine mitral valve phantom and three cine mode
scans were acquired at 30, 60 and 90 bpm.

Acquisition of simultaneous TEE and CT datasets

To use the 4D-CT scans of the mitral valve phantoms as ground truth in the TEE validation
study, simultaneous imaging with TEE and CT was performed. First, the submerged silicone
valve phantom and motorized valve manipulator was placed within the CT gantry with a TEE
probe positioned and secured at the esophageal view. Dynamic scans at the three different heart

rates were acquired. The same protocol was repeated with the submerged, stained bovine valve phantom and motorized valve manipulator.
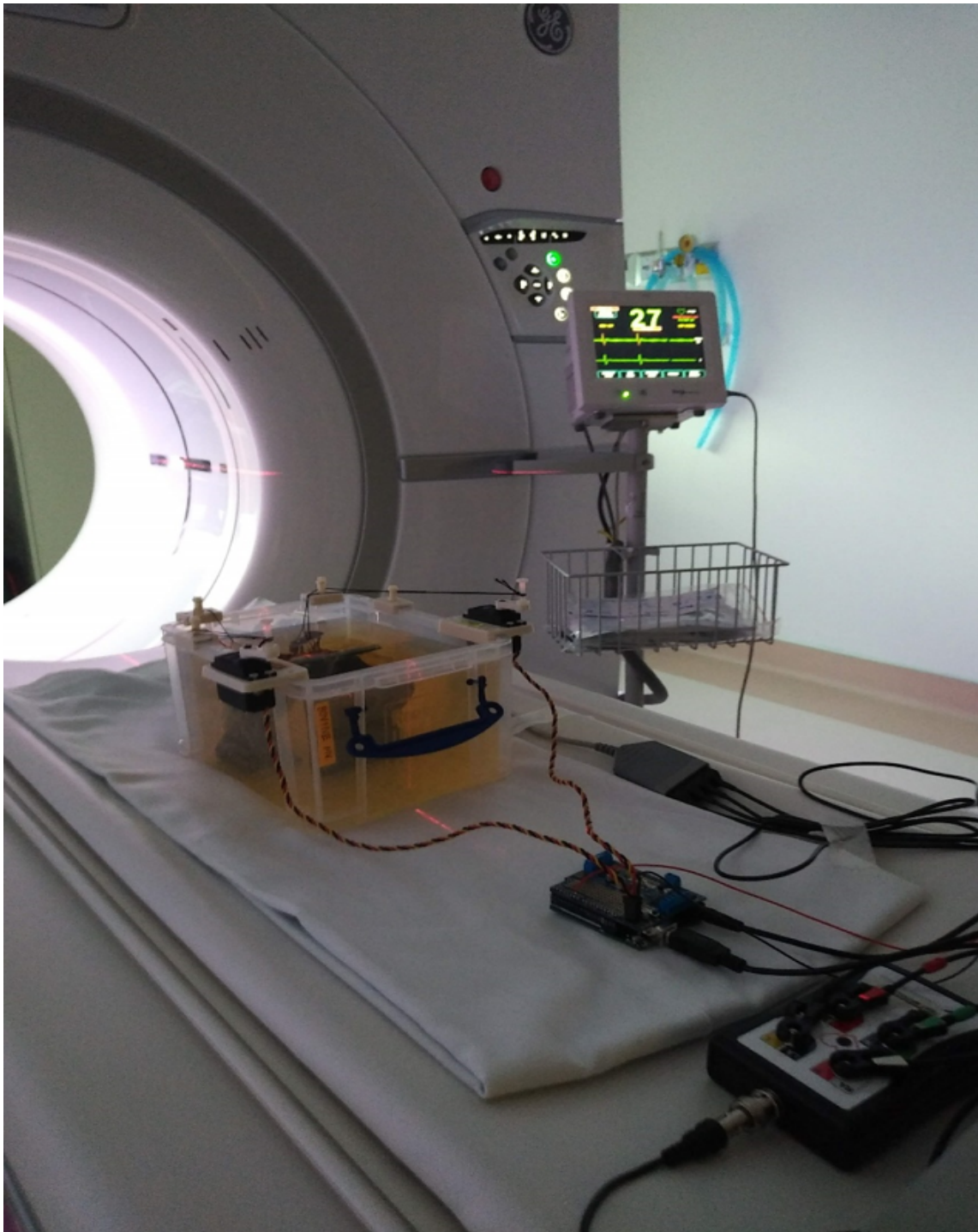
Figure 2.5: The GE Revolution Dynamic CT with the submerged, stained bovine valve in the scanner, Passive ECG Adapter device and the Arduino-controlled motorized valve manipulator

2.2.4   Image Processing and Analysis

After acquisition, the image data were processed for a quantitative assessment of the match between the static ground truth and the continuously-acquired scans. In addition, the image quality of the dynamic scans was evaluated for common CT artifacts such as streaking, and artifacts unique to 4D-CT such as duplicate, overlapping and incomplete structures.

Quantitative comparison and validation

For post-processing analysis, we applied the same pipeline to the three dynamically-acquired scans (with 30, 60 and 90 bpm heart rates) with the silicone mitral valve phantom imaged in air. The data from each scan was sorted and organized into six 3D volume pairs, matching the images based on the ECG-gating and angular rotation of the servomotors for each precise time-point. The six ground truth, static CT volumes were then aligned to the corresponding phase-matched dynamic CT scan at each time-point by homologous-point landmark-based registration in 3D Slicer 4.6.2 (https://www.slicer.org/). The fiducial landmarks used for this registration were the three 2mm-diameter holes punched around the silicone flange annulus. Next, both the anterior and posterior valve leaflets and chordae were segmented in MATLAB (https://www.mathworks.com/products/matlab.html) by continuous max flow [60] for each CT volume comprising the six phase-matched pairs for all three simulated heart rate scans. The segmented leaflets and chordae for each phase-matched pair were overlaid in CloudCompare (https://www.danielgm.net/cc/). This software platform was used to compute the mean Euclidean distance between the static and dynamic geometries for each time-point, in all three scans. The entire methodology for phantom assembly, image acquisition, image processing and analysis is presented in Figure 2.6.

Qualitative image artifacts

The second component of the analysis of dynamic 4D-CT for mitral valve imaging was a qualitative assessment of image quality and identification of any image artifacts that may corrupt the dyanmic datasets. These components were determined upon careful visual inspection of the 2D slices within a 3D CT volume from the original 4D-CT reconstruction of simulated 30, 60 and 90 bpm heart rates for both the silicone and bovine valves submerged in water. This experimental setup was chosen as the aqueous environment more closely matches human cardiac physiology than the silicone valve imaged in air.
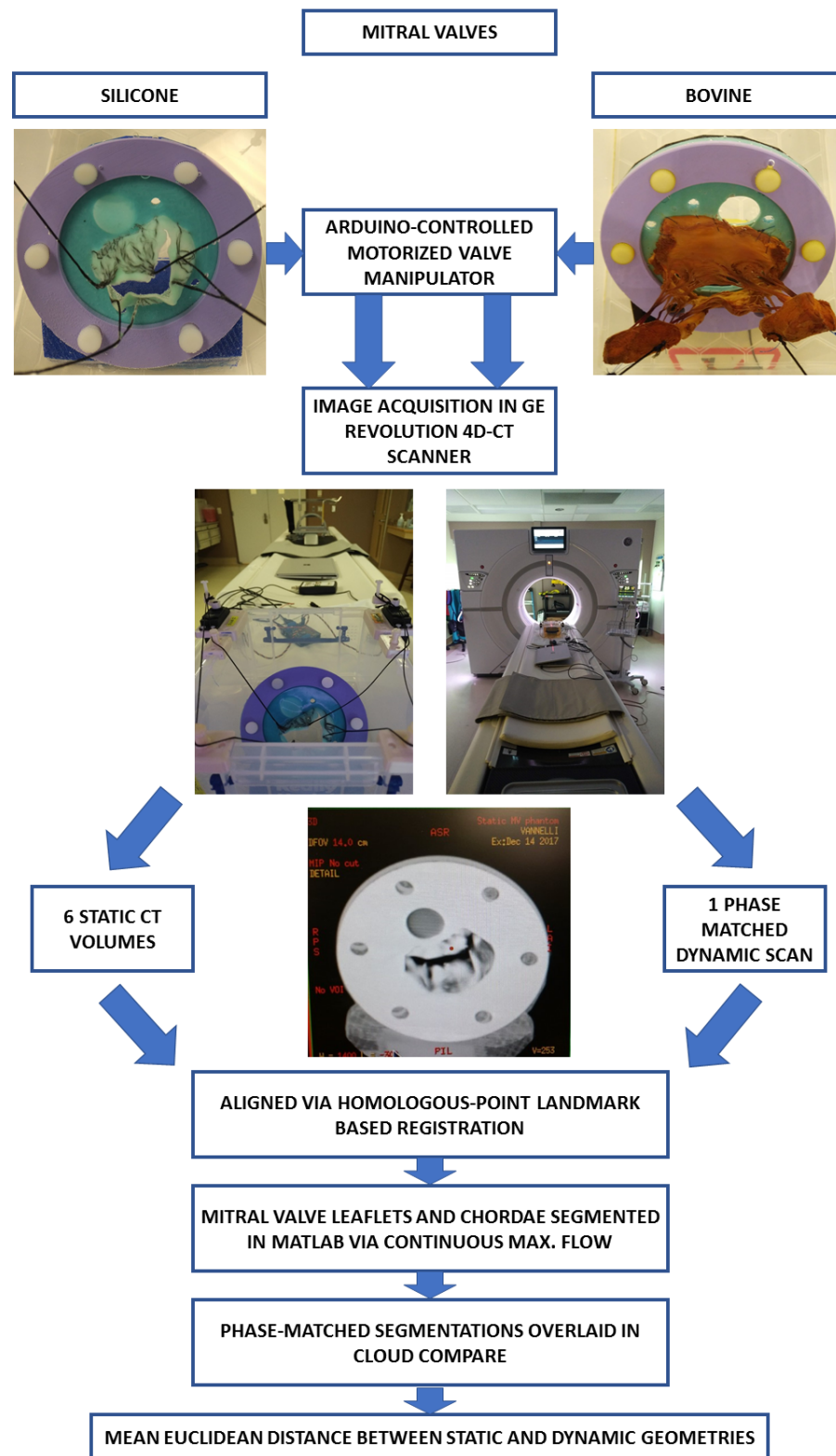
Figure 2.6: Workflow of methodology for silicone and bovine valve phantom assembley, image acquisiton, image processing and image anaylsis

2.3   Results

With this methodology, we constructed two mitral valve phantoms and a motorized valve manipulator which was capable of simulating realistic valve morphology over a range of heart rates. In addition, the valve phantoms could be arrested at distinct time-points over the cardiac cycle for construction of a static CT ground truth. These 3D volumes comprising the ground truth were compared with the corresponding dynamic volumes from the matching time-points, in order to determine the level of accuracy with which the dynamic CT captures mitral valve movement. We also assessed the dynamic valve phantom scans qualitatively, with a focus on motion artifacts which could corrupt or misconstrue structures within the images.

2.3.1   Quantitative comparison and validation

The phase-matched static and dynamic datasets were first aligned according to their corresponding time points. Figure 2.7 presents a side-by-side comparison between slice 656 (out of 1792 in the volume) of the silicone valve phantom, imaged in air and captured at time-point number four (Figure 2.4), with the valve in the pre-diastole position. Upon visual inspection there were some minor difference between the statically-aquired image (Figure 2.7a) and the image acquired dynamically with the motorized valve manipulator operating to simulate 60 bpm (Figure 2.7b). The differences were mainly localized to the positions of the chordae, since these structures have the largest and most rapid motion during the phantom cardiac cycle.
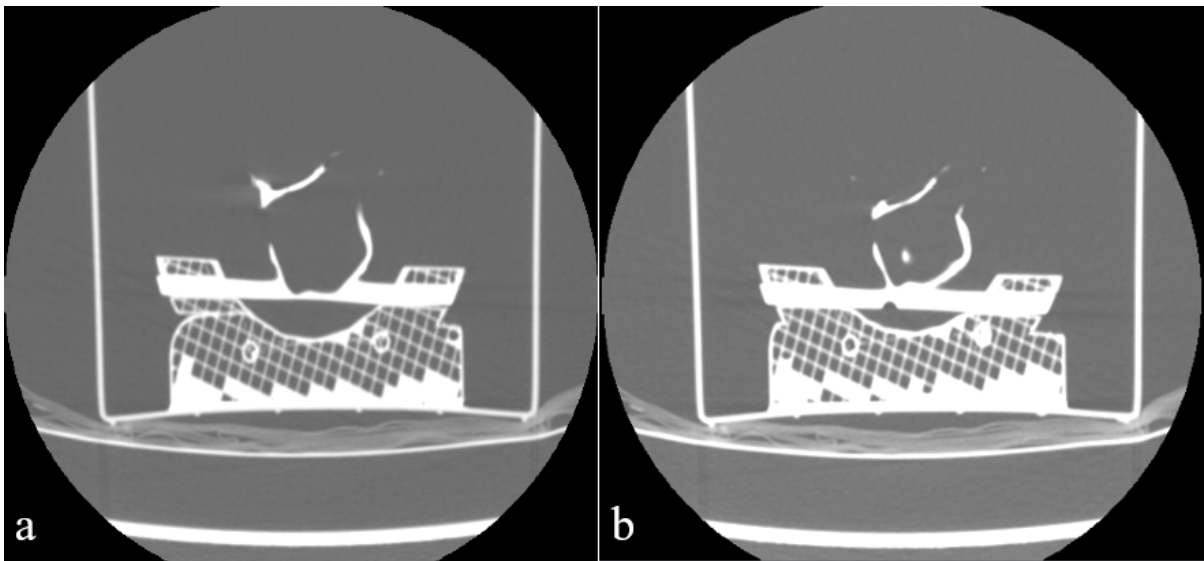
Figure 2.7: 2D slice (z = 656 out of 1792) through the leaflets of the silicone valve, imaged in air at 60 bpm captured at time-point 4 of the matched (a) static, ground truth dataset and (b) dynamic, continuously-acquired images

Our metric of quantitative comparison was the Mean Euclidean Distance (MED) computed between the phase-matched static and dynamic geometries in CloudCompare. This served as a metric of how accurately the continuous, dynamically-acquired scan captured the actual valve position at distinct points over the cardiac cycle. Generally, the MED for the 30, 60 and 90 bpm scans of silicone in air were relatively small, indicating that the continuous scan provides an accurate view of the valve in motion. For the higher heart rate of 90 bpm, the MED was larger than for slower movements at 30 and 60 bpm. The maximum MED between two phase-matched volumes at any of the six time points from the 90 bpm dataset was 3.55 mm, showing that the dynamically-acquired scan closely matches the corresponding ground truth. The regions of greatest difference between the static and dynamic volumes were predominately around the chordae (Figure 2.8).
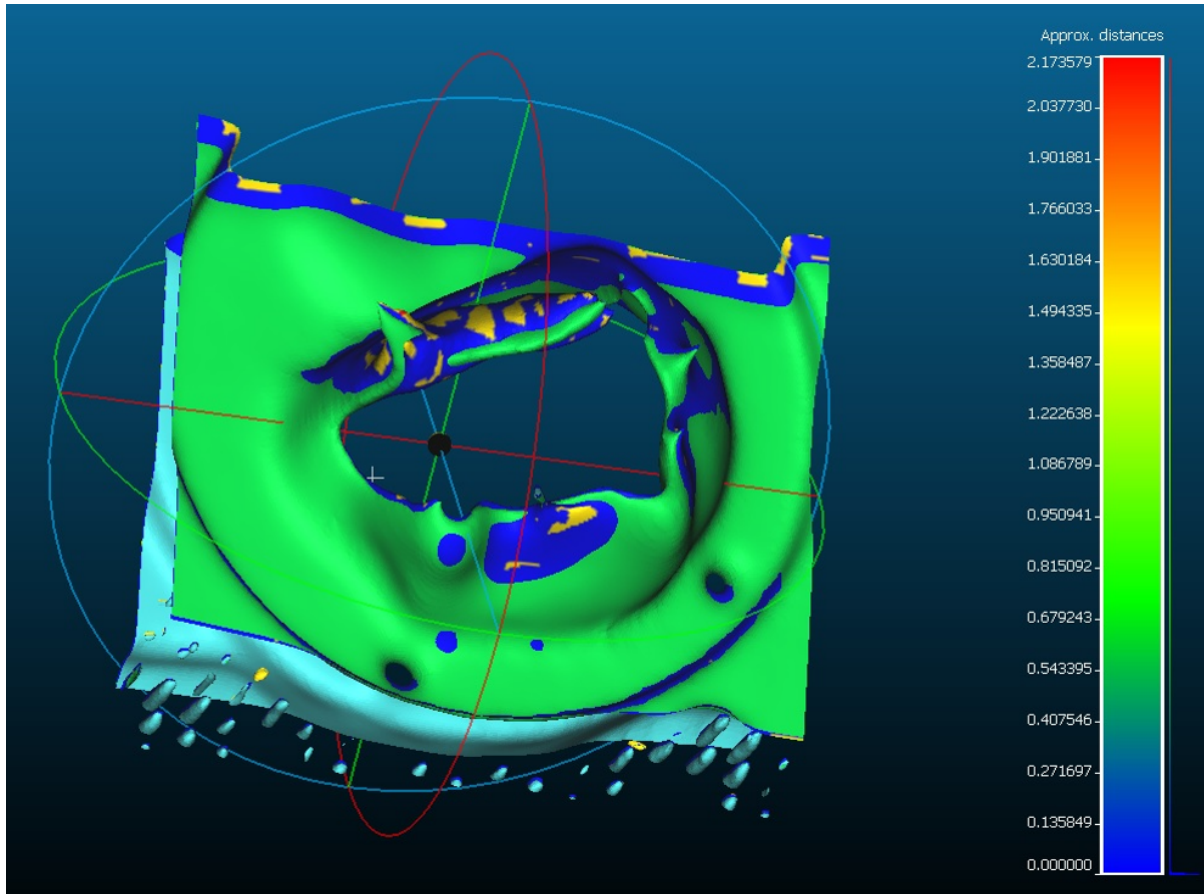
Figure 2.8: Distribution map of mean euclidean distance between phase-matched geometries segmented from static and dynamic scans of the silicone valve phantom imaged in air with simulated 60 bpm. The colour variation represents the increasing distance in mm between the two aligned geometries

2.3.2 Qualitative image artifacts

The second part of the analysis of the dynamic CT scans of the valve phantoms was a qualitative assessment of image artifacts. Overall, there was significant corruption of slices within 4D volumes acquired at 60 and 90 bpm due to motion artifacts. Most common was the duplicate structure artifact (Figure 2.9) where one or both of the leaflets appears twice on the image, making the correspondance to the actual leaflet position ambiguous. The general trend was that with larger and more rapid the motion of the valve leaflets and chordae (as simulated heart rates increased), the more prevalent motion artifacts appeared within the individual slices. In addition, the bovine valve presented a unique streaking artifact due to the stained papillary muscle motion (Figure 2.10).
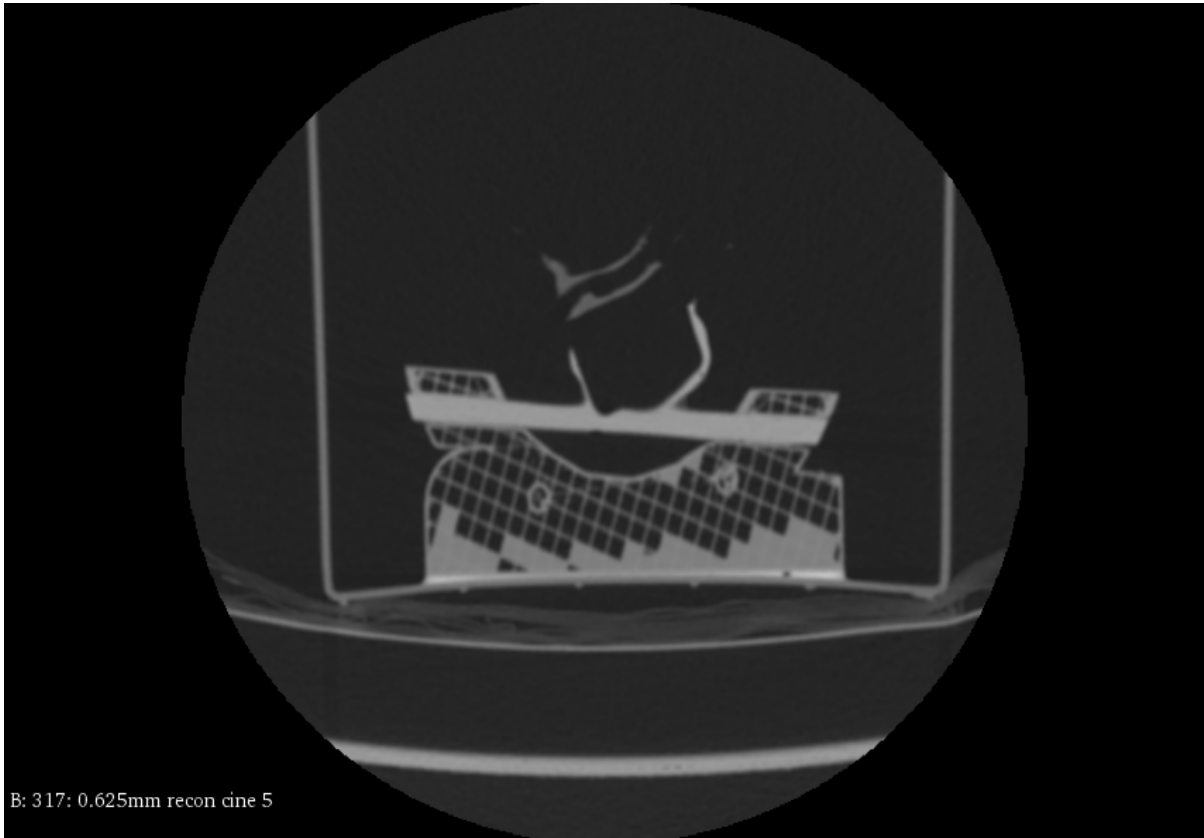
Figure 2.9: Example of duplicate leaflet structure image artifact found in one slice of 4D volume from dynamically-acquired scan of the silicone valve in air
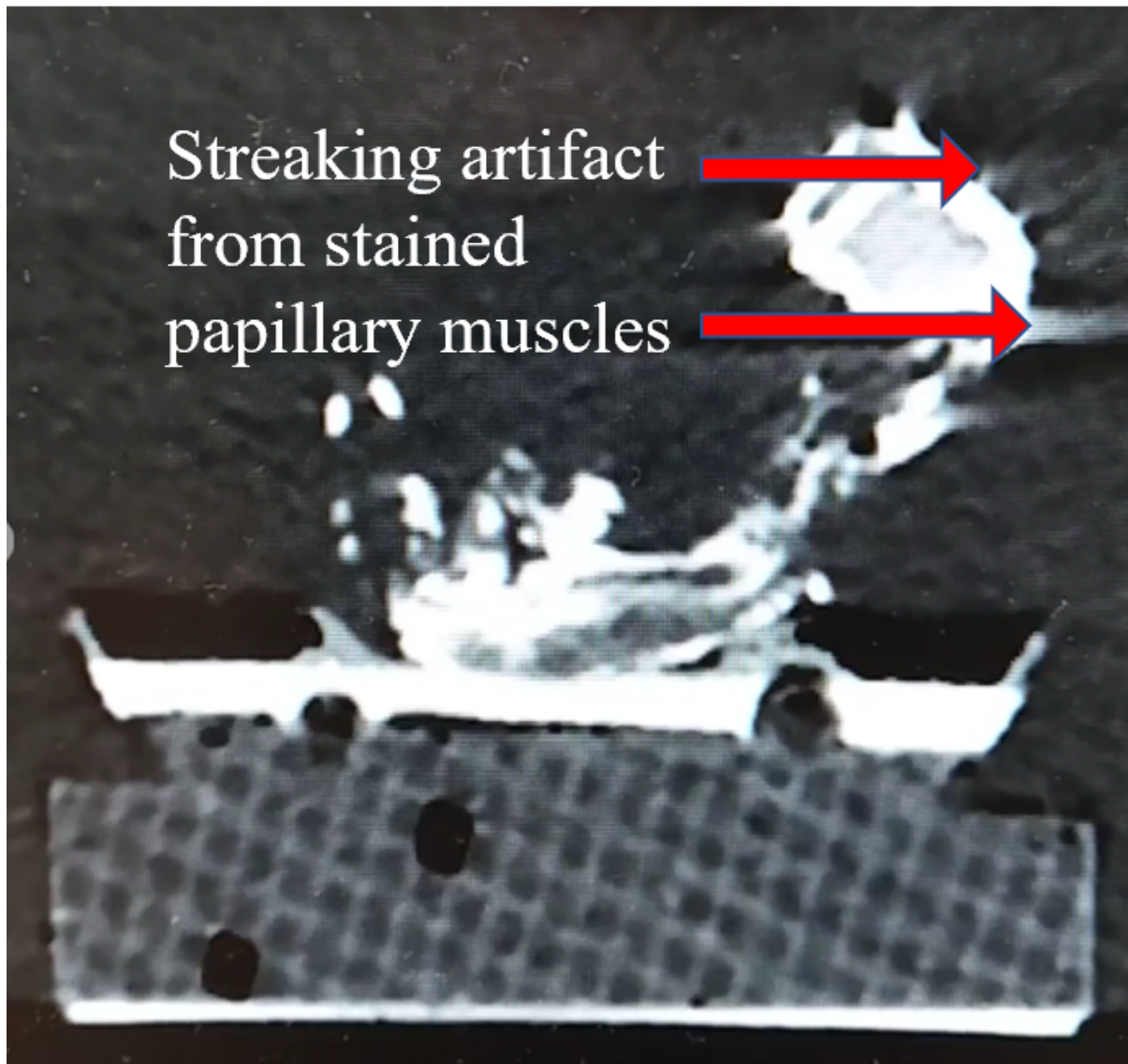
Figure 2.10: Example of streaking artifact due to stained papillary muscle movement within one slice of 4D volume from dynamically-acquired scan of the stained bovine valve in water operating at 30 bpm

2.4 Discussion

The primary motivation of this work was to investigate whether 4D-CT could be used as a ground truth to validate 3D reconstructions of the mitral valve from ultrasound. Dynamic cardiac CT is emerging as a modality well suited to provide high quality images capturing subvalvular anatomy and valve morphology over many cardiac phases. In order to assess the accuracy of dynamic CT for mitral valve imaging, we propose a workflow to compare gated, static CT images with phase-matched, dynamically-acquired images. In the work we showed that dynamic CT is reliable for imaging the beating mitral valve in a phantom.

The goals of this chapter were to explore the potential of dynamic CT for imaging a dynamic mitral valve phantom. To evaluate this, we designed two mitral valve phantoms (silicone and stained bovine) and constructed a motorized valve manipulator which simulates a range of physiologic heart rates, with the ability to arrest the valve at discrete points in the cardiac cycle. During image acquisition, we optimized parameters for the best possible temporal resolution, with the hope of fully capturing valve motion at the higher heart rates when movement became more rapid. We used mean euclidean distance (MED) as the metric for comparison between the static, ground truth datasets and the phase-matched volumes from the continuous scan. This gave us information about the ability of dynamic CT to accurately capture, represent and display the underlying valve movement at these different heart rates. Generally, we found good agreement between the static and dynamic volumes when the continuous scan captured 30 bpm, with the most discrepancy at the chordae positions. This is reasonable, as the chordae move the most in this experimental setup. As the simulated heart rate increased, the ability of the dynamic CT to accurately capture valve movement (as assessed by the MED between ground truth and dynamic volumes) declined. In addition, we wanted to investigate to what extent (if any) the image quality of the 4D-CT scans of dynamic mitral valve phantoms was affected. At simulated heart rates of 30 bpm, we found minimal to no artifacts in the resulting images. However, for 60 and especially at 90 bpm, there were nontrivial artifacts, mainly duplicate leaflet structures corrupting the images.

Dynamically-acquired, continuously-scanned volumes closely matched their phase-matched, static, ground truth counterparts. However, qualitatively we observed a high degree of motion artifacts–predominately duplicate structures–introduced with the dynamic scans. This effect became more pronounced as the simulated heart rate increased to the range typical of patients with valve regurgitation. However, improvements to the scanner itself are expected by next year where the temporal resolution will change from 280 ms to 80 ms, and this change alone could have a substantial impact on reducing artifacts. An observation unique to the bovine valve was the addition of streaking artifacts due to the papillary muscles. This indicates a spe-

cial consideration if extending this modality to valve imaging in humans where the presence of other organs could also introduce new artifacts. Still, CT for mitral valve disease patient use may be impractical since contrast-agent is required to provide contrast between valve and blood.

To conclude, the valve manipulator at 30 bpm with both silicone and bovine valves can serve as a ground truth phantom for a validation study with TEE. This work has demonstrated the ability of dynamic CT to serve as ground truth for TEE validation in the study performed and reported in Chapter 3 of this thesis.

Chapter 3

Accuracy of TEE for Mitral Valve Imaging

This chapter is largely based on the paper:

- "How accurately does transesophageal echocardiography identify the mitral valve?" Accepted for presentation at Statistical Atlases and Computational Modelling of the Heart (STACOM), a MICCAI Workshop in September 2018 in Granada, Spain and for publication in the IET Digital Library: Healthcare Technology Letters

3.1   Introduction

Due to the significant increase in life expectancy over the past century, valvular heart disease has come to the forefront of challenges facing modern medicine [12]. Mitral valve disease (MVD) classifies a range of different pathologies that cause regurgitation of blood into the left atrium during ventricular contraction. Mitral valve regurgitation (MVR) can occur from multiple pathologies, including prolapsed valves, as well as in the presence of flail leaflets with ruptured chordae tendineae [2]. Transesophageal echocardiography (TEE) is currently the state-of-the-art technique for diagnosis and evaluation of MVD. A diseased valve presents with regurgitation of high velocity blood which can be visualized with the TEE probe under Doppler [15]. Once diagnosed, a plan for intervention is decided upon based on patient's age, anatomy and in some cases additional cardiac computed tomography (CT) imaging. At present, this is a largely subjective process based mainly on images and clinician experience. There are limitations to using TEE for diagnosis and intervention of regurgitant mitral valves. A study of 242 patients who underwent TEE-guided mitral valve repair for degenerative MVD found the

rate of recurrence of regurgitation to be 5% after 1 month and 40% after 4 years [19].

Personalized analytical cardiac models have become a crucial component of the clinical workflow, especially with complex disorders such as valvular heart disease [39]. Patient-specific modelling provides an unparalleled opportunity for pre-operative planning and practice. The development of image-guided procedures enables minimally-invasive, beating-heart surgery, but poses new challenges and risks by removing the clinician's direct line of sight [46]. The success of these interventions relies on patient-specific simulators for pre-operative planning, including attempting different access routes, deployment of sutures and analyzing their accuracy, navigating variations in patient anatomy and repeating the procedure under image-guidance to reduce the cognitive load when performing the actual operation. Currently, the development of these models is limited by the quality of the patient images from which they are modelled. The mitral valve is segmented from a patient's diagnostic TEE, and rendered as a volume for rapid prototyping into a tissue-mimicking valve [24]. However, multiple pervading issues with the TEE datasets challenge the valve segmentation and successful implementation of this protocol. The first is the prevalence of signal dropout, appearing as gaps within the valve leaflet in regions that should present as contiguous tissue. For diagnosis, images corrupted by artifacts limit the clinicians' ability to determine the cause of regurgitation; for modelling, the valve cannot be completely segmented and the resulting models have holes. This results in a loss of some patient-specific morphology and the efficacy of the models is decreased. The second issue is the presence of high-intensity signal artefacts that appear in the TEE images and can be misconstrued as leaflets or other anatomical structures [40].

While an accurate valve segmentation of 3D TEE images is needed for patient-specific modelling, it is also a valuable diagnostic tool. Quantitative analysis is an integral part of the overall assessment of valve morphology and gives objective evidence for both classification and guiding intervention of regurgitation [23]. Current commercial 3D TEE imaging platforms can derive quantitative measurements and 3D visualizations of annular and leaflet geometry [56]. The software used for valve quantification and segmentation available from most vendors is semi-automated. Clinicians can calculate valve surface area, commissure-commissure lengths and leaflet area to identify various pathological features, evaluate MVR severity and inform subsequent interventions and treatment. Measurements made to evaluate lengths for neo-chordae, valve replacements and other volumetric data rely on intensities in TEE images as indications of valve and papillary muscle tissue [17]. Quantitative measurements and assessment is an essential step in the evaluation of patient-specific geometry, pathophysiologic mechanisms and abnormalities of the mitral valve.

The major challenge with 3D TEE segmentation is that a limited number of methods exist that can accurately and robustly isolate the mitral valve. These techniques vary in the extent
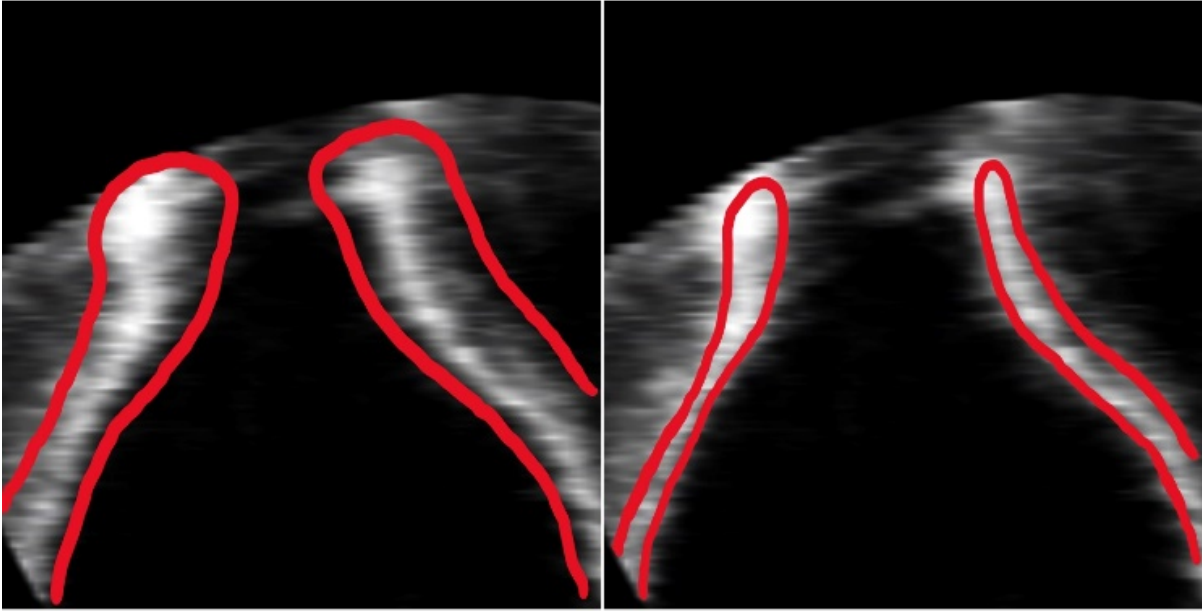
Figure 3.1: A 2D slice of a 3D TEE volume that demonstrates the two different ways to estimate the boundary (depicted in red). The edges of the bright intensity regions in valve TEE images are ambiguous and it is unclear if they are due to echoes or represent underlying valve tissue.

of user interaction required. Several anatomical details of the valve introduce nontrivial challenges to its segmentation. First, there is no intensity-based boundary between the leaflets and the adjacent heart tissue, which makes it difficult to identify the leaflet boundaries and annulus solely with image intensity information. As well, during diastole, the posterior leaflet is often pressed against the left ventricular wall, and the resulting echo image is characterized by signal dropout; this poses a challenge for an automated segmentation algorithm to capture the posterior leaflet geometry when the valve is opened. In addition, there is no intensity-based distinction between the anterior and posterior leaflets, and it is difficult to distinguish the coaptation zone during systole [56]. The majority of current ultrasound segmentation techniques involve and rely on intensity thresholds. Methods include intensity-based level sets, active contours graph cuts and thresholding to segment the valve [53]. However, it remains ambiguous whether regions of high intensity correspond to presence of mitral valve or papillary muscle tissue. As demonstrated in Figure 3.1, the leaflet boundaries are ambiguous, and an intensity-based approach cannot always accurately delineate the valve. Along the appearance of the tissue edge in particular, there is the option to over- or under-estimate the leaflet with intensity-based segmentation.

The goal of the present work is to evaluate the relationship between intensity values in 3D TEE images and underlying valve structure as seen in CT. This will inform intensity-based techniques for valve segmentation used in diagnosis, quantitative assessment and patient-

specific modelling of mitral valve regurgitation. To accomplish these goals, we propose the creation of ground truth CT datasets of silicone and bovine valve models for comparison to simultaneously acquired TEE images.

3.1.1   Contribution

The main contribution of this work is its analysis of the relationship between TEE intensities and underlying mitral valve tissue. With comparison to a CT ground truth, we have quantified the observed overestimation of valve structure in TEE [10]. Further, we have explored and demonstrated the efficacy of the centre line method for improved valve segmentation.

3.2   Materials and Methods

3.2.1   Overview

To meet the objectives of this study, our task was two-fold. First, we created a ground truth for mitral valve TEE image segmentation in both static and dynamic settings. Second, we employ this ground truth dataset to study the correspondence between mitral valve TEE image intensity distribution and the underlying valve morphology.

3.2.2   Ground Truth Creation

The silicone and bovine phantoms described in Chapter 2 were used, with both containers filled with water. An important requirement for creation of the ground truth dataset is simultaneous imaging of the mitral valve phantoms with CT and TEE. Because of CT's high resolution capability, we used the segmented valve from the CT image as the ground truth for comparison with the TEE images.

Image Acquisition

The data were acquired with simultaneous CT and TEE imaging of both the silicone and bovine valves. All of the 3D TEE scans were acquired using a Philips iE33 (Philips, Eindhoven, NL), using the X7-2t transesophageal probe. Three strategically placed holes on opposite sides of the annulus served as fiducials that were visible in both CT and TEE for landmark-based registration. The resulting dynamic image used for post-processing is an average over multiple TEE acquisitions. To create the static ground truth, the CT images were acquired in an O-arm (Medtronic, Minnesota, MN) at a resolution of 512 x 512 x 120 and the pixel spacing of 0.415
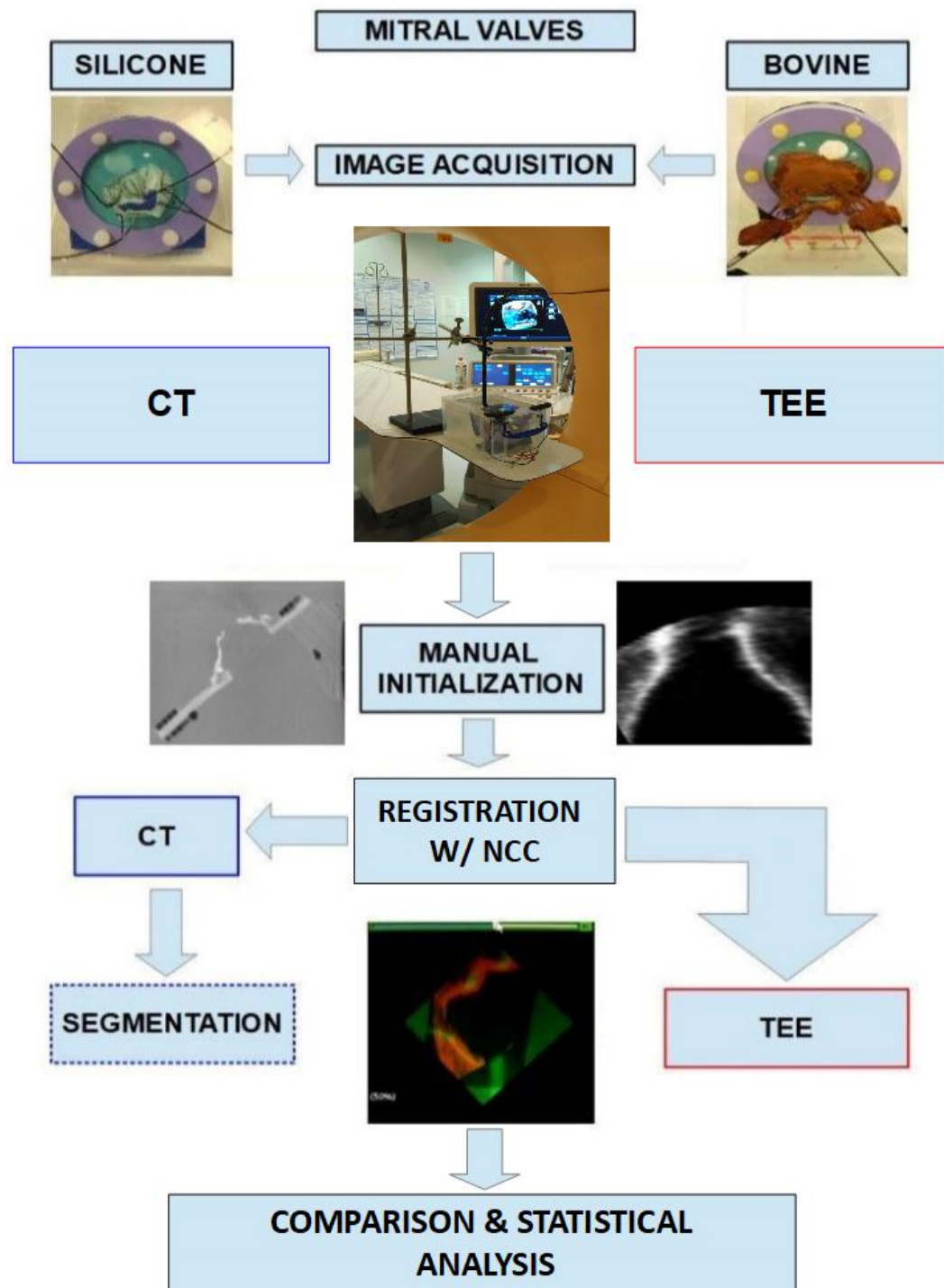
Figure 3.2: Pipeline for image acquisition, image processing and statistical analysis.

x 0.415 x 0.833mm. As outlined in Chapter 2, to obtain the dynamic ground truth, the 4D-CT scans were performed on the GE Revolution Discovery multi-slice scanner (GE Medical Systems, Waukesha, WI) in cine mode. These data were acquired with retrospective gating and the scan parameters were set as follows: 0.28 s gantry rotation, 2.2 s length of scan and 0.625 mm slice thickness. Each image reconstruction used data acquired from a full 360° rotation of the gantry.

Image Processing

Following acquisition, specific images were selected for further analysis based on visual inspection. Due to the poor image quality of TEE images during systole, this primarily consisted of selecting eight CT-TEE cardiac phases from end-diastole. In addition, we chose to use images with the motorized valve manipulator described in Chapter 2 operating at 30 bpm to avoid duplicate structure artifacts where a valve leaflet appears twice in one reconstructed slice in 4DCT. Once selected and sorted into image pairs, corresponding time frames were registered. The CT-TEE registration process was not trivial; to ensure a high degree of accuracy, most of the registration was performed manually. First, we placed landmarks in the centres of the holes visible in both CT and TEE, and the landmark-based registration was performed to act as a good initialization for CT-TEE registration. We then employed the BRAINS registration module in Slicer 4.6.2 (https://www.slicer.org/) to improve the alignment. Using this module, we implemented both Mutual Information (MI) and Normalized Cross Correlation (NCC) as our registration metrics, with NCC providing the more accurate alignment based on visual inspection. After automatic registration using NCC, the alignment was manually fine-tuned to further improve the registration accuracy. The aligned TEE and CT images were then apodized manually to focus on the valve region and to exclude the silicone flange and other supporting apparati that are also visible in the TEE and CT images. Finally, we applied the continuous max flow [72] algorithm to segment the processed CT images for subsequent use as ground truth. The workflow of the proposed ground truth creation pipeline is represented in Figure 3.2.

3.2.3 Image Analysis

With the ground-truth correspondence and registration established, we then completed both intensity-based and segmentation-based analyses of the static silicone (1 image pair), dynamic silicone (8 image pairs) and dynamic bovine (8 image pairs) CT segmentation and TEE image pairs.

Pixel based analysis

First, we directly studied the relationship between TEE image pixel intensity and the likelihood that a pixel belongs to the leaflet. Thus, for each discretized pixel intensity i ranging from 1 to 255, we computed the conditional probability of a pixel belonging to the valve region given its intensity by the following equation:

$$P(i) = P(x \in L | I(x) = i) = \frac{P(x \in L \cap I(x) = i)}{P(I(x) = i)}, \tag{3.1}$$

where $P(I(x) = i)$ represents the probability that a pixel in TEE images has intensity i, $P(x \in L)$ represents the probability that a pixel at location x belongs to the leaflet, and $P(x \in L \cap I(x) = i)$ represents the probability of the joint event. Thus, for any pixel location x, it can be determined if it is included in the leaflet by computing the dot product with the aligned CT segmentation at the same location x.

Segmentation based analysis

To further analyze the intensity correspondence of the TEE intensities and valve tissue, we also studied the performance of an advanced and commonly-used intensity-based segmentation approach. Aside from an optimization parameter, the two user inputs are a lower and upper threshold, which anticipate the intensity values of the background and foreground, or valve, respectively. Since we are interested in correctly predicting the location of the leaflet based on intensity, we used the positive predictive value (PPV) as our measurement of segmentation accuracy. This accounts for the fact that the majority of the TEE image is background, while we are concerned with correctly identifying valve regions. In the context of Receiver Operating Characteristic (ROC), the PPV is given as:

$$PPV = \frac{TP}{TP + FP}, \tag{3.2}$$

where TP represents the true positive rate and FP represents the false positive rate. Using this metric, we examined the PPV of the 3D continuous maxflow (3D CMF) algorithms. We ran the algorithm multiple times with different intensity threshold values for a thorough analysis of any improvements due to threshold optimization.

Centre-Line based analysis

From past observations, we noticed that the leaflets shown on TEE images were always thicker than those presented in CT. This could be an indication that the classification errors were mainly

located near the edges of the TEE segmentations, while the centre of the intensity-based segmentation is more likely to be part of the leaflet. Thus, as a preliminary study, we wanted to test a hypothesis that using the centre line of the TEE segmentation to represent the mitral valve is more accurate than using the segmentation surface to represent the valve surface. To test this hypothesis, we first computed the segmentations of the static silicone, dynamic silicone and dynamic bovine TEE images using the 3D CMF algorithm and then extracted the centre-lines from both TEE segmentations and CT segmentations. Then we compared the root mean squared distances between the surfaces of TEE and CT segmentations and the distance between TEE and CT centre-lines.

3.3 Results

In this study, we created a dynamic silicone phantom and a dynamic bovine phantom, which allowed us to image them in both static and dynamic states. Following the registration scheme shown in Figure 3.2, we created three sets of CT ground truth images for static silicone TEE, dynamic silicone TEE, and dynamic silicone TEE. For each dataset, we performed the pixel- and segmentation-based analyses as described in Section 3.2. Finally, we performed a center-line analysis using the static silicone dataset, as a pilot study, to prove the validity of our hypothesis given in Section 3.2.

3.3.1 Pixel based analysis

For each dataset, we computed the conditional probability of a pixel belonging to the valve region given its intensity following equation (1). The relationships between the likelihood and the TEE image intensity are shown in Figure 3.3. Generally, the results indicate that even with an optimized naive based threshold segmentation, only 40% of pixels are correctly classified as part of the valve.

The results shown in Figure 3.3 indicate the likelihood of any individual pixel intensity value corresponding to part of the valve. In Figure 3.3(a), we see that for the static silicone valve, there is a maximum 42% likelihood that any pixel would be classified as valve tissue, given its TEE intensity. From Figure 3.3(b), the maximum likelihood of intensity-based valve classification for the dynamic silicone valve is 35%. For the dynamic bovine valve, the maximum likelihood given its intensity is below 51%, as shown in Figure 3.3(c). As a result, our data suggest that classification based on intensity alone may be error-prone and subject to false positives.
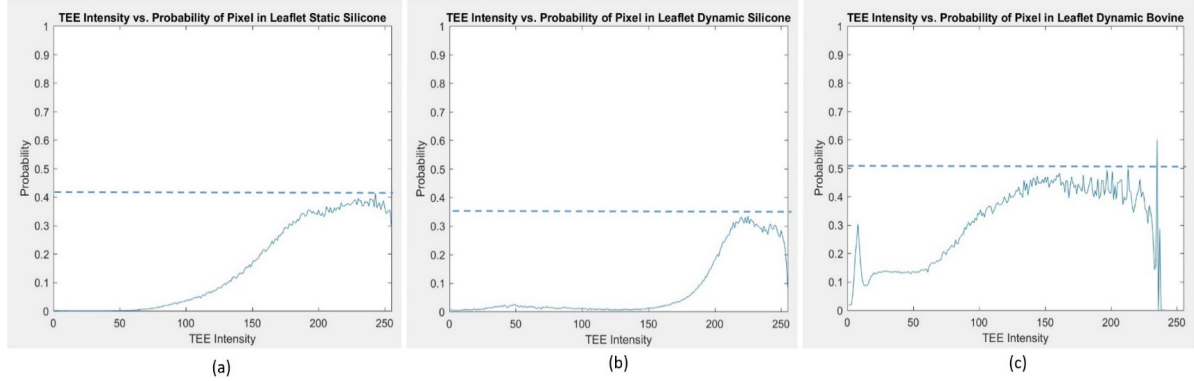
Figure 3.3: Plots of probability of each individual pixel intensity value in TEE images to correctly classify the pixel as part of the valve leaflet for (a) static silicone valve model (b) dynamic silicone valve model and (c) dynamic bovine valve model

3.3.2   Segmentation based analysis

After the pixel-based analysis was completed, we performed a 3D Continuous Max Flow (CMF) segmentation [72] on all three image pairs (static silicone, dynamic silicone and dynamic bovine). CMF is an advanced, intensity-based segmentation technique that needs both a lower and upper threshold to indicate the expected intensity value of the background and foreground, respectively.

The results from the 3D CMF segmentations are depicted in Figure 3.4. The multiple coloured lines represent the range of options for the lower threshold, and upper threshold varies along the x-axis. The algorithm begins with the initial lower threshold (the x-intercept) and runs through a search of all possible upper threshold values. Each line represents a different initial expected value for the background, and together these lines map all the possible combinations of lower and upper thresholds for 3D CMF. The y-axis includes the PPV value for each combination of lower and upper thresholds. Here, we investigated if any combination of user-defined parameters could optimize the segmentation accuracy.

From Figure 3.4(a), the maximum PPV is 40% for the 3D CMF segmentation of the static silicone valve. In Figure 3.4(b), the maximum PPV value is 31%, calculated over 8 averaged dynamic silicone volumes. Finally, in Figure 3.4(c), the 3D CMF segmentation of the dynamic bovine model yields a maximum averaged PPV value of 49%. Given that this is an advanced and commonly used technique for mitral valve segmentation, these results highlight the limitations of an intensity-only approach [60]. Thus, regardless of user-defined thresholds, mitral valve segmentation is limited by relying solely on intensity values of the ultrasound images.
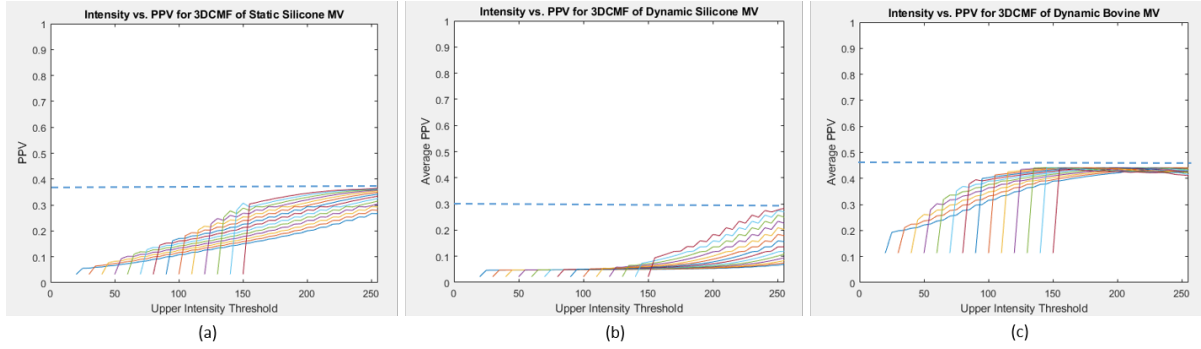
Figure 3.4: Plots of positive predictive value (PPV) for a range of lower and upper intensity thresholds for segmentation using 3DCMF of (a) static silicone valve model (b) dynamic silicone valve model and (c) dynamic bovine valve model. The coloured lines indicate different lower threshold values for a range of upper threshold values, tracked along the x-axis.

3.3.3 Centre-line Based Analysis

Following the description in Section 2.2, we performed a centre-line analysis on the static silicone image pairs. As an example, the overlayed 2D sections are shown in Figure 3.5, where Figure 3.5(a) demonstrates the overlayed centrelines and Figure 3.5(b) demonstrating the overlaid segmentations. The CT segmentation and centre-line is shown as green and the TEE segmentation and centre-line is shown in pink. As demonstrated by Figure 3.5(b), there are large distances between the edges of the TEE and CT segmentations, while from Figure 3.5(a), the distance between CT and TEE centre-lines is significantly smaller. Quantitatively, from 3D studies, the surface root mean squared distance (RMSD) between surfaces of the TEE and CT segmentations is 1.80 mm whereas the RMSD between the centre-lines extracted from the TEE and CT segmented volumes is 0.81 mm. Thus, these preliminary results support our hypothesis that the center line of the TEE segmentation is a better representation of the valve morphology than the solely intensity-based methods of leaflet edge delineation.

3.4 Discussion

Comprehensive visual and quantitative analysis of dynamic mitral valve morphology is necessary for identifying and correcting regurgitation. TEE is widely accepted as the gold standard for mitral valve imaging. The clinical workflow involves several applications of a mitral valve segmentation for quantifying and modelling patient-specific parameters and behavior. Most methods for valve segmentation are intensity-based, though it is unclear how the pixel values present in a TEE image correspond to underlying valve tissue. In this study, we evaluated the accuracy of TEE mitral valve imaging through construction of quasi-static silicone and bovine
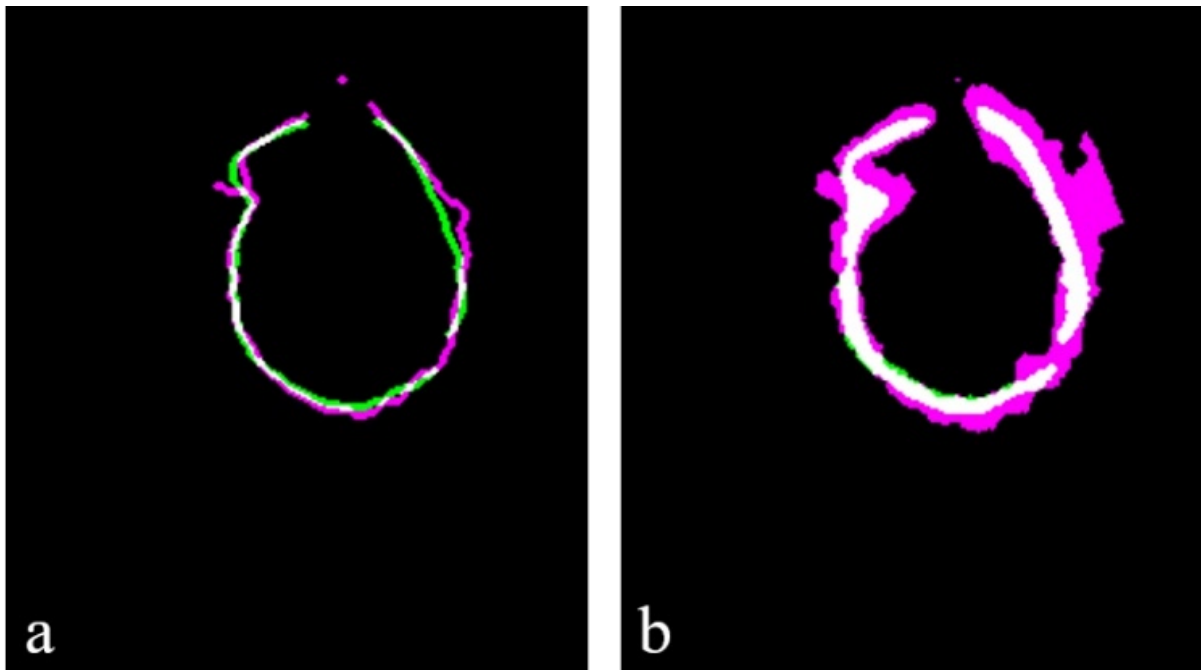
Figure 3.5: Overlaid segmentations of static silicone valve TEE (pink) and CT (green) images, and complete agreement between them (white) a) with centre-line extraction from 3DCMF segmentation and b) with 3DCMF segmentation only

valve phantom used to compare CT ground truth with simultaneously-acquired TEE images. The results provide evidence that reliance on intensity alone for segmentation cannot fully capture the valve structure, quantified by probability and positive predictive value metrics. The curves in Figure 3.3 present compelling evidence that individual pixel intensities in TEE do not have a consistent and obvious correspondence to underlying tissue. Comparisons across the three valve models (static silicone, dynamic silicone and dynamic bovine) demonstrate that the segmentation of the dynamic bovine TEE with 3DCMF is more accurate than images made with both static and dynamic silicone valves. This could indicate that individual pixel intensities in TEE images of biological tissue have a better correspondence to underlying structures than in silicone models. As such, further studies should be performed incorporating patient imaging data for a more comprehensive analysis of TEE for mitral valve imaging. The general trend present across all graphs in Figure 3.3 is that higher intensity values have a higher probability of identifying valve tissue. Although, with a maximum 50% likelihood of valve classification at any intensity, these results are compelling and motivate the use of new segmentation techniques that do not rely solely on intensities. Rather, valve segmentation should also incorporate some level of shape information about the valve structure. We demonstrate this by comparing an intensity-based segmentation with a centre-line analysis. These results demonstrate the efficacy of augmenting an intensity-based segmentation with information about the

shape and structure of the valve.

A limitation of this work is that the TEE images analyzed in this study were acquired from an older generation ultrasound system. As the technology continues to improve, a similar analysis should be conducted on future systems. Furthermore, we constructed our ground truth with the assumption that any motion artifacts due to valve motion in dynamic CT would be negligible. In reality, the resulting images had streaking artifacts and duplicate structures, with higher prevalence of artefact at higher simulated heart rates. To accomodate for and avoid these motion artifacts in our ground truth images, we selected 4DCT data from the 30bpm valve simulation. In addition, the analysis was restricted to 3 pairs of images due to limited acquisition time and TEE image quality. Further studies will evaluate a larger range of corresponding CT and TEE images of valve models at different cardiac phases.

This work has the potential to both inform current techniques for TEE imaging and segmentation as well as motivate the development of new methods for identifying valve structure in TEE from known correspondence to ground truth CT images. In future, being able to pair up ground truth CT images with actual TEE images may form the basis for improved reconstructions from TEE data. With CT data as a labelled training set, deep learning techniques can further extend this work to map between CT and TEE, and incorporate deep learning to predict the TEE segmentation from pre-existing CT segmentations.

Chapter 4

Conclusions and Future Work

4.1 Conclusions

The purpose of this thesis was first to develop a methodology for the design, implementation and assessment of a mitral valve phantom used to construct a dataset of ground truth images. The second aim of this work was to use this ground truth phantom in a validation study of transesophageal echocardiography imaging of the mitral valve. This thesis was as such divided into two chapters following the objectives stated in Chapter 1. Overall conclusions from both chapters will be discussed in this section.

In Chapter 2, our aim was to investigate whether 4D-CT could be used as a ground truth to validate 3D reconstructions of the mitral valve from TEE. We outlined the design of two mitral valve phantoms and construction of a motorized valve manipulator which simulates three different ECG-gated heart rates and can arrest the valve at precise, pre-selected points over the cardiac cycle. This has the ability to both inform and augment the use of TEE in mitral valve imaging for diagnosis and pre-operative models used in planning and practice. The results reported in Chapter 2 indicate that dynamic, 4D-CT has the potential to both extend and enhance the imaging of the mitral valve and subvalvular apparatus. However, we discovered that with simulated physiologic heart rates, the prevalence of motion artifacts increased such that duplicate leaflets and streaking both corrupted the resulting images. The phantom implemented and analyzed in Chapter 2 had a direct impact on the experiment reported in the subsequent chapter, from which more general conclusions can be drawn which are relevant to clinicians and researchers.

In Chapter 3, we performed an experiment with simultaneous TEE and CT imaging for a validation study. This primarily serves to validate the use of mitral valve segmentation in the workflows for MVD diagnosis and patient-specific modelling. We have demonstrated that reliance on intensity methods of segmentation alone do not closely identify underlying valve

tissue. Rather, valve segmentation from ultrasound should incorporate some level of shape information about the structure in addition to individual intensities. We hope that this will assist clinicians and engineers in future applications of mitral valve segmentation. In addition, this can be used to inform advanced techniques for classification of the mitral valve with deep and machine learning.

4.2 Future Work

These techniques have the potential to enable clinicians to acquire information for a thorough qualitative and quantitative assessment of regurgitant mitral valves. We have demonstrated that dynamic CT is a valuable tool for imaging mitral valve phantoms as a means of validating the use of transesophageal echocardiography in the clinical workflow for valvular disease. Current techniques for TEE imaging and segmentation of the mitral valve are limited by the prevalence of signal dropout, artifacts and limited field of view. One course of future direction will be to apply the accuracy analysis and validation pipelines to imaging machines with upgraded hardware and software. Within the next year, the Revolution CT will have an increased gantry speed from 280ms to 200ms; this improved temporal resolution could reduce the prevalence of image aritfacts at higher heart rates. Additionally, we plan to develop another prototype of the quasi-static phantom with subvalvular components and more physiologically-relevant features to improve the strength of these findings. With regards to the validation study in Chapter 3, we plan to extend the results to derive a mapping function between the intensities from dynamic CT and ultrasound in order to predict and inform the mitral valve segementation. Eventually, this will be developed into a neural network for deep learning of the relationship between dynamic CT and TEE, with a large database of patient images used to train the network for diagnosis and segmentation of regurgitant valves.

Each focus of the future work is aimed to improve the clinical workflow for mitral valve disease from diagnosis, pre-operative planning and preparation to intervention and post-operative monitoring. We have completed a novel, first-of-its-kind assessment of dynamic CT for this application. Currently we have demonstrated some intriguing results for the role that dynamic CT can play in the valvular disease workflow. We hope that this this thesis has laid the ground work for a further investigation of dynamic CT for mitral valve imaging, such that furure research can build on this work and continue to develop tools and systems which will improve surgical outcomes for heart disease patients.

Bibliography

[1] Mitral regurgitation. Columbia University Department of Surgery http://columbiasurgery.org/heart/mitral-regurgitation, 2015. 19.

[2] Eirini Apostolidou, Andrew D Maslow, and Athena Poppas. Primary mitral valve regurgitation: Update and review. *Global Cardiology Science & Practice*, 2017(1), 2017.

[3] Anthony D Bai, Marilyn Steinberg, Adrienne Showler, Lisa Burry, R Sacha Bhatia, George A Tomlinson, Chaim M Bell, and Andrew M Morris. Diagnostic accuracy of transthoracic echocardiography for infective endocarditis findings using transesophageal echocardiography as the reference standard: a meta-analysis. *Journal of the American Society of Echocardiography*, 30(7):639–646, 2017.

[4] S Barry Issenberg, William C McGaghie, Emil R Petrusa, David Lee Gordon, and Ross J Scalese. Features and uses of high-fidelity medical simulations that lead to effective learning: a beme systematic review. *Medical teacher*, 27(1):10–28, 2005.

[5] Ricardo Benenstein and Muhamed Saric. Mitral valve prolapse: role of 3d echocardiography in diagnosis. *Current opinion in cardiology*, 27(5):465–476, 2012.

[6] Thomas M Binder, Raphael Rosenhek, Gerold Porenta, Gerald Maurer, and Helmut Baumgartner. Improved assessment of mitral valve stenosis by volumetric real-time three-dimensional echocardiography. *Journal of the American College of Cardiology*, 36(4):1355–1361, 2000. 20.

[7] Jeremy Blum. *Exploring Arduino: tools and techniques for engineering wizardry*. John Wiley & Sons, 2013.

[8] F Edward Boas and Dominik Fleischmann. Ct artifacts: causes and reduction techniques. *Imaging Med*, 4(2):229–240, 2012.

[9] A Carpentier, S Chauvaud, JN Fabiani, A Deloche, J Relland, A Lessana, CL d'Allaines, PH Blondeau, A Piwnica, and CH Dubost. Reconstructive surgery of mitral valve incompetence: ten-year appraisal. *The Journal of thoracic and cardiovascular surgery*, 79(3):338–348, 1980.

[10] Pei G Chew, Katrina Bounford, Sven Plein, Dominik Schlosshan, and John P Greenwood. Multimodality imaging for the quantitative assessment of mitral regurgitation. *Quantitative imaging in medicine and surgery*, 8(3):342, 2018.

[11] Jacob P Dal-Bianco and Robert A Levine. Anatomy of the mitral valve apparatus: role of 2d and 3d echocardiography. *Cardiology clinics*, 31(2):151–164, 2013. 13.

[12] JL d'Arcy, BD Prendergast, JB Chambers, SG Ray, and B Bridgewater. Valvular heart disease: the next cardiac epidemic, 2010. 2.

[13] Tirone E David, Robert J Burns, CM Bacchus, and MN Druck. Mitral valve replacement for mitral regurgitation with and without preservation of chordae tendineae. *The Journal of Thoracic and Cardiovascular Surgery*, 88(5 Pt 1):718–725, 1984.

[14] JM Ferrão de Oliveira and Manuel J Antunes. Mitral valve repair: better than replacement. *Heart*, 92(2):275–281, 2006.

[15] Milind Y Desai, Francesco Grigioni, Marco Di Eusanio, Matteo Saccocci, Maurizio Taramasso, Francesco Maisano, Rakesh M Suri, and A Marc Gillinov. Outcomes in degenerative mitral regurgitation: current state-of-the art and future directions. *Progress in cardiovascular diseases*, 2017.

[16] P Joy Dunmore-Buyze, Elsbeth Tate, Fu-li Xiang, Sarah A Detombe, Zengxuan Nong, J Geoffrey Pickering, and Maria Drangova. Three-dimensional imaging of the mouse heart and vasculature using micro-ct and whole-body perfusion of iodine or phospho-tungstic acid. *Contrast media & molecular imaging*, 9(5):383–390, 2014.

[17] Sarah Eibel, Edwin Turton, Chirojit Mukherjee, Carmine Bevilacqua, and Joerg Ender. Feasibility of measurements of valve dimensions in en-face-3d transesophageal echocardiography. *The international journal of cardiovascular imaging*, 33(10):1503–1511, 2017.

[18] Milad El-Segaier, O Lilja, S Lukkarinen, Leif Sörnmo, R Sepponen, and Erkki Pesonen. Computer-based detection and analysis of heart sound and murmur. *Annals of Biomedical Engineering*, 33(7):937–942, 2005.

[19] Willem Flameng, Paul Herijgers, and Kris Bogaerts. Recurrence of mitral valve regurgitation after mitral valve repair in degenerative valve disease. *Circulation*, 107(12):1609–1613, 2003. 4.

[20] Elyse Foster. Mitral regurgitation due to degenerative mitral-valve disease. *New England Journal of Medicine*, 363(2):156–165, 2010.

[21] Lisa A Freed, Daniel Levy, Robert A Levine, Martin G Larson, Jane C Evans, Deborah L Fuller, Birgitta Lehman, and Emelia J Benjamin. Prevalence and clinical outcome of mitral-valve prolapse. *New England Journal of Medicine*, 341(1):1–7, 1999.

[22] Oliver Gaemperli, Roberto Corti, and A Gruntizig. Mitraclip for the treatment of mitral regurgitation. *Cardiovasc Med*, 15:276–286, 2012. 6.

[23] Madalina Garbi and Mark J Monaghan. Quantitative mitral valve anatomy and pathology. *Echo research and practice*, pages ERP–15, 2015.

[24] Olivia Ginty, John Moore, Wenyao Xia, Dan Bainbridge, and Terry Peters. Patient-specific indirectly 3d printed mitral valves for pre-operative surgical modelling. In *Medical Imaging 2017: Image-Guided Procedures, Robotic Interventions, and Modeling*, volume 10135, page 1013517. International Society for Optics and Photonics, 2017.

[25] Alexandra Gonçalves, Carla Sousa, José Alberto de Agustín, Pedro Marcos-Alberca, C Fernández-Golfín, and JL Zamorano. Full-volume color flow quantification in mitral regurgitation. *US Cardiology*, 8(2):94–97, 2011.

[26] Jasmine Grewal, Sunil Mankad, William K Freeman, Roger L Click, Rakesh M Suri, Martin D Abel, Jae K Oh, Patricia A Pellikka, Gillian C Nesbitt, Imran Syed, et al. Real-time three-dimensional transesophageal echocardiography in the intraoperative assessment of mitral valve disease. *Journal of the American Society of Echocardiography*, 22(1):34–41, 2009. 18.

[27] Jan N Hilberath, Daryl A Oakes, Stanton K Shernan, Bernard E Bulwer, Michael N DAmbra, and Holger K Eltzschig. Safety of transesophageal echocardiography. *Journal of the American Society of Echocardiography*, 23(11):1115–1127, 2010.

[28] SY Ho. Anatomy of the mitral valve. *Heart*, 88(suppl 4):iv5–iv10, 2002. 14.

[29] Razvan Ioan Ionasec, Dime Vitanovski, and Dorin Comaniciu. Morphological and functional modeling of the heart valves and chambers. In *Patient-Specific Modeling in Tomorrow's Medicine*, pages 157–187. Springer, 2011. 3.

[30] Hoda Javadikasgari, Rakesh M Suri, Bassman Tappuni, and A Marc Gillinov. Minimally invasive mitral valve repair. *Heart*, 104(10):861–867, 2018.

[31] Christine Jellis and Teerapat Yingchoncharoen. Assessment of mitral valve function. In *An Atlas of Mitral Valve Imaging*, pages 17–30. Springer, 2015.

[32] Somsupha i Kanjanautha. Mitral valve anatomy: Overview, gross anatomy, microscopic anatomy. Medscape https://emedicine.medscape.com/article/1878301-overview, September 2015. 11.

[33] Bob Kiaii and Michael Chu. Verbal communication with Dr. Bob Kiaii, London Health Sciences Center (LHSC) University Hospital Chief of Cardiac Surgery and Dr. Michael Chu, Cardiac Surgeon for LHSC., 2013. 7.

[34] Richard E. Klabunde. Cardiovascular physiology concepts: https://www.cvphysiology.com/heart 8.

[35] Hyun Jung Koo, Dong Hyun Yang, Sang Young Oh, Joon-Won Kang, Dae-Hee Kim, Jae-Kwan Song, Jae Won Lee, Cheol Hyun Chung, and Tae-Hwan Lim. Demonstration of mitral valve prolapse with ct for planning of mitral valve repair. *Radiographics*, 34(6):1537–1552, 2014.

[36] Sandra V Kotsis and Kevin C Chung. Application of see one, do one, teach one concept in surgical training. *Plastic and reconstructive surgery*, 131(5):1194, 2013.

[37] Robert A Levine, Albert A Hagége, Daniel P Judge, Muralidhar Padala, Jacob P Dal-Bianco, Elena Aikawa, Jonathan Beaudoin, Joyce Bischoff, Nabila Bouatia-Naji, Patrick Bruneval, et al. Mitral valve diseasemorphology and mechanisms. *Nature Reviews Cardiology*, 12(12):689, 2015.

[38] Feng P Li, Martin Rajchl, John Moore, and Terry M Peters. A mitral annulus tracking approach for navigation of off-pump beating heart mitral valve repair. *Medical physics*, 42(1):456–468, 2015.

[39] Magnus Lindroos, Markku Kupari, Juhani Heikkilä, and Reijo Tilvis. Prevalence of aortic valve abnormalities in the elderly: an echocardiographic study of a random population sample. *Journal of the American College of Cardiology*, 21(5):1220–1225, 1993.

[40] Azad Mashari, Mario Montealegre-Gallegos, Ziyad Znio, Lu Yeh, Jelliffe Jeganathan, Robina Matyal, Kamal R Khabbaz, and Feroze Mahmood. Making three-dimensional echocardiography more tangible: a workflow for three-dimensional printing with echocardiographic data. *Echo research and practice*, pages ERP–16, 2016.

[41] Karen P McCarthy, Liam Ring, and Bushra S Rana. Anatomy of the mitral valve: understanding the mitral valve complex in mitral regurgitation. *European Journal of echocardiography*, 11(10):i3–i9, 2010. 15.

[42] William C McGaghie, S Barry Issenberg, Ms Elaine R Cohen, Jeffrey H Barsuk, and Diane B Wayne. Does simulation-based medical education with deliberate practice yield better results than traditional clinical education? a meta-analytic comparative review of the evidence. *Academic medicine: journal of the Association of American Medical Colleges*, 86(6):706, 2011.

[43] A Jonathan McLeod, John Moore, Pencilla Lang, Dan Bainbridge, Gordon Campbell, Doug L Jones, Gerard M Guiraudon, and Terry M Peters. Evaluation of mitral valve replacement anchoring in a phantom. In *Medical Imaging 2012: Image-Guided Procedures, Robotic Interventions, and Modeling*, volume 8316, page 83162Q. International Society for Optics and Photonics, 2012.

[44] A Jonathan McLeod, John T Moore, and Terry M Peters. Beating heart mitral valve repair with integrated ultrasound imaging. In *Medical Imaging 2015: Image-Guided Procedures, Robotic Interventions, and Modeling*, volume 9415, page 941504. International Society for Optics and Photonics, 2015.

[45] Stephanie L Mick, Suresh Keshavamurthy, and A Marc Gillinov. Mitral valve repair versus replacement. *Annals of cardiothoracic surgery*, 4(3):230, 2015.

[46] John T Moore, Michael WA Chu, Bob Kiaii, Daniel Bainbridge, Gerard Guiraudon, Chris Wedlake, Maria Currie, Martin Rajchl, Rajni V Patel, and Terry M Peters. A navigation platform for guidance of beating heart transapical mitral valve repair. *IEEE Transactions on Biomedical Engineering*, 60(4):1034–1040, 2013.

[47] Yoshihisa Morimoto and Takaki Sugimoto. Alfieri stitch for temporary severe functional mitral regurgitation after aortic valve replacement. *Surgical case reports*, 4(1):4, 2018.

[48] Michael F Morris, Joseph J Maleszewski, Rakesh M Suri, Harold M Burkhart, Thomas A Foley, Crystal R Bonnichsen, Nandan S Anavekar, Phillip M Young, Eric E Williamson, James F Glockner, et al. Ct and mr imaging of the mitral valve: radiologic-pathologic correlation. *Radiographics*, 30(6):1603–1620, 2010.

[49] Dariush Mozaffarian, Emelia J Benjamin, Alan S Go, Donna K Arnett, Michael J Blaha, Mary Cushman, Sarah De Ferranti, Jean Pierre Despres, Heather J Fullerton, Virginia J Howard, et al. Executive summary: heart disease and stroke statistics-2015 update: a report from the american heart association. *Circulation*, 131(4):434–441, 2015. 1.

[50] Rick A Nishimura, Alec Vahanian, Mackram F Eleid, and Michael J Mack. Mitral valve diseasecurrent management and future challenges. *The Lancet*, 387(10025):1324–1334, 2016.

[51] Vuyisile T Nkomo, Julius M Gardin, Thomas N Skelton, John S Gottdiener, Christopher G Scott, and Maurice Enriquez-Sarano. Burden of valvular heart diseases: a population-based study. *The Lancet*, 368(9540):1005–1011, 2006. 5.

[52] Thilo Noack, Philipp Kiefer, Razvan Ionasec, Ingmar Voigt, Tammaso Mansi, Marcel Vollroth, Michael Hoebartner, Martin Misfeld, Friedrich-Wilhelm Mohr, and Joerg Seeburger. New concepts for mitral valve imaging. *Annals of cardiothoracic surgery*, 2(6):787, 2013.

[53] J Alison Noble and Djamal Boukerroui. Ultrasound image segmentation: a survey. *IEEE Transactions on medical imaging*, 25(8):987–1010, 2006.

[54] Kikuko Obase, Valluvan Jeevanandam, Ken Saito, Kimberly Kesner, Aaron Barry, Andrew Hollatz, Farhan Farooqui, Karima Addetia, Joseph D Roberts, Takeyoshi Ota, et al. Visualization and measurement of mitral valve chordae tendineae using three-dimensional transesophageal echocardiography from the transgastric approach. *Journal of the American Society of Echocardiography*, 28(4):449–454, 2015.

[55] AS Omran, AA Arifi, and AA Mohamed. Echocardiography of the mitral valve. *Journal of the saudi Heart Association*, 22(3):165–170, 2010.

[56] Alison M Pouch, Hongzhi Wang, Manabu Takabe, Benjamin M Jackson, Joseph H Gorman III, Robert C Gorman, Paul A Yushkevich, and Chandra M Sehgal. Fully automatic segmentation of the mitral leaflets in 3d transesophageal echocardiographic images using multi-atlas joint label fusion and deformable medial modeling. *Medical image analysis*, 18(1):118–129, 2014.

[57] Manuel K Rausch, Wolfgang Bothe, John-Peder Escobar Kvitting, Julia C Swanson, D Craig Miller, and Ellen Kuhl. Mitral valve annuloplasty. *Annals of biomedical engineering*, 40(3):750–761, 2012.

[58] Mansour Razminia, Atul Trivedi, Janos Molnar, Monther Elbzour, Mayra Guerrero, Yasser Salem, Aziz Ahmed, Sandeep Khosla, and David L Lubell. Validation of a new formula for mean arterial pressure calculation: the new formula is superior to the standard formula. *Catheterization and cardiovascular interventions*, 63(4):419–425, 2004.

[59] Pankaj Saxena, Joseph F Malouf, Roger Click, and Rakesh M Suri. 3 d echocardiography in cardiac surgery. *Journal of Cardiac Surgery: Including Mechanical and Biological Support for the Heart and Lungs*, 29(1):51–54, 2014.

[60] Robert J Schneider, Douglas P Perrin, Nikolay V Vasilyev, Gerald R Marx, J Pedro, and Robert D Howe. Mitral annulus segmentation from 3d ultrasound using graph cuts. *IEEE Transactions on Medical Imaging*, 29(9):1676–1687, 2010.

[61] Yasushige Shingu, Tomonori Ooka, Hiroki Katoh, Tsuyoshi Tachibana, Suguru Kubota, and Yoshiro Matsui. Feasibility and limitations of mitral valve repair, with or without left ventricular reconstruction in non-ischemic dilated cardiomyopathy. *Journal of cardiology*, 71(4):329–335, 2018.

[62] William P Shuman, Kelley R Branch, Janet M May, Lee M Mitsumori, David W Lockhart, Theodore J Dubinsky, Bill H Warren, and James H Caldwell. Prospective versus retrospective ecg gating for 64-detector ct of the coronary arteries: comparison of image quality and patient radiation dose. *Radiology*, 248(2):431–437, 2008.

[63] Jeffrey J Silbiger and Raveen Bazaz. Contemporary insights into the functional anatomy of the mitral valve. *American heart journal*, 158(6):887–895, 2009. 17.

[64] Edwin Wilberforce Turton and Jörg Ender. Role of 3d echocardiography in cardiac surgery: Strengths and limitations. *Current anesthesiology reports*, 7(3):291–298, 2017.

[65] Heart & Vascular Institute George Washington University. Anatomy and function of the heart valves. http://www.gwheartandvascular.org/education/anatomy-and-function-of-the-heart-valves/, 2018. 10.

[66] Rice University. *Anatomy and Physiology: 19.2 Cardiac Muscle and Electrical Activity*. OpenEd, 2016. 9.

[67] Alec Vahanian, Helmut Baumgartner, Jeroen Bax, Eric Butchart, Robert Dion, Gerasimos Filippatos, Frank Flachskampf, Roger Hall, Bernard Iung, Jaroslaw Kasprzak, et al. Guidelines on the management of valvular heart disease: The task force on the management of valvular heart disease of the european society of cardiology. *European heart journal*, 28(2):230–268, 2007.

[68] Gerda L van Rijk-Zwikker, Ben J Delemarre, and Hans A Huysmans. Mitral valve anatomy and morphology: relevance to mitral valve replacement and valve reconstruction. *Journal of cardiac surgery*, 9:255–261, 1994. 12.

[69] Claire Vannelli, John Moore, Jonathan McLeod, Dennis Ceh, and Terry Peters. Dynamic heart phantom with functional mitral and aortic valves. In *Medical Imaging 2015: Image-Guided Procedures, Robotic Interventions, and Modeling*, volume 9415, page 941503. International Society for Optics and Photonics, 2015.

[70] Tokihiro Yamamoto, Ulrich Langner, Billy W Loo Jr, John Shen, and Paul J Keall. Retrospective analysis of artifacts in four-dimensional ct images of 50 abdominal and thoracic radiotherapy patients. *International Journal of Radiation Oncology* Biology* Physics*, 72(4):1250–1258, 2008.

[71] EDWARD L Yellin, CHARLES Peskin, CHAIM Yoran, Mordecai Koenigsberg, MASAYUKI Matsumoto, SHLOMO Laniado, D McQueen, D Shore, and RW Frater. Mechanisms of mitral valve motion during diastole. *American Journal of Physiology-Heart and Circulatory Physiology*, 241(3):H389–H400, 1981.

[72] Jing Yuan, Egil Bae, Xue-Cheng Tai, and Yuri Boykov. A continuous max-flow approach to potts model. In *European conference on computer vision*, pages 379–392. Springer, 2010.

[73] William A Zoghbi, Maurice Enriquez-Sarano, Elyse Foster, Paul A Grayburn, Carol D Kraft, Robert A Levine, Petros Nihoyannopoulos, Catherine M Otto, Miguel A Quinones, Harry Rakowski, et al. Recommendations for evaluation of the severity of native valvular regurgitation with two-dimensional and doppler echocardiography. *Journal of the American Society of Echocardiography*, 16(7):777–802, 2003.

Curriculum Vitae

Name: Claire Marie Regan Vannelli

Post-Secondary   Bachelor of Engineering, Biomedical Engineering
Education and   Duke University, Durham, NC, USA
Degree: 2011 - 2015

Related Work   Teaching Assistant
Experience: The University of Western Ontario
                      2016-2018

Journal Manuscripts: (* - primary author)

Vannelli, C.*, Moore, J., Xia, W., So, A., & Peters, T.M., Accuracy of Dynamic CT for Mitral Valve Imaging *International Journal of Computer Assisted Radiology and Surgery* (In preparation).

Vannelli, C.*, Xia, W., Moore, J., & Peters, T.M., Accuray of Transesophageal Echocardiography for Identifying the Mitral Valve *The Institution of Engineering and Technology: Healthcare Technology Letters* (Accepted for publication).

Conference Proceedings: (* - primary author)

Vannelli, C*, Xia, W., Moore, J., & Peters, T.M., How accurately does transesophageal echocardiography identify the mitral valve? *MICCAI Workshop in Statistical Atlases and Computatoinal Modelling of the Heart*, Spain, 2018. (Poster presentation)

Vannelli, C.*, Moore, J., Xia, W., So, A., & Peters, T.M., Accuracy of mitral valve imaging in dynamic CT *International Conference of Computer Assisted Radiology and Surgery*, Germany, 2018. (Podium presentation)

Vannelli, C.*, Moore, J., McLeod, A.J., Ceh, D. & Peters, T.M. Dynamic heart phantom with functional mitral and aortic valves *Society of Photographic Instrumentation Engineers Proceedings in Medical Imaging*, FL, USA, 2015. (Podium presentation)

Research Abstracts: (* - primary author)

Vannelli, C.*, Moore, J., Xia, W., So, A., and Peters, T.M. Accuracy of mitral valve imaging in dynamic computed tomography. *Robarts Research Retreat*, London, ON, 2018. (Poster presentation)

Vannelli, C.*, Moore, J., Xia, W., So, A., and Peters, T.M. Accuracy of mitral valve imaging in dynamic computed tomography. *Imaging Network Ontario*, Toronto, ON, 2018. (Poster presentation)

Vannelli, C.*, Moore, J., Xia, W., So, A., and Peters, T.M. Accuracy of mitral valve imaging in dynamic computed tomography. *London Health Research Day*, London, ON, 2018. (Poster presentation)

Vannelli, C.*, Xia, W., Moore, J., and Peters, T.M., Image Fusion for Improved Ultrasound Mitral Valve Segmentation and Modelling.*Robarts Research Retreat*, London, ON, 2017. (Poster presentation)

Vannelli, C*, Xia, W., Moore, J., and Peters, T.M., Image Fusion for Improved Ultrasound Mitral Valve Segmentation and Modelling.*Imaging Network Ontario*, London, ON, 2017. (Poster presentation)

Honours and Awards:	Graduate Student Innovation Scholar (Institutional) Western University, London ON, 2017
	Weaver James Corrigan Postgraduate Scholar (Regional) Duke Universiy, Durham, NC, 2015
	All-ACC Academic Team Selection (Regional) Duke University, Durham, NC, 2015
	Graduation with Distinction, *cum laude* (Institutional) Duke University, Durham, NC, 2015
	Deans Honor List With Distinction (Institutional) Duke University, Durham, NC, 2012-2015

CRCA Scholar Athlete Recipient (National)
Duke University, Durham, NC, 2011-2015

Baldwin Scholar (Institutional)
Duke University, Durham, NC, 2011-2015

Leadership/   Presented at over six outreach sessions for students aged 10-18
Volunteer   Discovery Day in Health Sciences; The Canadian Medical Hall of Fame
Activities: Robarts Research Institute, London, ON
                     2016-2017

                     Coordinator of Weekly Department Seminar Series
                     School of Biomedical Engineering, Western University
                     2017-2018